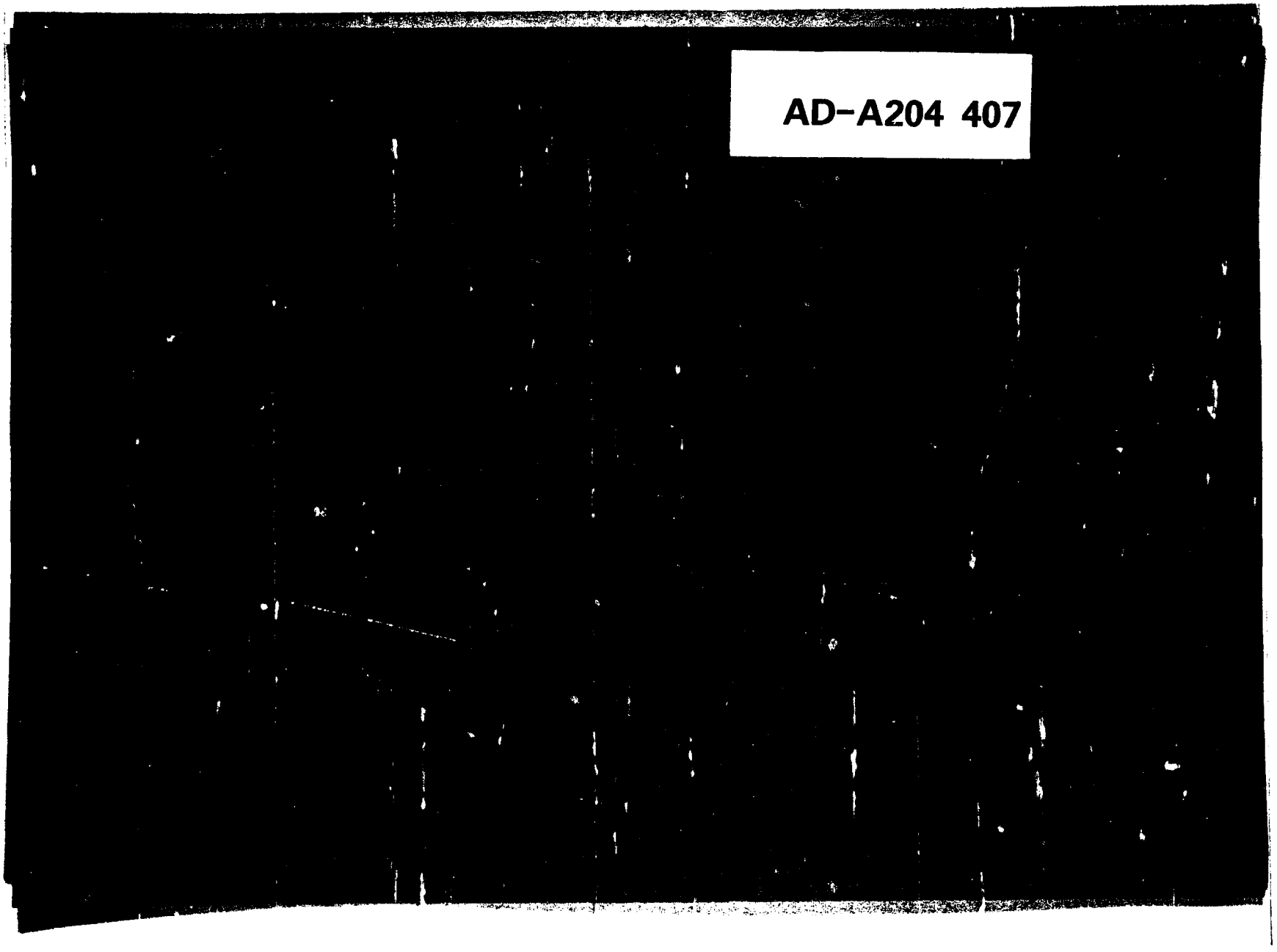

Laser Studies of Gas Phase Radical Reactions

Final Technical Report

by

G. Hancock

January 1989

United States Army

EUROPEAN RESEARCH OFFICE OF THE U.S. ARMY

London England

Contract Number DAJA45-85-C-0034

Physical Chemistry Laboratory, Oxford University

Approved for Public Release; distribution unlimited

Unclassified
SECURITY CLASSIFICATION OF THIS PAGE

REPORT DOCUMENTATION PAGE

1a. REPORT SECURITY CLASSIFICATION Unclassified	1b. RESTRICTIVE MARKINGS
2a. SECURITY CLASSIFICATION AUTHORITY	3. DISTRIBUTION/AVAILABILITY OF REPORT Approved for public release; distribution unlimited
2b. DECLASSIFICATION/DOWNGRADING SCHEDULE	
4. PERFORMING ORGANIZATION REPORT NUMBER(S)	5. MONITORING ORGANIZATION REPORT NUMBER(S) R&D 5016-CH-01
6a. NAME OF PERFORMING ORGANIZATION Physical Chemical Laboratory Oxford University 6b. OFFICE SYMBOL (If applicable)	7a. NAME OF MONITORING ORGANIZATION USARDSG(UK)
6c. ADDRESS (City, State, and ZIP Code) South Parks Road Oxford OX1 3QS United Kingdom	7b. ADDRESS (City, State, and ZIP Code) Box 65 FPO New York 09510-1500
8a. NAME OF FUNDING/SPONSORING ORGANIZATION USARDSG(UK) 8b. OFFICE SYMBOL (If applicable) AMXSN-UK-RC	9. PROCUREMENT INSTRUMENT IDENTIFICATION NUMBER DAJA45-85-C-0034
8c. ADDRESS (City, State, and ZIP Code) Box 65 FPO New York 09510-1500	10. SOURCE OF FUNDING NUMBERS PROGRAM ELEMENT NO: 61102A PROJECT NO.: 1L161102BH57 TASK NO: 08 WORK UNIT ACCESSION NO: DA308990
11. TITLE (Include Security Classification) (U) Laser Studies of Gas Phase Radical Reactions	
12. PERSONAL AUTHOR(S) G. Hancock	
13a. TYPE OF REPORT Final 13b. TIME COVERED FROM Sep 85 TO Dec 88 14. DATE OF REPORT (Year, Month, Day) 1989, January 15. PAGE COUNT 40	
16. SUPPLEMENTARY NOTATION hydrogen fluoride carbon monoxide	

17. COSATI CODES			18. SUBJECT TERMS (Continue on reverse if necessary and identify by block number)
FIELD	GROUP	SUB-GROUP	
07	04		carbon dioxide
07	02		

Sigma

19. ABSTRACT (Continue on reverse if necessary and identify by block number)

A series of measurements on free radicals produced by chemical reaction and photodissociation has been made, using laser methods for formation and in some cases, detection. Highly exothermic reactions between oxygen atoms and both CF_2 and CHF radicals have been studied by time resolved Fourier transform infrared emission spectroscopy, yielding information on the reaction pathway, emitting products, kinetics of formation and quenching, and the nascent vibrational distributions. Emitting species HCl, HF, CO and CO_2 have been identified in these systems. In a second study, the quantum state distributions and polarisations of OH and OD($A^2\Sigma^+$) products of the two photon dissociation of H_2O and D_2O at 266 nm have been measured. Results show the importance of long lived trajectories in determining the photodissociation dynamics, but the unexpected observation of low fragment alignment is unable to clarify the two photon state responsible for the excitation step. A third project has concentrated on

hydrogen chloride

Continued over.

over

20. DISTRIBUTION/AVAILABILITY OF ABSTRACT ☒ UNCLASSIFIED/UNLIMITED ☒ SAME AS RPT ☐ DTIC USERS	21. ABSTRACT SECURITY CLASSIFICATION Unclassified
22a. NAME OF RESPONSIBLE INDIVIDUAL Dr. Robert J. Campbell	22b. TELEPHONE (Include Area Code) (01) 409 4423 22c. OFFICE SYMBOL AMXSN-UK-RC

DD FORM 1473, 84 MAR 83 APR edition may be used until exhausted. All other editions are obsolete

SECURITY CLASSIFICATION OF THIS PAGE
Unclassifed

(1)

Block 19 continued.

measurements of radiative lifetimes of the CF($A^2\Sigma^+$) state, with new information on the A-X spectroscopy and on the O + CF($X^2\Pi$) reaction rate constant found. Finally, preliminary measurements on the nascent CO rotational distribution in the O + CS reaction is reported, and some additional experiments concerning the formation of carbene radicals in liquid phase enzyme cleavage studies are described.

carbon difluoride, water, deuterium, (oxygen)

Laser Studies of Gas Phase Radical Reactions

G. Hancock

Physical Chemistry Laboratory, Oxford University,
South Parks Road, Oxford, OX1 3QZ, U.K.

ABSTRACT

A series of measurements on free radicals produced by chemical reaction and photodissociation has been made, using laser methods for formation and in some cases, detection. Highly exothermic reactions between oxygen atoms and both CF_2 and CHF radicals have been studied by time resolved Fourier transform infrared emission spectroscopy, yielding information on the reaction pathway, emitting products, kinetics of formation and quenching, and the nascent vibrational distributions. Emitting species $HC\ell$, HF, CO and CO_2 have been identified in these systems. In a second study, the quantum state distributions and polarisations of OH and OD($A^2\Sigma^+$) products of the two photon dissociation of H_2O and D_2O at 266 nm have been measured. Results show the importance of long lived trajectories in determining the photodissociation dynamics, but the unexpected observation of low fragment alignment is unable to clarify the two photon state responsible for the excitation step. A third project has concentrated on measurements of radiative lifetimes of the CF($A^2\Sigma^+$) state, with new information on the A–X spectroscopy and on the O + CF($X^2\Pi$) reaction rate constant found. Finally, preliminary measurements on the nascent CO rotational distribution in the O + CS reaction is reported, and some additional experiments concerning the formation of carbene radicals in liquid phase enzyme cleavage studies are described.

Keywords Laser, kinetics, fluorescence, infrared, fluorocarbene, hydroxyl

Index

1. Time Resolved Fourier Transform Infrared Emission Studies of Atom plus Radical Reactions

INTRODUCTION

Infrared emission from the products of bimolecular chemical reactions was one of the first experimental methods to be used to study the nascent distributions of internal energy, and thus to learn about the molecular dynamics of the reactive encounter [1]. Since the early experiments of Polanyi's group, a number of workers [2,3] have concentrated on obtaining such information by observations at low pressures under conditions in which the products' nascent rotational and vibrational distributions are preserved. Such low pressures (where the reaction vessel dimensions are smaller than the mean free path of the products) do not allow a second aspect of the reaction to be studied, namely the bulk bimolecular rate constant, and this is normally obtained from separate studies at higher pressures.

Almost all of the information obtained from such studies is on atom plus stable molecule reactions, in particular for reactions of hydrogen or halogen atoms with hydrogen halide as the product. Discharges have been generally used to produce the atomic species [1,3,4] and the observations have been carried out by averaging the weak emission in a CW fashion. The alternative method of photolytic production of one of the reagents has been used with success by Sloan's group, formerly at NRC Ottawa [2], for reactions of $O(^1D)$ with a variety of molecules, the $O(^1D)$ being formed by photolysis of ozone. This group have also exploited the advantages of Fourier transform techniques in extracting information from the very weak signals in the infrared observed from rotationally and vibrationally nascent products, and more recently this technique has been applied to time resolved observations of nascent fragments from the uv photolysis of $CH_2 = CFC\ell$ by Leone et al. [5].

Atom plus radical reactions have been little studied because of the difficulties of producing sufficient concentrations of two unstable species in the low pressure fast flow systems employed. Even measurements of vibrational state populations for such reactions are rare: an example is in the O + CS reaction, for which vibrational populations were measured in the early 1970s [6] and whose rotational distribution is still unknown, (although, as described later in this report, progress has been made in our laboratory in determining the rotational populations in high vibrational levels.) During the grant period we have built and successfully operated a time resolved Fourier Transform Infrared

Spectrometer for the study of such reactions. We have identified emission from vibrationally excited HCℓ, HF, CO and CO_2 formed in a variety of photochemical and bimolecular collision processes, obtained kinetic information on the production and relaxation rates of these species, and explored the mechanisms of their formation from analyses of the nascent vibrational state distributions.

EXPERIMENTAL

Fig. 1.1 shows a block diagram of the essential features of the FTIR system. A commercial teaching Michelson Interferometer (Ealing UK Ltd.) was modified for use in the infrared by replacement of the glass optics by coated CaF_2 components. Detection of IR emission was accomplished by cooled InSb photoconductive detectors, allowing wavelengths up to ~ 8 μm to be detected (although for most experiments emission between 2–5 μm was selected by using appropriate filters). The interferometer path difference was controlled by fringe counting from a reference HeNe laser beam, thus eliminating non linearity in the (relatively crude) stepper motor drive to the movable mirror. Resolution of the instrument is controlled by the mirror path difference. Currently this is 1 cm^{-1} but can be extended: in the time resolved experiments reported here the path difference used was such as to give a resolution of $\gtrsim$ 4 cm^{-1}.

Operation of the instrument was as follows. The interferometer was set at a known path difference. Chemical reaction was initiated at time zero by laser photolysis of a suitable precursor molecule. The ir detector then observed a time resolved signal, generally rising to a maximum and falling with a slower rate, and an example is shown in Fig. 1.2. This time resolved output was digitised and stored: if averaging was required then this process was repeated for more laser shots in order to build up a suitable signal to noise ratio. Then the interferometer path difference was incremented, and the whole process repeated, thus building up a series of time resolved signals for each path difference, and typically ~ 2000 such signals were recorded. By examination of this data it can be seen that at each point in time we have 2000 points on an interferogram, and Fourier transformation of this interferogram yields an ir emission spectrum. Thus a complete two dimensional picture (time and wavelength) of the ir emission is built up.

The reactions are initiated at time t=0 by pulsed infrared multiple photon dissociation (IRMPD) of a suitable precursor molecule in the presence of the second (atomic) reagent, by means of a line tunable TEA CO_2 laser. The reactions studied so far are those of CF_2 and CHF radicals with oxygen atoms, and these were formed by IRMPD

of a low pressure (a few mTorr) of $CF_2HC\ell$ and CH_2F_2 respectively in a flow of excess O atoms (~ 20–30 mTorr) in ~ 5 Torr Ar (O atoms do not react with the precursor molecule to any appreciable extent). IRMPD has the advantage over most uv photolysis processes in that it produces radicals with low vibrational excitation [7] so that ground state reactions predominate in the subsequent kinetics. The pressures of Ar used are such that although rotational states are thermalised, vibrational state populations should be preserved at least at early times in the process, and thus information on nascent vibrational distributions should be extractable from the data.

Figure 1.3 gives an example of an inteferogram at 200 μs delay following the IRMPD of ~ 7 mTorr $CF_2HC\ell$ in 20 mTorr O atoms and 5 Torr Ar. No signal averaging was used here: 1 CO_2 laser shot was taken for each value mirror separation for a total of 2000 points at a resolution of 15 cm^{-1}. The lower part of the Figure shows the transformed spectrum at this delay between 1500 and 4500 cm^{-1}.

RESULTS AND DISCUSSION

(a) The O + CF_2 reaction

The O + CF_2 reaction has been proposed, from analyses of stable products in a flow system, to proceed in two stages [8]

$$O + CF_2 \longrightarrow FCO + F \qquad 1a$$

$$\longrightarrow CO + F_2(2F) \qquad 1b$$

$$O + FCO \longrightarrow CO_2 + F \qquad 2$$

with 1a predominating over 1b. The combined removal rate constant for CF_2 radicals, k(1a + 1b) has been measured in two laboratories (including our own) [8,9], as 1.8 x 10^{-11} cm^3 $molecule^{-1}$ s^{-1} at 298 K, with reaction 2 a factor of 5 faster than this [8].

Figure 1.4 shows spectra at 3 different times following reaction initiation in the presence of 20 mTorr O atoms. Three emission regions can be identified:

(i) a region ~ 2000 cm^{-1}, in which the emission rises and falls with time whilst exhibiting a shift to higher wavenumber

(ii) weak emission around 2900 cm^{-1} which falls rapidly with time

(iii) a strong and well structured emission near 3700 cm^{-1}, which rises more slowly than feature (i) and again shifts to higher wavenumber with time.

Figure 1.5 shows an expanded version of feature (ii), showing that it is vibrationally excited $HC\ell$ emitting in the (1–0) band. This feature is also present without oxygen present, and is clearly due to $HC\ell$ formed by the photolysis step

$$CF_2HC\ell \longrightarrow CF_2 + HC\ell$$

with some internal excitation observable in the product despite the predominance of low excitation energy in the fragments expected by IRMPD. Figure 1.6 shows that feature (iii) is from HF with some vibrational excitation (clearly visible as relaxing between 75 and 380 μs in Figure 1.4). HF is formed by F atom reaction with either $HC\ell$ or $CF_2HC\ell$, consistent with reactions 1 and 2 being the F atom source.

Figure 1.7 shows the 2000 cm^{-1} region in more detail, with the wavenumber ranges expected for emission from CO (reaction 1b, with F_2 formed as co–product) and CO_2 in the (0,0,n $\longrightarrow$ 0,0,n–1) transitions, CO_2 formed from reaction 2. Emission at long times is undoubtedly from CO_2(0,0,1), as experiments with a cell containing ground state CO_2 placed in the path of the beam eliminated this emission completely. In contrast, no effect was seen with a comparable CO filter. Although we need to carry out more experiments on this system to be sure of the conclusions, it appears that CO_2 is the main emitter, and that this is consistent with its production in reaction 2. Kinetic evidence supports this conclusion: the rising and falling rates are both linearly dependent upon the oxygen atom concentration and independent of precursor; the maximum signal is linearly dependent on precursor and independent of oxygen atoms. We suggest the mechanism

$$O + CF_2 \xrightarrow{k_1} FCO + F$$

$$O + FCO \xrightarrow{k_2} CO_2‡‡ + F$$

$$CO_2‡‡ + O \xrightarrow{k_3} CO_2‡ + O$$

with $k_2 > k_1 > k_3$, a reaction scheme which would predict the kinetic dependences observed above, and which agrees with known kinetic behaviour of CF_2 and FCO radicals in reactions with O atoms [8,9].

As is clear from this report, these data are preliminary, and have been obtained in the last few months of the grant period. We fully intend to explore the kinetics and dynamics of this system more thoroughly in work currently in progress.

(b) The O + CHF reaction

Infrared emission from CO, HF and $CO_2(001)$ has been seen in our limited studies in the O + CHF system. HF formed by IRMPD of the precursor CH_2F_2 is observed: in the presence of O atoms, additional HF signal, plus CO emission is seen, the CO(1–0) band being identified by its absorption with a cold CO gas filter. CO emission extends to shorter wavenumbers than in the O + CF_2 system (Fig. 1.7), right up to the InSb detector cut–off. The evidence points to the reaction sequence

$$O + CHF \longrightarrow CO^{\ddagger\ddagger} + HF^{\ddagger\ddagger}$$
$$CO^{\ddagger\ddagger} + O \longrightarrow CO^{\ddagger} + O$$
$$HF^{\ddagger\ddagger} + O \longrightarrow HF^{\ddagger} + O$$

producing vibrationally excited diatomics which undergo relaxation with O atom collisions. As yet the vibrational distribution in this system is unknown, but a measure of the total removal of IR emission caused by insertion of a cold CO filter gives an indication of the percentage of CO(v=1) present in the system: the results are consistent with the observations of Hsu et al. [10] that CO is formed with a distribution of energies that can be adequately described by statistical partitioning in the HFCO excited adduct.

CO_2 appears to be formed by the reaction

$$O_2 + CO^{\ddagger\ddagger} \longrightarrow CO_2 + O$$

where $CO^{\ddagger\ddagger}$ is vibrationally excited. This step has already been invoked to explain the quenching of highly vibrationally excited CO (with enough energy to cross to the A $^1\Pi$ state) by O_2 in studies of the vuv emission accompanying the O + CHF reaction [11].

(c) Future reactions

The successful operation of the FTIR instrument has opened up a huge range of potential reactions. Table 1.1 lists some of these, together with available kinetic information. The N + NCO reaction is already under investigation in our laboratory by separate LIF experiments, and shortly ir emission from $CO^{\ddagger}$ will be investigated.

TABLE 1.1

Possible reactions for study involving halocarbene, CN and NCO radicals producing potential IR emitting products

	$\Delta H^{\ominus}_{298}$/kJ mol^{-1}	k^{298}/cm^3 molecule^{-1}s^{-1}
(i) Reactions with O and N atoms		
$O + CF_2 \longrightarrow CO + F_2(2F)$	–178(–25)	(a) 1.8×10^{-11}
$\longrightarrow FCO + F$	–159	
$O + CHF \longrightarrow CO + HF$	–795	(a) 1.5×10^{-10}
$\longrightarrow CO + H + F$	–231	
$\longrightarrow$ other products		
$N + CHF \longrightarrow CN + HF$	–476	(b) 2.5×10^{-10}
$\longrightarrow HCN + F$	–422	
$O + CC\ell_2 \longrightarrow CO + C\ell_2$	–598	(c) –
$O + CFC\ell \longrightarrow CO + FC\ell$	–439	(c) 2.9×10^{-12}
$\longrightarrow FCO + C\ell$	–330	
$O + CN \longrightarrow CO + N(^4S)$	–309	(d) 2.1×10^{-11}
$\longrightarrow CO + N(^2D)$	– 78	
$O + NCO \longrightarrow NO + CO$	–422	(c) –
$\longrightarrow N + CO_2$	–324	
$N + NCO \longrightarrow N_2 + CO$	–737	(c) –
(ii) Other reactions of interest		
$NO + NCO \longrightarrow N_2 + CO_2$	–638	(a) 3.4×10^{-11}
$\longrightarrow N_2O + CO$	–273	
$O + CHF \longrightarrow NCO + HF$	–370	(e) 7.0×10^{-12}
$O_2 + CN \longrightarrow NCO + O$	– 31	(f) 2.2×10^{-11}
$\longrightarrow CO + NO$	–461	
$CN + HI \longrightarrow HCN + I$	–208	(g) 6.6×10^{-11}
$CN + NH_3 \longrightarrow HCN + NH_2$	– 77	2.8×10^{-11}

NOTES

(a) See main text.

(b) CN(A–X) and (B–X) emission seen, and deduced to be from initially formed CN(X,v′) undergoing rapid internal conversion in collisions with N atoms.

(c) No product channels known.

(d) Branching ratio 80% to form N^2D; CO(v) distribution observed, via laser absorption, to be bimodal.

(e) Vibrationally excited NCO has been inferred from the temporal behaviour of the radical observed by LIF.

(f) NCO is the major product.

(g) For CN reactions with hydrogen halides, the reaction with HI is the fastest and most exothermic.

REFERENCES

[1] J.C. Polyanyi and P.E. Charters, Disc. Far. Soc. **33**, 107 (1962).

[2] J.E. Butler, R.G. McDonald, D.J. Donaldson and J.J. Sloan, Chem. Phys. Lett. **95**, 183 (1983).

[3] P.M. Aker, D.J. Donaldson and J.J. Sloan, J. Phys. Chem. **90**, 3110 (1986).

[4] D.J. Bogan, D.W. Setser and J.P. Sung, J. Phys. Chem. **81**, 888 (1977), **81**, 898 (1977); B.S. Agrawalla, A.S. Manocha and D.W. Setser, J. Phys. Chem. **85**, 2873 (1981); D. Klenerman and I.W.M. Smith, JCS Far. Trans. II **83**, 229 (1987).

[5] T.R. Fletcher and S.R. Leone, J. Chem. Phys. **88**, 4720 (1988).

[6] G. Hancock, B.A. Ridley and I.W. M. Smith, JCS Far. Trans. II **68**, 2117 (1972).

[7] D.E. Heard, Part II Thesis, Oxford University (1986).

[8] I.C. Plumb and K.R. Ryan, Plasma Chem. Plasma Process **4**, 271 (1984).

[9] G. Hancock, P.D. Harrison and A.J. MacRobert, JCS Far. Trans. II **82**, 647 (1986).

[10] D.S.Y. Hsu, R.G. Shortridge and M.C. Lin, Chem. Phys. **38**, 285 (1978).

[11] C.J. Astbury, Part II Thesis, Oxford University (1985).

FIGURE CAPTIONS

Figure 1.1 Block diagram of the Michelson interferometer used for Fourier Transform Infrared Emission studies of atom plus radical reactions.

Figure 1.2 Time resolved behaviour of the full infrared emission ($1800 - 4500\ cm^{-1}$) observed following the initiation of the reaction sequence between oxygen atoms and CF_2 radicals by infrared multiple photon dissociation of CF_2HCl precursor. The behaviour shown is for one specific position of the movable mirror, and hence represents a convolution of all the observed frequencies of emission with their separate time profiles.

Figure 1.3 Interferogram recorded from the $O + CF_2$ reaction sequence at 200 μs delay under conditions given in the text. One laser pulse per mirror separation was used: 2000 points in total were taken (giving a resolution of $15\ cm^{-1}$). The lower trace shows the resultant spectrum obtained from a Fourier transform of the interferogram. Features at high and low wavenumber are ascribed to HF and CO_2 respectively.

Figure 1.4 Spectra observed at three different times in the $O + CF_2$ reaction sequence, showing the three different emitting species observed and their behaviour as a function of time.

Figure 1.5 Emission near $2900\ cm^{-1}$ following IRMPD of $CF_2HC\ell$ in the presence of O atoms. The feature is compared with a simulated $HC\ell$ (1–0) spectrum (lower trace), and is due to $HC\ell$ formed directly in the photodissociation step with some internal excitation.

Figure 1.6 Emission near 3700 cm^{-1} following initiation of the O + CF_2 reaction. The features are identified as those of HF in v=3,2,1, with the species arising from reactions of F atoms either with HCℓ or with $CF_2HC\ell$ precursor. This observation confirms the presence of F atoms from the chemical reactions in the system.

Figure 1.7 Emission near 2000 cm^{-1} in the O + CF_2 reaction at three different times. Emission at long times (after relaxation by O atoms) is from CO_2 (001). At early times potential emitters are CO, CO_2 and FCO, with the regions expected for the emission marked on the Figure. Our present experimental data point to CO_2, formed in the O + FCO reaction, as the most likely candidate.

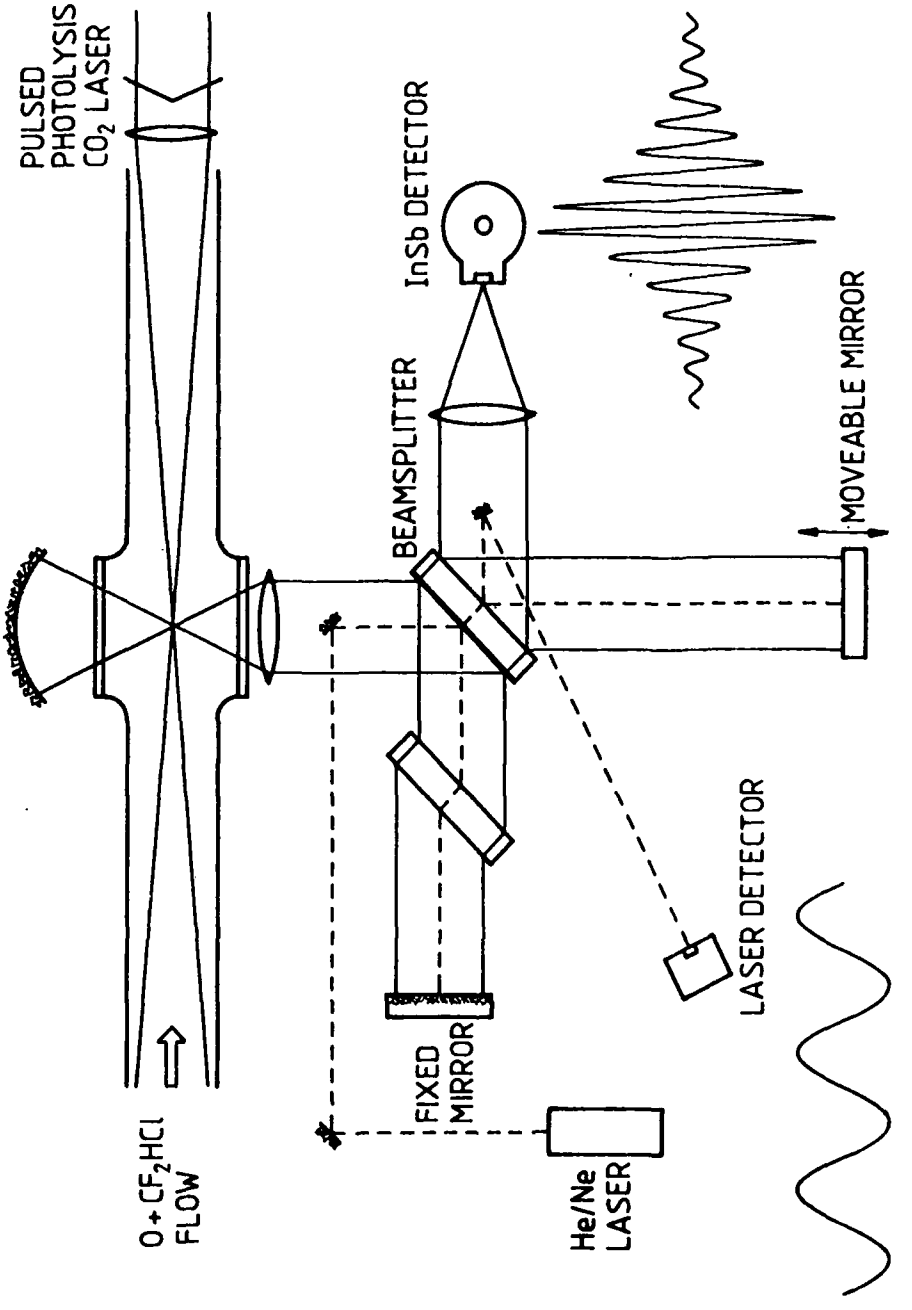
PULSED PHOTOLYSIS CO_2 LASER
InSb DETECTOR
BEAMSPLITTER
MOVEABLE MIRROR
LASER DETECTOR
FIXED MIRROR
He/Ne LASER
O + CF_2HCl FLOW

Fig 1.1

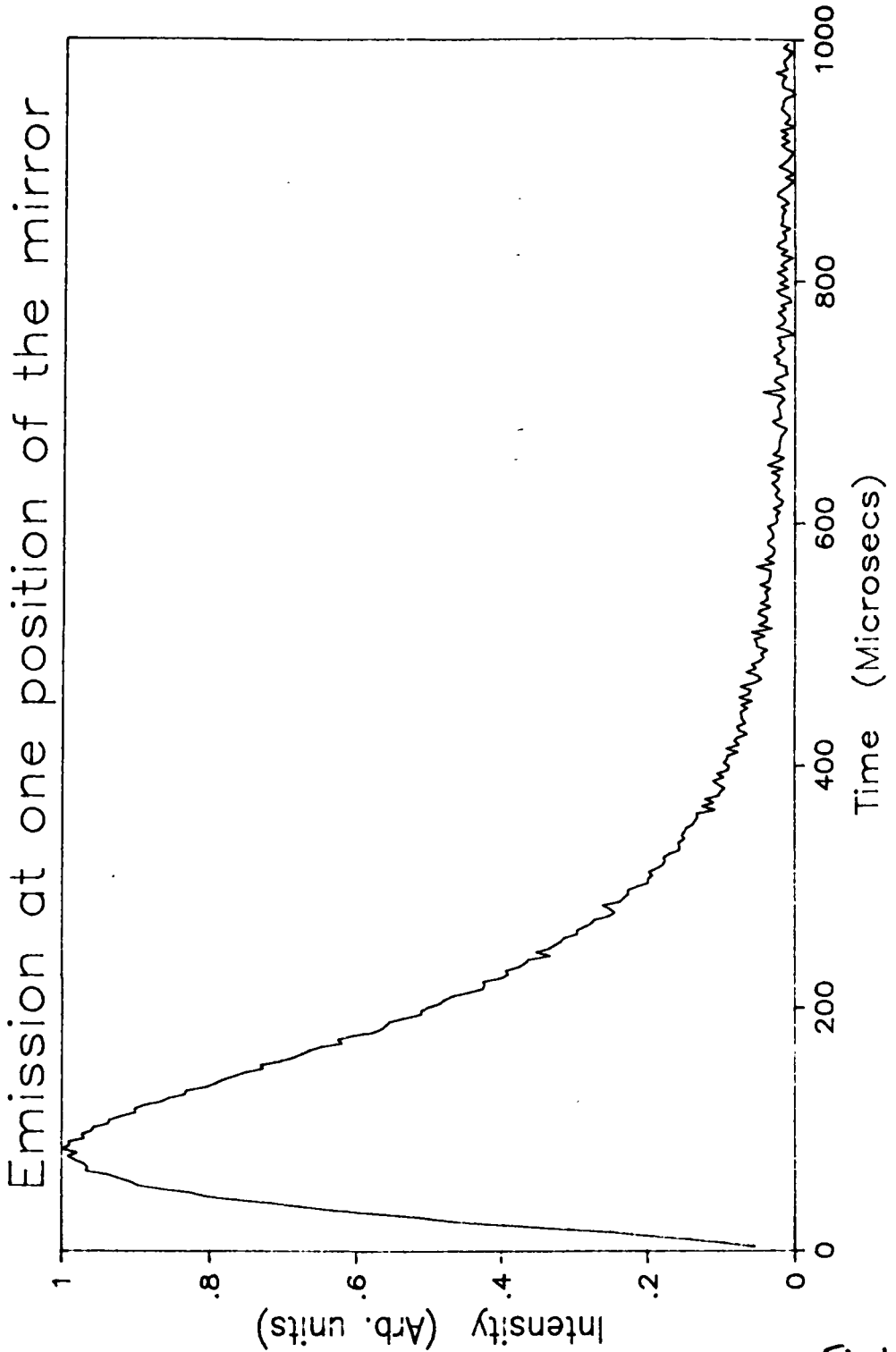
Emission at one position of the mirror
Intensity (Arb. units)
0
.2
.4
.6
.8
1
0
200
400
600
800
1000
Time (Microsecs)

Fig 1.2

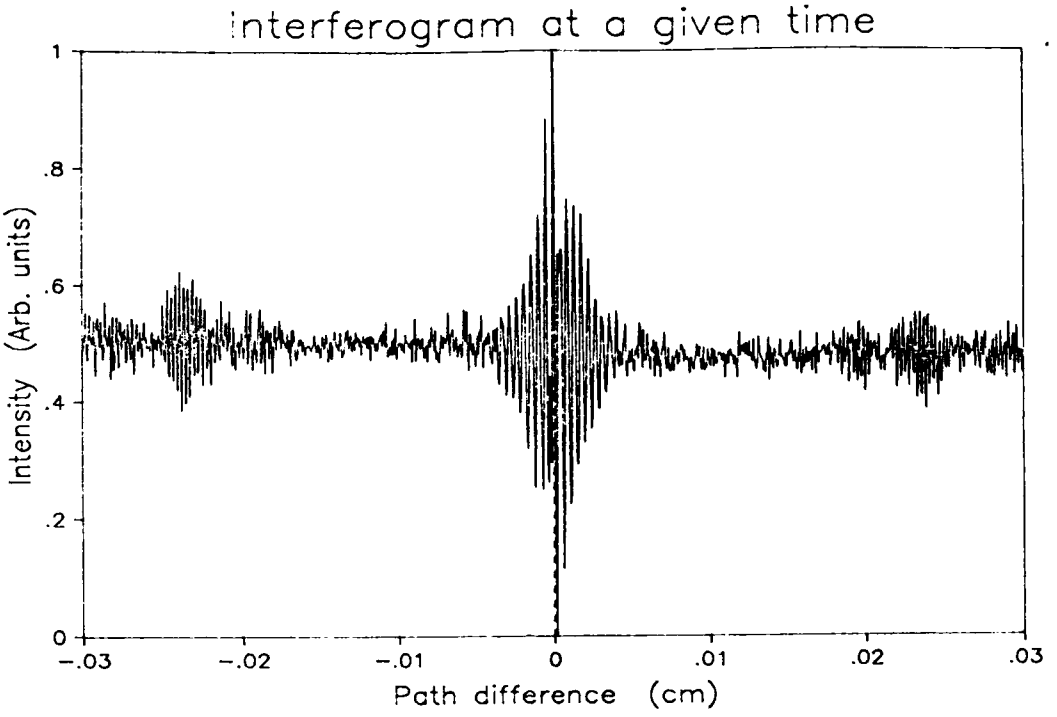
Interferogram at a given time
Intensity (Arb. units)
1
.8
.6
.4
.2
0
−.03
−.02
−.01
0
.01
.02
.03
Path difference (cm)

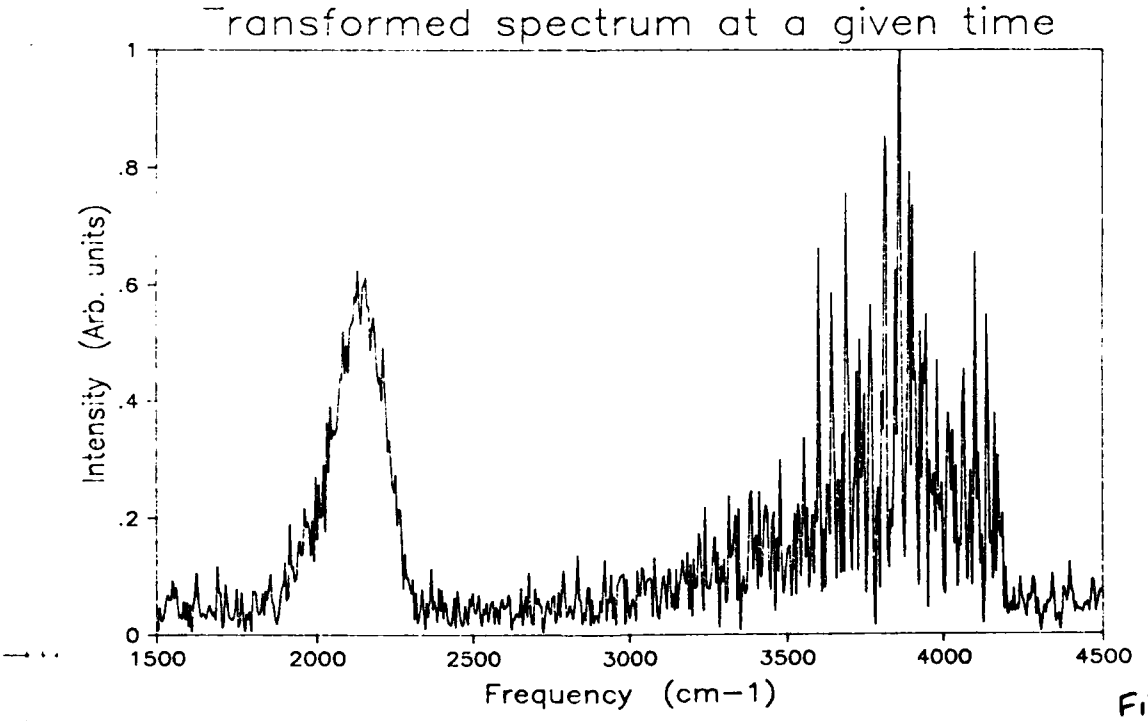
Transformed spectrum at a given time
Intensity (Arb. units)
1
.8
.6
.4
.2
0
1500
2000
2500
3000
3500
4000
4500
Frequency (cm−1)

Fig 1.3.

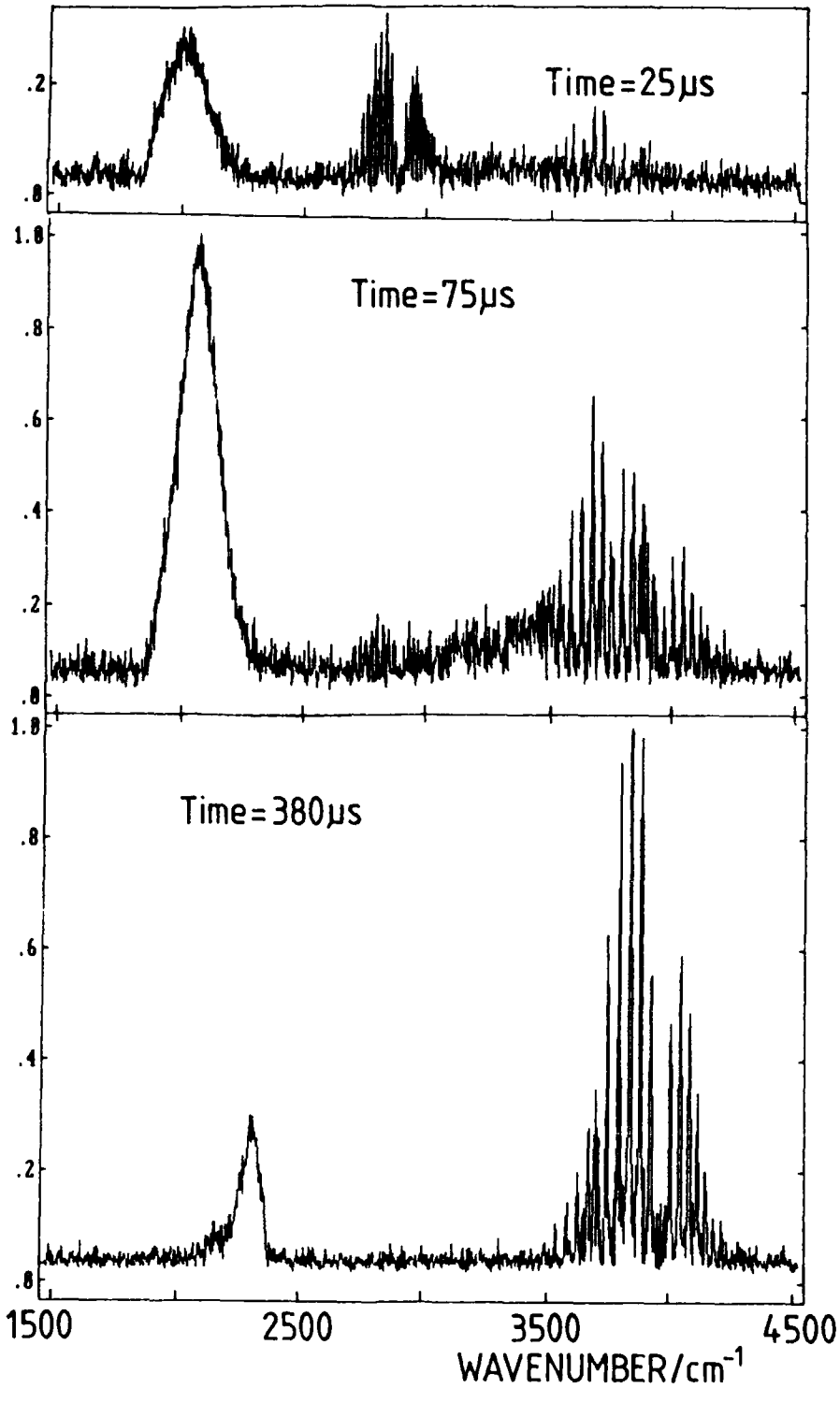
Time=25μs
Time=75μs
Time=380μs
.2
.8
1.0
.6
.4
1500
2500
3500
4500
WAVENUMBER/cm^{-1}

Fig 1.4

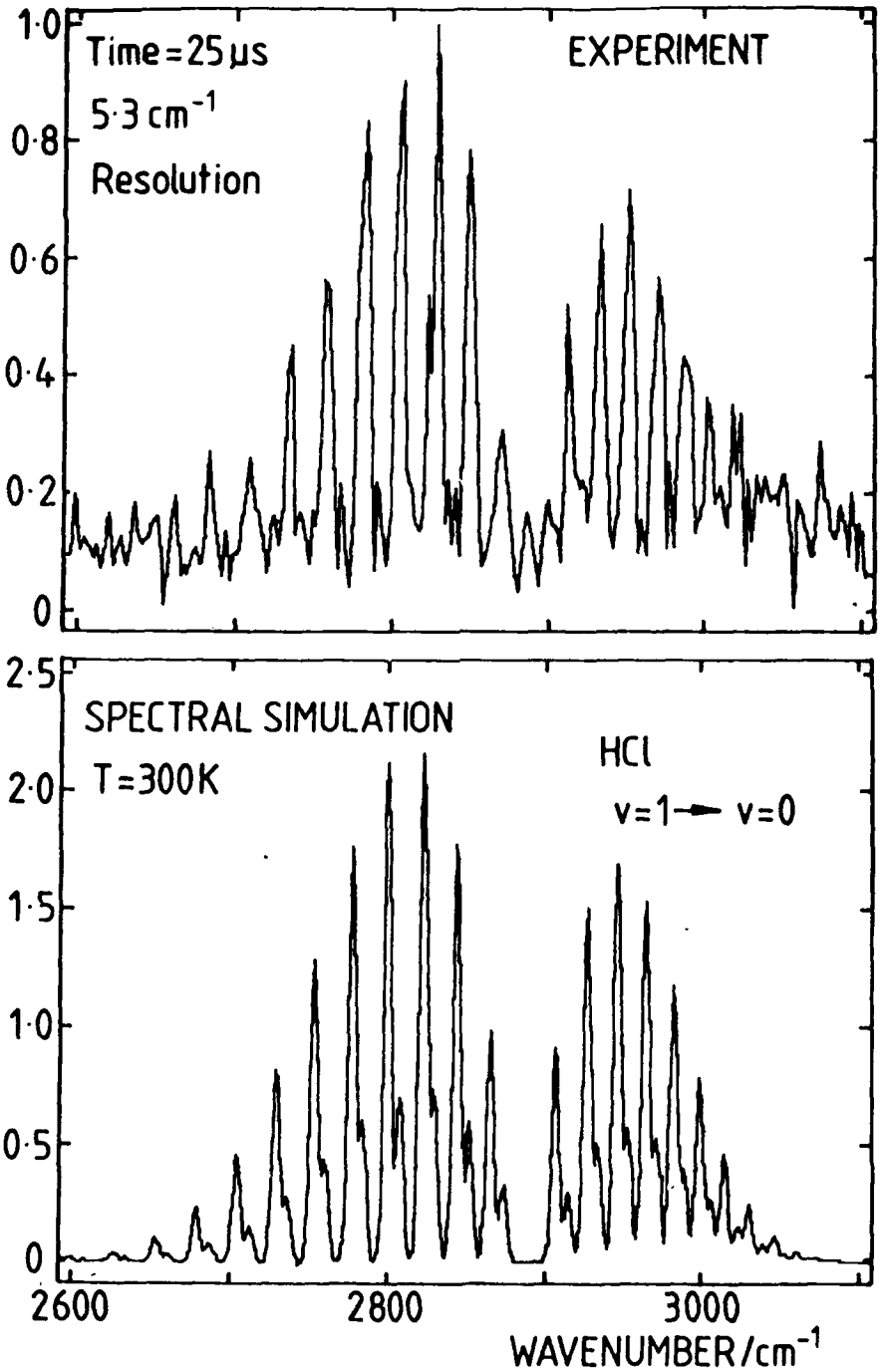
Time = 25 μs
5·3 cm⁻¹
Resolution
EXPERIMENT
1·0
0·8
0·6
0·4
0·2
0
SPECTRAL SIMULATION
T = 300K
HCl
v=1 → v=0
2·5
2·0
1·5
1·0
0·5
0
2600
2800
3000
WAVENUMBER/cm⁻¹

Fig 1.5

Figure 3

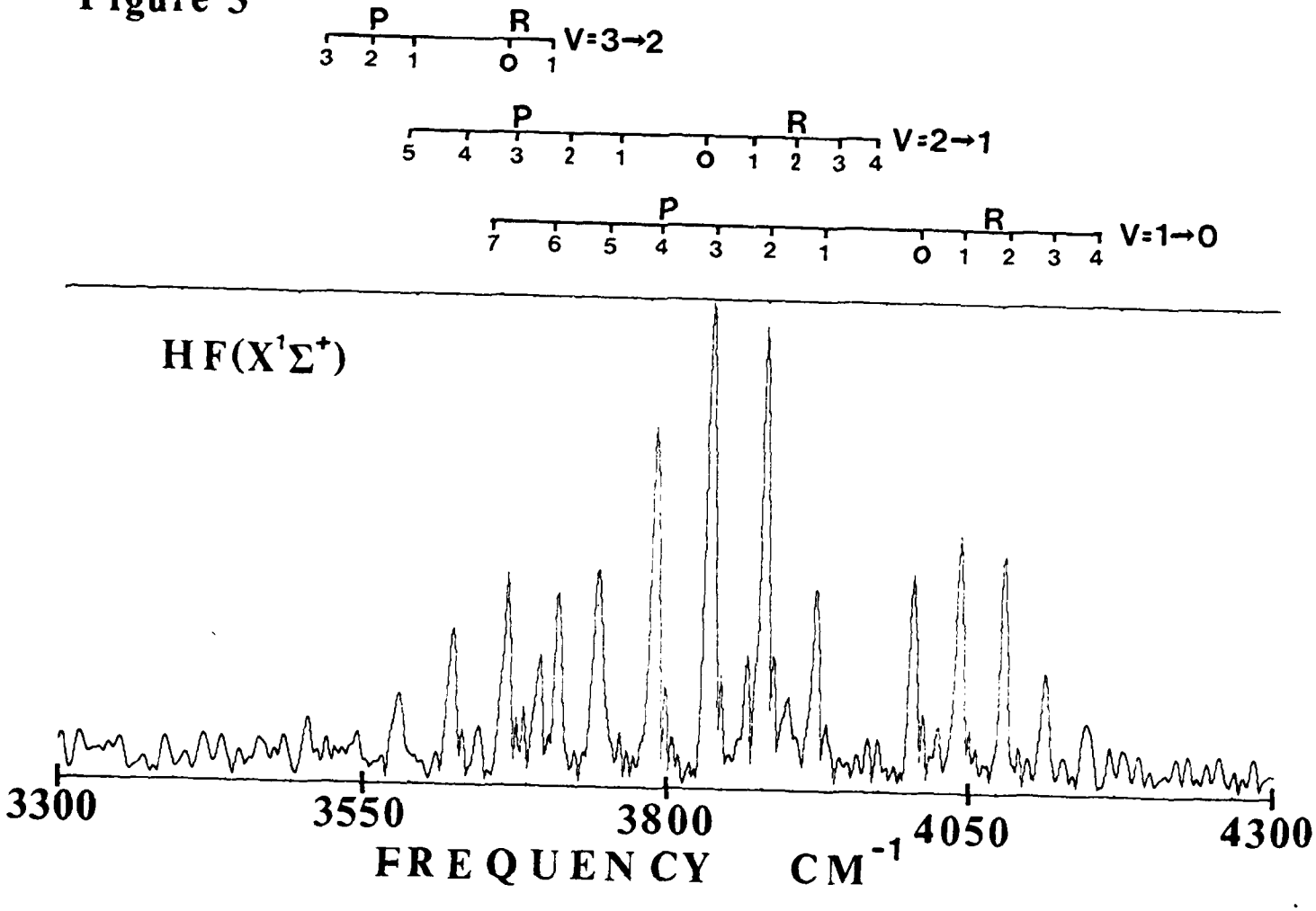

Fig 1.6

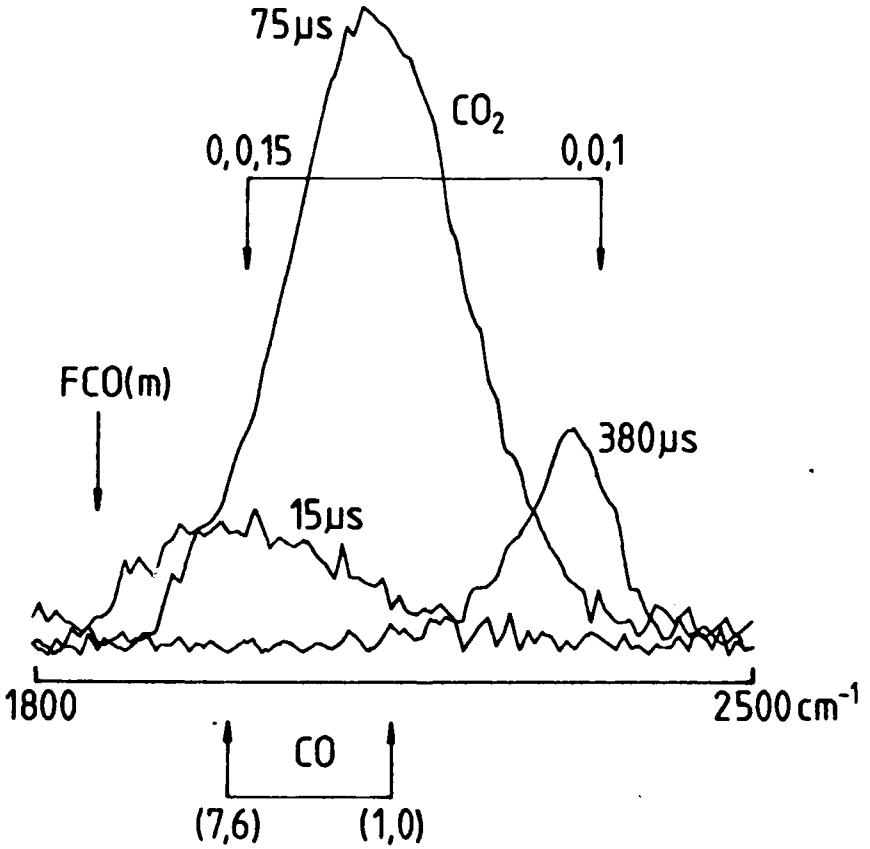
75µs
CO_2
0,0,15
0,0,1
FCO(m)
380µs
15µs
1800
2500 cm^{-1}
CO
(7,6)
(1,0)

2. The Two Photon Dissociation of H_2O and D_2O at 266 nm

INTRODUCTION

The energy required to produce electronically excited OH or OD($A^2\Sigma^+$) radicals from the photolysis of H_2O or D_2O corresponds to the absorption of a single photon of wavelength $\lesssim$ 137 nm. The absorption spectrum of H_2O below this wavelength consists of a diffusely structured band peaking at around 130 nm, and assigned to a $\tilde{B}^1A_1 \leftarrow \tilde{X}^1A_1$ transition which, at lower wavelengths is overlapped by sharp bands associated with Rydberg transitions [1], and the dissociation dynamics in this region have been extensively studied, largely through measurements of the OH and OD($A^2\Sigma^+$) internal state distributions [2–6] and alignments [5–8]. Although the $\tilde{B}$ state correlates adiabatically with the $A^2\Sigma^+$ state of the diatomic fragment, the quantum yield for production of the excited species is low ($\lesssim$ 10%) [3,9], with the majority of dissociating molecules crossing to the H_2O (D_2O) $\tilde{A}^1B_1$ or $\tilde{X}^1A_1$, states, and forming ground state OH or OD($X^2\Pi$) [10]. Recently this channel has been explored for the first time through measurements of the photofragment spectroscopy of the H atom following photodissociation at ~ 125 nm [11].

Both OH($A^2\Sigma^+$) and ($X^2\Pi$) state fragments produced from photolysis via the $\tilde{B}$ state show a high degree of rotational excitation, with this being particularly marked for photolysis at wavelengths shorter than the $\tilde{B}$ state maximum absorption [2–6,11]. The development of potential energy surfaces for the $\tilde{B}$, $\tilde{A}$ and $\tilde{X}$ states [12–14] has stimulated trajectory calculations [15–17], leading to predicted energy distributions in the OH $A^2\Sigma^+$ and $X^2\Pi$ states. Particularly impressive agreement has been found between theory [17] and experiment [5,11] for excitation near 125 nm, where approximately 1 eV of energy is available for partitioning in the products, and where rotational distributions peak close to the maximum allowed by energy conservation. At wavelengths above 130 nm (where only one experimental study of rotationally resolved fragment distributions has been reported [5]), calculations for dissociation on the $\tilde{B}$ state surface have shown that trajectories are either direct or can undergo at least one vibration within the deep $\tilde{B}$ surface well [15,18]. The influence of these so called trapped [15] or indirect [18] trajectories on the diffuse structure of the $\tilde{B}$ state absorption spectrum [18] and on the OH($A^2\Sigma^+$) rotational energy distribution [15] has been calculated, with the latter study showing a marked effect of the

form of the distribution on the precise region of the surface accessed by absorption (and thus on the photodissociation wavelength) [15].

This report describes the rotational energy distributions and alignments in OH and OD($A^2\Sigma^+$) produced by the two photon dissociation of H_2O and D_2O at 266 nm. Its motivation was twofold: first to test whether the distribution resembled the one photon case near this dissociation energy (the nearest such study being at 130.4 nm [5]) or whether the distribution was 'cooler' because of a trapped trajectory (predicted to occur near 133 nm [15]), and secondly to see if the energy distribution or the alignment gave any indication of the involvement of a state other than $\tilde{B}^1A_1$ in the two photon absorption step. A state of $^1A_2$ symmetry has long been predicted to exist in this energy region [13,19] and suggestions have been made about its influence on the H_2O electron impact [20,21] and multiple photon ionisation [22] spectra and on the OH($A^2\Sigma^+$) fluorescence polarization [7] and rotational energy distributions [4]. No direct evidence for this $^1A_2$ state has been found, although the other two components arising from the promotion of an electron in the ground state $1b_1$ orbital to a 3p orbital (the $\tilde{D}^1A_1$ and $\tilde{C}^1B_1$ states corresponding to the $3pb_1$ and a_1 components respectively) are known [1,22], and a state of A_2 symmetry at higher energies, assigned as a $3db_2 \leftarrow 1b_1$ transition has been identified [22]. Single photon absorption from the ground $^1A_1$ state to a $^1A_2$ state is forbidden, but it can be accessed (as can the $\tilde{B}^1A_1$ state) by two photon excitation, and in principle it might be expected that the influence of this state would be revealed by differences in the $A^2\Sigma^+$ rotational state distributions and alignments between one and two photon excitation. For dissociation energies corresponding to single photon absorption near 124 nm, alignment studies have shown that the $^1A_2$ state is not involved, the $\tilde{B}$ state being the principal carrier of the two photon continuum in this region [6]. Our results show a rotational distribution very similar (when scaled to the fractional energy appearing in rotation) to the single photon case at 130.4 nm [5]. The OH A–X polarization data however show that the alignment is considerably lower than that observed in the 1 photon case [5,8].

EXPERIMENTAL

Gas phase H_2O and D_2O were photolysed in a stainless steel chamber using the frequency quadrupled output of a Nd^{3+} YAG laser (J.K. Lasers 2000 L). The linearly polarised laser output (~ 40 mJ $pulse^{-1}$) was focussed into the vessel with a 20 cm focal length spectrosil lens, and the fluorescence output detected at right angles to both the laser

beams propagation axis and its electric vector via a monochromator (Spex 1870 C) fitted with a cooled EMI 9816 QKB photomultiplier. For the measurements of wavelength resolved emission the fluorescence was passed into the monochromator with no deliberate selection of the polarisation vector. For the polarisation measurements, the monochromator was set at a fixed wavelength and the fluorescence intensities parallel ($I_{\parallel}$) and perpendicular ($I_{\perp}$) to the photolysis beam's electric vector were selected by the use of uv transparent polarising film.

The detection system in these experiments is polarisation sensitive (due to the monochromator grating), and thus the observed signals needed to be corrected for this. A series of calibration experiments was carried out using either a quartz halogen lamp or an RF excited plasma to generate emission in the 308–310 nm range polarised in such a way as to correspond to either $I_{\parallel}$ or $I_{\perp}$, and measurements were made of the relative system response as a function of wavelength. Care was taken to ensure that equal intensities were emitted from the calibration sources at the two orientations.

Experiments were carried out at H_2O and D_2O pressures up to 250 mTorr. Under these conditions any effect of collisional scrambling of either the upper state OH population or its polarisation is negligible [5] due to the very rapid electronic quenching of $OH(A^2\Sigma^+)$. The monochromator was operated typically with 100 μm slit width, giving a resolution of $\sim$ 0.1 nm at 300 nm. The voltage output from the detection system was digitised, corrected for variations in the laser intensity, and summed for a preset number of shots at each wavelength setting.

RESULTS AND DISCUSSION

For H_2O, Figure 2.1 shows the fluorescence spectrum in the region 306–314 nm, with features clearly identified as arising from the formation of $OH(A^2\Sigma^+)$ with values of N' between 0 and 10. The signal was found to vary with the square of the laser power (and this dependence was used in the normalisation of the signal for fluctuations in the laser intensity), and the rotational levels populated are consistent with those expected for the 2 photon dissociation of H_2O at 266 nm. The available energy from this process for partitioning into the H + $OH(A^2\Sigma^+)$ fragments is 1503 cm^{-1} if internal energy in H_2O is neglected, and this is enough to populate $N'_{MAX} = 9$ in OH $A^2\Sigma^+$: the small population observed in $N' = 10$ is presumably the result of a contribution from internally excited H_2O molecules.

Fluorescence from electronically excited species generated by photolysis is expected to be polarized, and the degree of polarisation can be a sensitive function of the level excited and of the branch observed [23]. Extraction of populations from such fluorescence spectra thus need to take polarisation into account, particularly (as in the present case) if the detection system is polarisation sensitive. Separate measurements on the degree of polarisation on isolated features of the spectrum shown in Fig. 2.1 (see later) indicate that the polarisation index R_ϵ (defined as $(I_{/\!/} - I_\perp)/(I_{/\!/} + 2I_\perp)$ where $I_{/\!/}$ and $I_\perp$ are the intensities of emission parallel and perpendicular to $\underline{\epsilon}$, the electric vector of the photolysis beam) is close to zero for all wavelengths studied, and that such corrections were unnecessary. Populations in the F_1 and F_2 components of the N′ levels were extracted by measuring the intensities of isolated features in spectra such as that of Fig. 2.1 (at higher resolution where necessary). In some cases peak intensities were due to emission from a single upper level (for example, for the high P_{11} lines at long wavelengths). For peaks which consisted of overlapped lines (either from satellite branches at the same value of N′ but different J′, or from sets of lines at different N′) peak intensities were expressed as sums of contributions from different levels, and resultant sets of simultaneous equations were solved for the upper state populations. In all cases intensities were related to populations by using the Einstein A coefficients of Chidsey and Crosley [24]. Table 2.1 shows the populations derived for separate F_1 and F_2 components. Spectral simulations carried out with these values were indistinguishable, within the accuracy of the experimental data, from those in which both components were set at the average of those in Table 2.1, and these average values are shown in Figure 2.2 as a plot of relative population versus N'/N'_{MAX}, with $N'_{MAX} = 9$. Figure 2.1 shows a simulation carried out using these values (with populations for the undetermined N′ = 0 and 2 levels interpolated from the data of Fig. 2) showing excellent agreement with the experimental data.

Fig. 2.3 shows the fluorescence spectrum obtained from $OD(A^2\Sigma^+)$. As the line spacing for the heavier species is less than that for OH, the weakness of the fluorescence signal precluded measurements on isolated features in order to obtain the rotational level populations. Simulations were thus carried out to fit the experimental data by successively refining the populations. The results showed that the OH and OD populations, when scaled to the N'_{MAX} value in each case (9 for OH, 8 for OD) were very similar in overall shape, showing a peaking close to the maximum allowed by energy conservation, but with a pronounced portion of the rotational distribution in low N′ levels, in contrast to the almost complete absence of low N′ population in photolyses at considerably higher energies [5,6].

Figure 2.2 also shows that the population distribution obtained from the one

photon dissociation of H_2O at 130.4 nm by [illegible]-workers [5], when scaled to the same N'_{MAX} value, is very similar to that o[illegible]udy, apart from a rather higher population observed at low N′ values (0 – 2) in the la[illegible]ter case. Both distributions peak at ~ 75% of the maximum value, somewhat less than the very high rotational energies seen at lower photolysis wavelengths [2,3,5,6]. If the difference in excitation energies in the two cases is neglected, then at first sight this result would be consistent with the same dissociation dynamics for one and two photon excitation, i.e. both initially populating the $\tilde{B}^1A_1$ state from which $A^2\Sigma^+$ OH fragments are formed. However, marked differences in the fragment fluorescence polarisation are seen in the two cases. Single photon excitation of H_2O to produce $OH(A^2\Sigma^+)$ via a state of $^1A_1$ symmetry can produce a limiting value of –0.4 for $A_0^{(2)}$, the quadrupole moment of the J′ vectors of OH relative to $\underline{\epsilon}$, which is directly related to the experimentally measured R_ϵ [5,23]. Simons et al. found $A_0^{(2)}$ to be a function of N′, decreasing from –0.1 at low N′ to a minimum of –0.35 at N'_{MAX}, close to the limiting value [5]. The lower alignment at low N′ was attributed to H_2O molecules with trapped trajectories on the $\tilde{B}$ state surface (as predicted by Segev and Shapiro [15]) and thus with relatively long lifetimes, reducing the $A_0^{(2)}$ value. Two photon excitation to the $\tilde{B}^1A_1$ state would predict a limiting value for $A_0^{(2)}$ of +1.14 [25] if the intermediate (virtual) state were of $^1B_1$ symmetry, and this has been suggested to be the case for two photon excitation to the continuum at energies corresponding to a single photon absorption near 124 nm, with the $\tilde{A}^1B_1$ state making the major contribution to the transition moment as an intermediate [6]. Excitation to a $^1A_2$ state was eliminated as a possibility in this study [6], as the maximum value of $A_0^{(2)}$ experimentally found, 0.6 at high N′, was larger than the limiting value of 0.29 expected for $^1A_2 \leftarrow \tilde{X}^1A_1$ excitation with two photons [25]. Our preliminary polarisation results, although not yet fully analysed, are summarised in Table 2.2. Values of $I_\perp/I_\parallel$ all cluster around 0.9, irrespective of the wavelength and thus of the rotational quantum number N′ probed, and application of the standard formulae for converting these ratios to values of $A_0^{(2)}$ [5] result in alignment parameters which themselves cluster around an average value of zero. It should be pointed out that the fluctuations around zero shown by the data of Table 2.2 are physically unreasonable: P or R branch lines from OH should be polarised oppositely from Q branch lines [5], i.e. if $I_\perp/I_\parallel$ < 1 for p,R lines, it should be > 1 for Q branches. Thus a constant ratio of 0.9 implies that there is an experimental fault, and the most obvious is that the correction made to the original data for the polarisation sensitivity of the monochromator is incorrect by 10%, that the true value of $I_\perp/I_\parallel$ is close to unity and hence that $A_0^{(2)}$ is close to zero. This

result, although lying closer to the $^1A_2$ limiting value that the $^1A_1$, is unable to distinguish between the two, as lifetime lengthening could be invoked in either case to bring the predicted values into the experimental range (in contrast to the clear distinction possible following excitation near 124 nm [6]).

We make the following points:

(i) If excitation is to the $\tilde{B}^1A_1$ state, then a mechanism is needed to reduce the anisotropy (i.e. to make $A_0^{(2)}$ closer to zero) from values seen, at high N′ following single photon dissociation at 130.4 nm. Long lived trajectories have been suggested to reduce the anisotropy at low N′ values in the single photon case [5], but are calculated to lead to high populations in low N′ levels (if predissociation of the $\tilde{B}$ state is neglected): Figure 2.2 shows the predicted distribution at 133.7 nm where such trajectories lead to a resonance [15], which is clearly different from the present results (although it should be pointed out that two photon excitation at 266 nm corresponds to absorption on the shoulder of this predicted resonance, where a higher rotational excitation would occur). Predissociation of the $\tilde{B}$ state has been suggested to explain the lack of low N′ population generally observed in the $OH(A^2\Sigma^+)$ state [5,26], as longer lived trajectories which lead to low N′ values have a higher probability of crossing from the $\tilde{B}$ state to, for example, the $\tilde{A}^1A_1$ state to form ground state products [26]. However, the present results would require $\tilde{B}$ state H_2O molecules leading to high N′ fragments to be longer lived than those following 130.4 nm excitation: long lived behaviour is predicted to be more important as the excitation energy decreases [18], but whether this is sufficient to explain the present behaviour is unclear.

(ii) If excitation is to the $^1A_2$ state, then less reduction in the anisotropy is required, but a crossing to the $\tilde{B}^1A_1$ surface is needed for OH $A^2\Sigma^+$ fragments to form (the $^1A_2$ state does not correlate adiabatically with OH $(A^2\Sigma^+)$ [28]). A crossing at large HO – H distances between the $\tilde{B}^1A_1$ and $^1A_2$ states (which now become $^1A'$ and $^1A''$ in C_s symmetry) has been predicted [27].

(iii) An alignment factor close to zero could occur by fortuitous cancelling of alignments of different sign in the two photon absorption to the $\tilde{B}^1A_1$ state, the differences caused by differing intermediate state symmetries. This could occur for the sequences $^1A_1 \longleftarrow (^1A_1 \text{ or } ^1B_2) \longleftarrow {}^1A_1$ and $^1A_1 \longleftarrow (^1B_1) \longleftarrow {}^1A_1$ which yield limiting $A_0^{(2)}$ values

of –0.57 and +1.14 respectively [25]. The former would thus need to dominate (presumably via the $\tilde{X}^1A_1$ ground state as intermediate), in contrast to two photon excitation near 124 nm, where the predominant intermediate state is clearly $\tilde{A}^1B_1$ [6].

(iv) The similarity between the H_2O and D_2O distributions is a result which has also been found for single photon photolyses at shorter wavelengths [5]. It suggests that the observations are characteristic of dissociation where relatively little energy is available for partitioning into rotation in the electronically excited product, and are not due to chance overlap with a "resonance" [15] in the absorption spectrum.

FURTHER EXPERIMENTAL STUDIES ON H_2O AND D_2O

During the grant period two further types of study were carried out. In one of these, attempts were made to observe the ground electronic state (and thus predominant) OH product by laser induced fluorescence (LIF), using two photon dissociation at 266 nm followed by single photon LIF of the $A^2\Sigma^+ - X^2\Pi$ transition in OH near 308 nm. LIF signals were detected, but from their pressure dependence it was clear that the levels observed (relatively low J'' in $v''=0$) were being formed by collisional relaxation of higher quantum states, and were <u>not</u> produced directly in the two photon process. This result is entirely in accord with observations of Krautwald et al. [11] on the ground state channel by time–of–flight spectroscopy of the H atom. Only very high rotational levels of OH($v''=0$) were seen; these levels cannot be directly observed by LIF due to rapid predissociation of the $A^2\Pi$ quantum states to which optical transitions from such high J'' states are allowed.

In a second experiment, the identity of ions produced in the 266 nm irradiation of H_2O and D_2O were studied. A small time–of–flight mass spectrometer was built, calibrated (by REMPI of NO) and used to analyse the products of low pressure (10^{-5} Torr) photolysis. H_2O^+ (and D_2O^+) were the major products, with some evidence of a low intensity channel to form H^+. The very large ion signals that are observed when 266 nm radiation is focussed into H_2O and D_2O is consistent with the dissociation step to H + OH(A and X) being a relatively minor channel, and that further up–pumping to ions may dominate.

PUBLICATIONS

One publication from this work [28] accompanies this report; a second (on the dissociation of D_2O) has been submitted to Chemical Physics Letters, and a third, on the detailed analysis of the polarisation and LIF experiments, is in preparation.

TABLE 2.1

N′	Populations	
	F_1	F_2
1	0.53	0.57
2	–	–
3	–	0.65
4	0.89	0.72
5	0.83	0.86
6	1.00	0.80
7	0.87	0.95
8	0.69	0.60
9	0.70	0.76
10	0.36	0.38

Relative populations in the F_1 and F_2 components of $OH(A^2\Sigma^+, N')$ produced by the two photon dissociation of H_2O at 266 nm.

TABLE 2.2

Wavelength/nm	Feature	$I_\perp/I_\parallel$	$A_0^{(2)}$
306.2	R_{11}(head)	0.89 ± .07	− .23 ± .16
309.3	$Q_{11}(8) + Q_{22}(6)$	0.88 ± .13	+ 10 ± .12
312.7	$P_{11}(9) + P_{22}(8)$	0.92 ± .10	− .17 ± .23
311.7	$P_{11}(7) + P_{22}(6)$	0.87 ± .08	− .36 ± .24
308.6	$Q_{11}(5)$	0.95 ± .12	+ .05 ± .11

Polarisation data for the $OH(A^2\Sigma^+)$ fragment from 266 nm two photon dissociation of H_2O. $I_\perp/I_\parallel$ values are converted to $A_0^{(2)}$ using the correction factors allowing for nuclear and electron spin effects of ref. 5. Errors quoted are the sum of the standard deviations from the repeated measurements of $I_\perp/I_\parallel$ and the monochromator polarisation correction factors.

REFERENCES

[1] M.N.R. Ashfold, M.T. Macpherson and J.P. Simons, Top. Curr. Chem. **86**, 1 (1979).

[2] T. Carrington, J. Chem. Phys. **41**, 2012 (1964); H. Okabe, J. Chem. Phys. **72**, 6642 (1980); A. Gedanken, J. Mol. Spectrosc. **82**, 246 (1980).

[3] I.P. Vinogradov and F.I. Vilesov, Opt. Spectrosc. **40**, 32 (1976); **44**, 653 (1978).

[4] C. Fotakis, C.B. McKendrick and R.J. Donovan, Chem. Phys. Lett. **80**, 598 (1981); R.J. Donovan, C. Fotakis, A. Hopkirk, C.B. McKendrick and A. Torre, Can. J. Chem. **61**, 1023 (1983).

[5] J.P. Simons, A.J. Smith and R.N. Dixon, J. Chem. Soc., Faraday 2 **80**, 1489 (1984).

[6] A. Hodgson, J.P. Simons, M.N.R. Ashfold, J.M. Bayley and R.N. Dixon, Chem. Phys. Lett. **107**, 1 (1984); Mol. Phys. **54**, 351 (1985).

[7] M.T. Macpherson and J.P. Simons, Chem. Phys. Lett. **51**, 261 (1977).

[8] J.P. Simons and A.J. Smith, Chem. Phys. Lett. **97**, 1 (1983).

[9] L.C. Lee, L. Oren, E. Phillips and D.L. Judge, J. Phys. B **11**, 47 (1978); L.C. Lee, J. Chem. Phys. **72**, 4334 (1980); O. Dutuit, A. Tabche–Fouhaile, I. Nenner, H. Frohlich and P.M. Guyon, J. Chem. Phys. **83**, 584 (1985); L.C. Lee and M. Suto, Chem. Phys. **110**, 161 (1986).

[10] R.N. Dixon, Mol. Phys. **54**, 333 (1985); M.P. Docker, A. Hodgson and J.P. Simons, Mol. Phys. **57**, 129 (1986).

[11] H.J. Krautwald, L. Schnieder, K.H. Welge and M.N.R. Ashfold, Faraday Disc. Chem. Soc. **82**, 99 (1986).

[12] F. Flouquet and J.A. Horsley, J. Chem. Phys. **60**, 3767 (1974).

[13] G. Theodorakopoulos, I.D. Petsalakis and R.J. Buenker, Chem. Phys. **96**, 217 (1985).

[14] V. Staemmler and A. Palma, Chem. Phys. **93**, 63 (1985).

[15] E. Segev and M. Shapiro, J. Chem. Phys. **77**, 5604 (1982).

[16] L.D. Dunne, H. Guo and J.N. Murrell, Mol. Phys. **62**, 283 (1987).

[17] K. Weide and R. Schinke, J. Chem. Phys. **87**, 4627 (1987).

[18] R. Schinke, V. Engel, S. Hennig, K. Weide and A. Untch, Ber. Bunsenges. Phys. Chem. **92**, 295 (1988).

[19] J.W.C. Johns, Can. J. Phys. 41, 209 (1963); 49, 944 (1971); R.J. Buenker and S.D. Peyerimhoff, Chem. Phys. Letters 29, 253 (1974); N.W. Winter, W.A. Goddard and F.W. Bobrowicz, J. Chem. Phys. 62, 4325 (1975); G. Theodorakopoulos, I.D. Petsalakis, R.J. Buenker and S.D. Peyerimhoff, Chem. Phys. Letters 105, 253 (1984); G. Theodorakopoulos, C.A. Nicolaides, R.J. Buenker and S.D. Peyerimhoff, Chem. Phys. Letters 89, 164 (1982).

[20] D. Yeager, V. McKoy and G.A. Segal, J. Chem. Phys. 61, 755 (1974).

[21] F.W.E. Knoop, H.H. Brongersma and C.J. Oosterhoff, Chem. Phys. Letters 13, 20 (1973).

[22] M.N.R. Ashfold, J.M. Bayley and R.N. Dixon, Can. J. Phys. 62, 1806 (1984).

[23] C.A. Greene and R.N. Zare, Ann. Rev. Phys. Chem. 33, 119 (1982); M.T. Macpherson, J.P. Simons and R.N. Zare, Mol. Phys. 38, 2049 (1979).

[24] I.L. Chidsey and D.R. Crosley, J. Quant, Spectry. Rad. Trans. 23, 187 (1980).

[25] G.W. Loge and J.R. Wiesenfeld, J. Chem. Phys. 75, 2795 (1981).

[26] R.N. Dixon, Mol. Phys. 54, 333 (1985).

[27] S. Tsurubuchi, Chem. Phys. 10, 335 (1975).

[28] C.G. Atkins, R. Briggs, J.B. Halpern and G. Hancock, Chem. Phys. Letters 152, 81 (1988).

FIGURE CAPTIONS

Figure 2.1 $OH(A^2\Sigma^+)$ fluorescence spectrum following two photon excitation of H_2O at 266 nm. Upper trace is the experimental spectrum, lower trace is that simulated using the populations shown in Fig. 2. The assignments show the branches numbered with N' values.

Figure 2.2 Rotational populations in $OH(A^2\Sigma^+)$ plotted as a function of N'/N'_{MAX}, where N'_{MAX} is the maximum value of N' allowed by energy conservation for dissociation of H_2O with zero internal energy. The experimental points from the present study are given as filled circles, (obtained as described in the text), the two open circles are interpolated values to give the best fit to the experimental data. The solid line is the single photon dissociation result of Simons et al. at 130.4 nm [5], the dashed line is the predicted distribution for dissociation at a 'resonance' at 133.7 nm by Segev and Shapiro [15].

Figure 2.3 $OD(A^2\Sigma^+)$ fluorescence spectrum following the two photon excitation of D_2O at 266 nm. The assignments show the branches numbered with N' values.

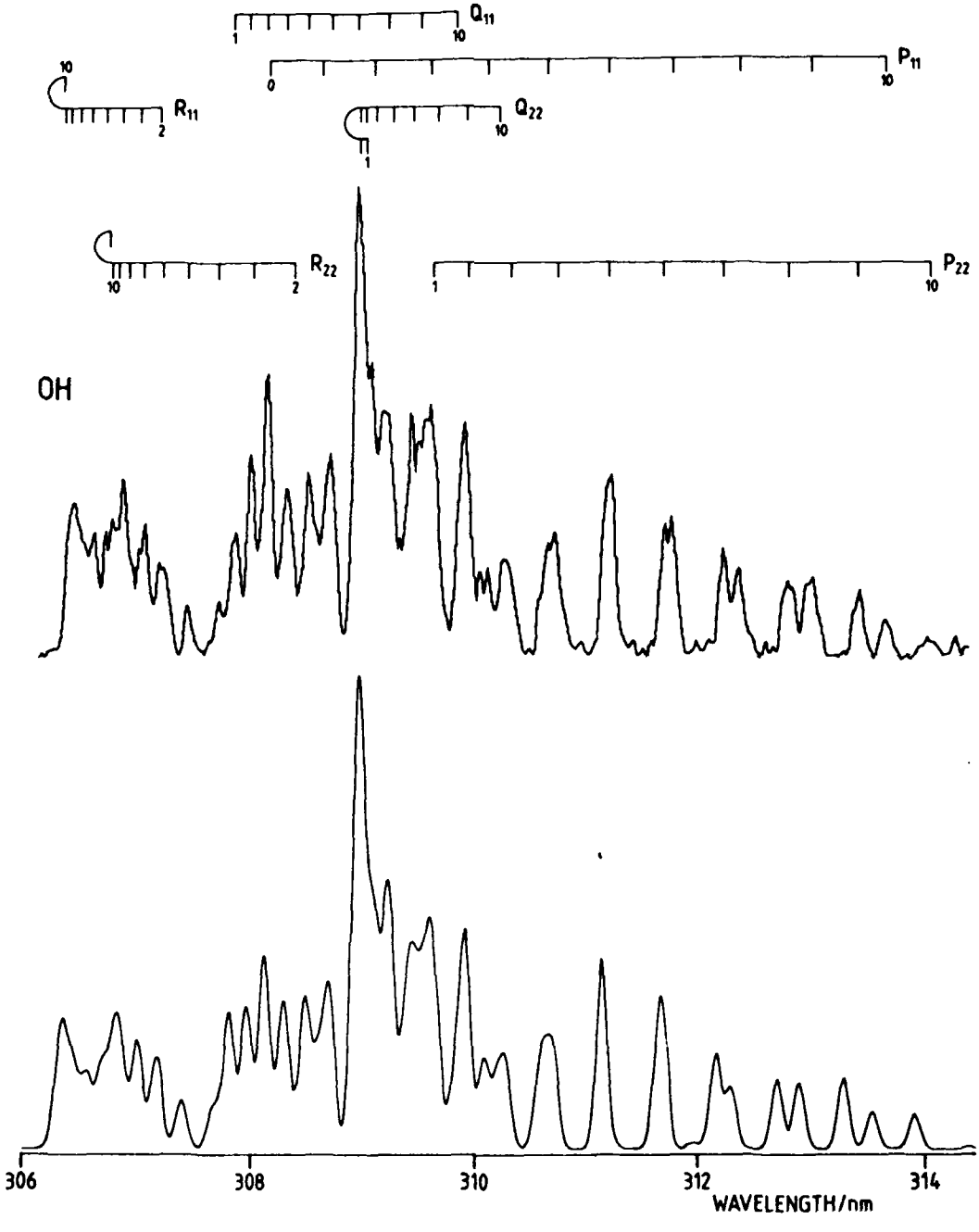

Fig 2.1

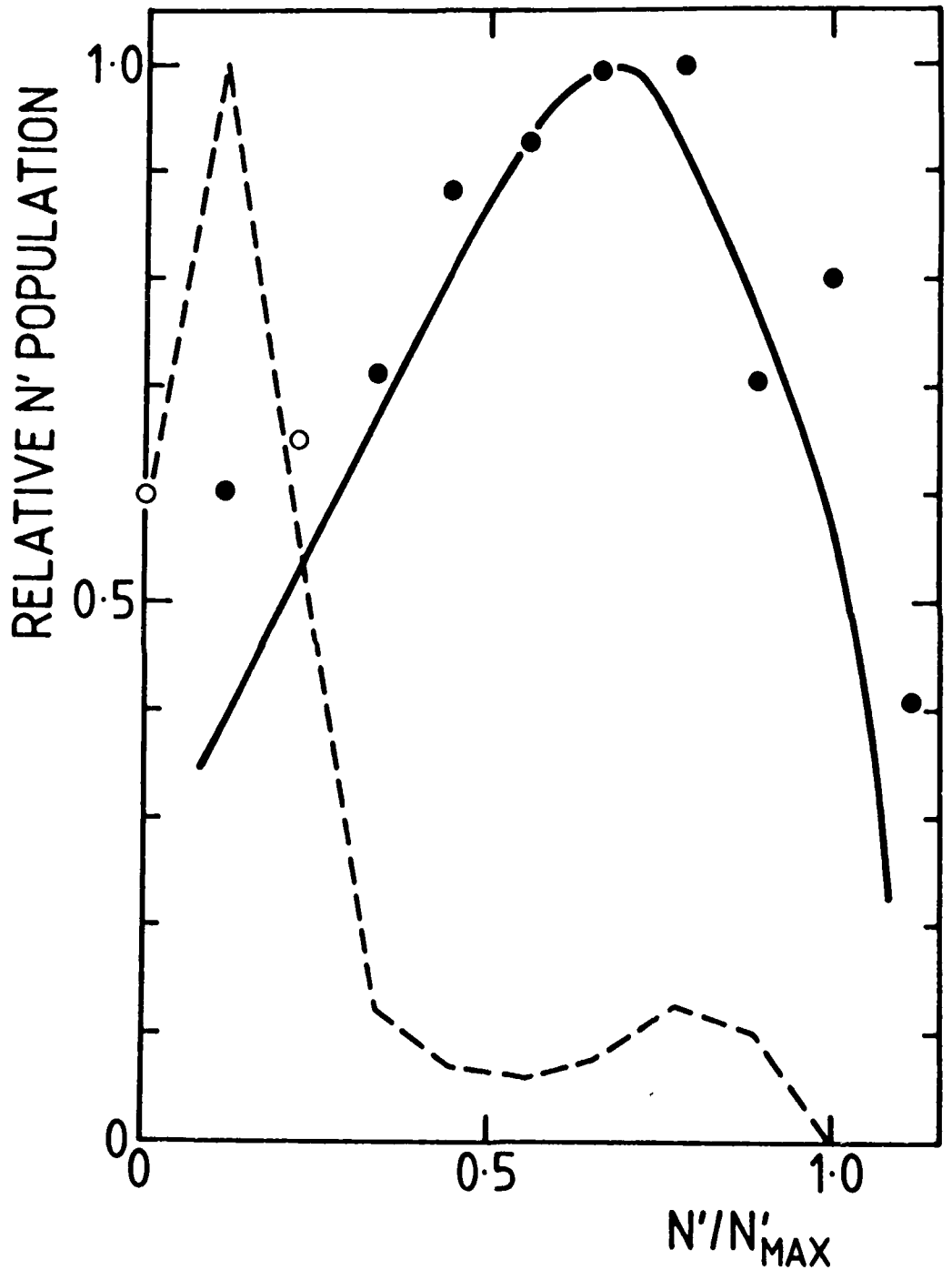

Fig 2.2

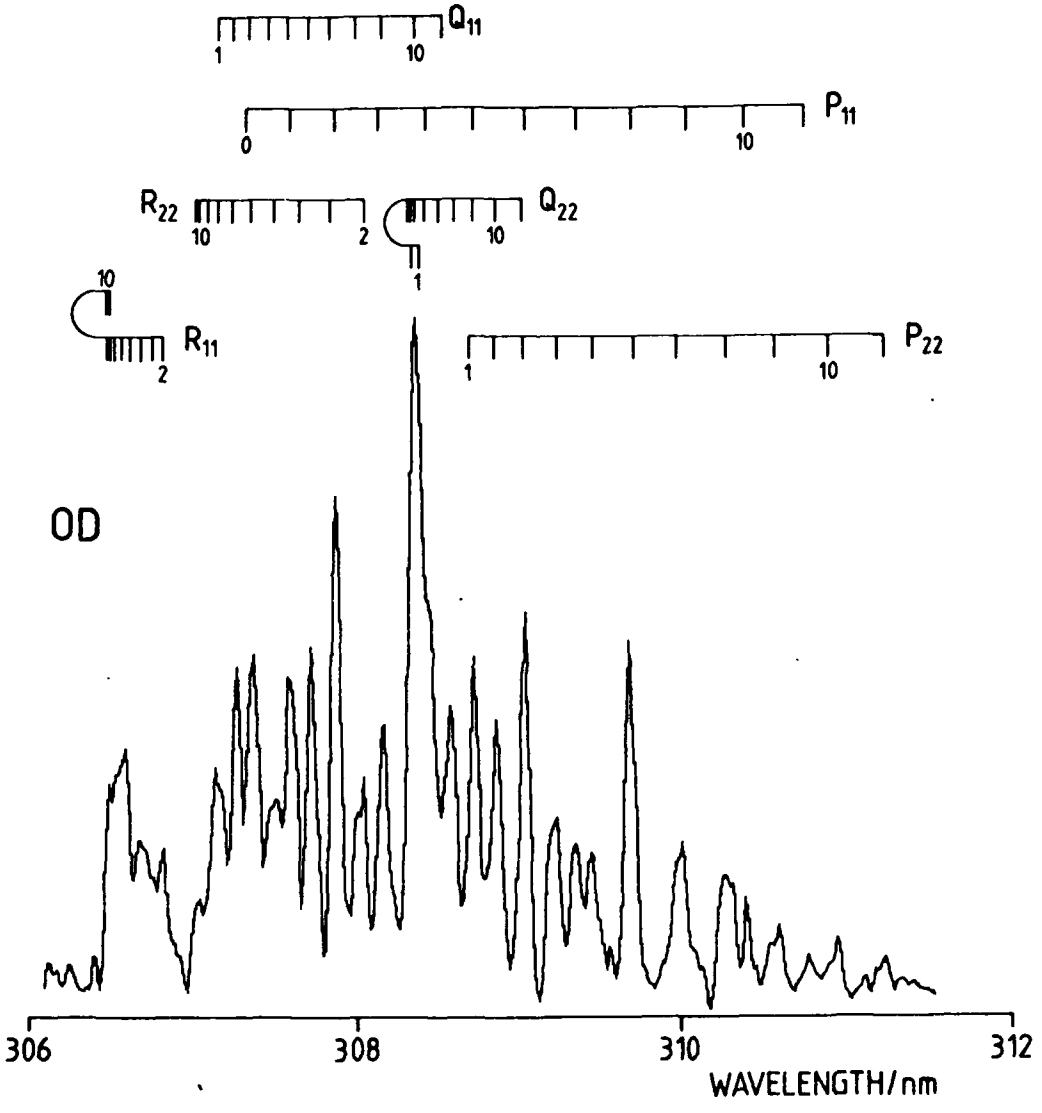
Q11
1
10
P11
0
10
R22
10
2
Q22
10
1
10
R11
2
P22
1
10
OD
306
308
310
312
WAVELENGTH/nm

Fig 2.3

3. Studies on the CF Radical

3.1 The Radiative Lifetime of CF($A^2\Sigma^+$)

INTRODUCTION

The measurement of absolute concentrations of free radicals by laser induced fluorescence (LIF) is most conveniently carried out by the use of a 'fluorescence actinometer', i.e. by comparing the magnitude of the LIF signal from the radicals with that from a species at known concentration excited under the same conditions. We have recently used this method to determine the absolute concentration of CF($X^2\Pi$) and $CF_2(\tilde{X}^1A_1)$ radicals in RF plasmas of fluorinated hydrocarbons under conditions similar to those used in the reactive ion etching of Si and SiO_2 features in VLSI manufacture [1]. For CF($X^2\Pi$, $v''=0$) the most convenient actinometer is NO($X^2\Pi$, $v''=1$), with the latter concentration known from the thermal population of a measured NO pressure at room temperature. Both species can be excited to their $A^2\Sigma^+$ upper states at similar wavelengths (232.9 nm for the CF(0,0) band, 236.1 nm for the NO(0,1) band). To relate the LIF signals to the CF concentration, values of the transition dipole moments are needed, and these can be deduced from the radiative lifetimes of the $A^2\Sigma^+$ upper states. For NO($A^2\Sigma^+$, $v'=0$) the lifetime is well known [2]: this report describes a direct measurement of the CF $A^2\Sigma^+$ radiative lifetimes τ_R for the $v'=0$ and $v'=1$ levels.

Two previous measurements of τ_R have been reported, both from time resolved emission following pulsed electron impact excitation of fluorinated hydrocarbons, with values of 19±2 ns for $v'=1$ [3] and 18±2 ns for $v'=0$ [4] obtained. In addition, two shock tube measurements of the transition dipole moment have resulted in values (2.31 [5] and 2.3 [6] Debye) corresponding to τ_R=20 ns. The direct measurement of τ_R reported here is some 30% greater than these results, with the discrepancy larger than the combined error limits.

EXPERIMENTAL

The reaction vessel used was a commercial plasma etching chamber (Plasma Technology RIE 80). The CF radical was generated by a 13.56MHz discharge (25 to 250W) in a volume of 2.3ℓ of pure CF_4, at pressures between 50 and 1000 mTorr, measured

with a capacitance manometer (Baratron 220AHS). Radiation at 220–240 nm was generated by an excimer pumped dye laser operating at 50 Hz (Lambda Physik EMG201MSC and FL2002), using coumarin 47 dye, and frequency doubled with a potassium pentaborate (KPB) crystal. Fluorescence emitted perpendicular to the laser beam was collected and focussed with two spectrasil B lenses into a monochromator (Edinburgh Instruments 121S15, f4, resolution 1.5 nm with .25 mm slits), and detected with an EMI 9813QKB photomultiplier. Special attention was paid to the design of the photomultiplier voltage divider chain to ensure rapid linear response.

For the recording of fluorescence excitation spectra the photomultiplier output was terminated to ground with a 3kΩ resistor, giving a time response of 3μs. This signal was recorded with a dual channel transient digitiser (Datalab DL912) interfaced to an IBM PCXT computer, and the signal integrated over the peak for 1μs to measure the total emitted fluorescence. The energy of the ultra–violet laser beam was monitored with a photodiode (Vactec VTB6061UV) connected to the second channel of the digitiser, allowing shot–by–shot normalisation of the signal. Typically the signal was averaged for 50 shots of the laser for each point in the spectrum, before changing the dye laser wavelength in increments of 3.5×10^{-4} nm. For the lifetime measurements, a fast gated sampler (Stanford Research Systems SR 255, 1 ns gate) was used to monitor the time behaviour of the photomultiplier output. The sampler was triggered by a signal from a photodiode illuminated by a small portion of the output from the excimer beam.

In order to remove interference from the intense cw emission from the plasma, the RF power was modulated off for a period of 300 μs each 20 ms, and the laser was fired 200 μs into this period. The continuous emission from the plasma decays to zero after 50 μs, whereas the concentration of the ground state CF decays in an approximately exponential fashion with a time constant of about 2ms. The sampling gate delay was scanned from 0 to 100 ns in 0.5 ns intervals, incrementing after each shot, and repeating the scan 500 times to allow averaging and estimation of the uncertainty of the measurement at each point, whilst eliminating systematic errors due to slowly varying fluctuations in conditions. Careful attention was paid to the method used for subtraction of the background noise level, caused by electrical interference from the excimer laser discharge, and instability of the zero signal level of the sampling gate output. For the smallest signals measured it was necessary to use a synchronised chopper (Rofin 7500) to block the laser beam on alternate shots to allow background subtraction. Signal due to scattered laser light was negligible.

The combination of the laser pulse shape and the time response function of the

measuring system was estimated by filling the chamber with atmospheric pressure air and tuning the monochromator to resonance with the laser frequency to observe scattered radiation.

RESULTS AND DISCUSSION

Figure 3.1 shows part of the excitation spectrum of CF as the laser wavelength is tuned through the $A^2\Sigma^+ - X^2\Pi(1,0)$ transition, with the monochromator set to pass (1,1) emission. Assignments shown were taken from the data of Porter et al. [7]. In this spectral region no fluorescence was observed which could be assigned to species other than CF, and thus the strong P_{11} band head at 223.82 nm was used for the lifetime measurements. In contrast the (0,0) excitation spectrum showed additional bands which were attributed to CF_2 $\tilde{A}^1B_1 - \tilde{X}^1A_1(0,11,0) - (0,0,0)$ and $(0,12,0) - (0,0,0)$ transitions around 234.2 and 231.5 nm respectively [8]. In order to avoid any fluorescence contribution from CF_2 to the observed signal an isolated CF feature, an overlap of the $Q_{21}+R_{11}(14.5)$ and $Q_{22}+R_{12}(21.5)$ lines, was chosen for the lifetime measurements.

Figure 3.2 shows the measured laser pulse shape and the LIF decay for (1,0) excitation. The measured laser pulse shape, a convolution of the true pulse width with the photomultiplier response function, is approximately Gaussian with a full–width at half maximum of $\sim$ 16 ns. Values of the fluorescence lifetime (which are of the same order as this measured pulse width) were extracted by non–linear least squares fitting a single exponential decay convoluted with the measured laser pulse shape to the experimentally observed time dependence of the CF fluorescence signal. An example of the experimental data together with 1σ error bars and the best fit convolution is shown in Figure 3.2. A series of measurements at 50 mTorr total pressure showed no systematic variation of the observed lifetime with applied RF power over the range 25–250 Watts, and under the conditions the fluorescence lifetime was measured to be 25.6±1.8 ns. The error quoted is twice the standard deviation of the weighted mean of a series of measurements, the weighting being derived from the standard deviations of the non–linear least squares fitting to the observed time profiles, together with an estimate of the uncertainty in the time measurement in the gated sampler.

At a pressure of 50 mTorr CF_4, collisional quenching of the $CF(A^2\Sigma)$ upper state would need to proceed at a rate constant of 2×10^{-10} cm^3 molecule^{-1} s^{-1} (i.e. the gas kinetic rate) in order to shorten the true radiative lifetime by 1%. Measurements were carried out

at CF_4 pressures between 50 and 1000 mTorr. At the higher pressures the quality of the fits was not as good as those at 50 mTorr, but it was apparent that between these limits there was no systematic lowering of the fluorescence lifetime. We conclude that at 50 mTorr quenching by CF_4 or by other species in the plasma is negligible. Shortening of the true lifetime by predissociation was also eliminated: predissociation in CF $A^2\Sigma^+$ $v''=2$ has been reported [9], but for $v'=1$ laser excitation spectra were observed with J' values ≤ 29.5 with no deviations seen from the calculated line intensities. We conclude that the value observed represents the true radiative lifetime τ_R of CF($A^2\Sigma^+$ $v'=1$).

For $v'=0$ excited at 232.15 nm, a lifetime of 26.7±1.8 ns was obtained under the same conditions. At other wavelengths contributions from underlying $CF_2(\tilde{A}-\tilde{X})$ LIF were observed, lengthening the observed decay times. As a check on the behaviour of the fluorescence detection system the fluorescence lifetime of the CF_2 $\tilde{A}^1B_1(0,2,0)$ level was measured as 51±2 ns, in good agreement with the value of 50±5 ns obtained recently [10].

Our values for τ_R are thus approximately one third larger than those previously observed, with the discrepancy being outside the range of the combined error limits. In the electron impact experiments, cascading of population from levels above CF $A^2\Sigma^+$ $v'=0,1$ would tend to make the measured value of the fluorescence lifetime an overestimate of τ_R and thus cannot explain the discrepancy: such cascading was observed [3] when CF was produced from electron impact dissociation of perfluorobutadiene. Electron impact spectra of CF precursors do show evidence of continuous emission in the CF(A–X) region [4], and a contribution from this, were it to arise from a state of short lifetime and be observed together with the CF(A–X) emission, would lead to an underestimate of τ_R for the $A^2\Sigma^+$ state. The shock tube studies, which produce radiative lifetimes some 25% smaller than the present measurements, depend upon values of the heats of formation of radical species to calculate the absolute CF concentrations, and any uncertainties in these values can lead to marked differences in the estimated transition moment [11].

3.2 Spectroscopy and Kinetics on CF

In order to fit the observed LIF spectrum of CF, the tabulated values of spectroscopic constants [7] were found to be adequate. However, with the availability of more accurate constants for the CF ground state [12], it was found that the previously reported $A^2\Sigma^+$ state constants needed to be slightly revised in order to fit the best spectroscopic data [7]. Table 3.2.1 lists the revised values together with the most accurate

previously accepted spectroscopic constants.

More spectroscopic analyses on the CF(A–X) emission is in progress, namely experimental measurements of the relative emission intensities of (v'–v'') transitions (v'=0,1). When published values of the (A–X) Franck Condon factors are used [11], the experimental data indicates a marked variation of the electronic dipole moment with v''. New calculations have been carried out in the last month on both the Franck Condon factors and the r–centroid, and these are presently being combined with the experimental data.

An estimate has been made of the rate constant for the O + CF reaction at room temperature. Ideally for this reaction one would like to have a clean photolytic source of CF in the presence of O atoms (as was, for example, used in our laboratory for the O + CF_2 reaction [13]) but this has not proved possible. Instead the following method was used. An RF discharge was struck in a mixture of CF_4 and O_2, and (in separate experiments) CF_2 and CF in their ground electronic states were observed by LIF. The discharge was then rapidly (< 5 μs) extinguished, and the decay of both radicals monitored. Both decayed exponentially: from the rate of the O + CF_2 decay, the known rate constant for the O + CF_2 reaction [13], and the measured CF and CF_2 absolute concentrations [14] the oxygen atom concentration was obtained, and shown to be in excess of both CF and CF_2. From the rate of the CF decay in the presence of a known O atom concentration the rate constant could be found: from a series of experiments a value of $(1.0 \pm 0.2) \times 10^{-10}$ cm^3 molecule^{-1} s^{-1} at 320 K was obtained.

TABLE 3.2.1

Rotational constants for the $A^2\Sigma^+$ state of CF

	Porter et al. [7]	Present work
B_e	1.72486 ± .00010	1.724360 ± .000030
α_e	0.02445 ± .00010	0.024535 ± .000030
D_e	6.65×10^{-6}	$(6.595 \pm .045) \times 10^{-6}$
β_e	0.30×10^{-6}	$(2.45 \pm .45) \times 10^{-7}$

REFERENCES

[1] J.P. Booth, G. Hancock, M.J. Toogood and N.D. Perry, Proc. Mat. Res. Soc. Symp. 117, (1988) in press.

[2] G.D. Greenblatt and A.R. Ravishankara, Chem. Phys. Letters 136, 501 (1987).

[3] J.E. Hesser and K. Dressler, J. Chem. Phys. 45, 2518 (1968); J.E. Hesser, J. Chem. Phys. 48, 2518 (1968).

[4] H.A. Van Sprang, H.H. Brongersma and F.J. DeHeer, Chem. Phys. 35, 51 (1978).

[5] J. Harrington, A.P. Modica and D.R. Libby, J. Chem. Phys. 44, 3380 (1966); 45, 2720 (1966).

[6] A.P. Monyakin, I.A. Svyatkin, N.G. Ovsyannikova, L.A. Kuznetsova and Yu. Ya Kuzyakov, Moscow University Chemistry Bulletin 32, 38 (1977).

[7] T.L. Porter, D.E. Mann and N. Acquista, J. Mol. Spectrosc. 16, 228 (1965).

[8] C.W. Mathews, Can. J. Phys. 45, 2355 (1967).

[9] W.P. White, Ph.D. Dissertation, Ohio State University, 1971.

[10] W. Hack and A. Wilms, J. Phys. Chem. 90, 4007 (1986).

[11] T. Wentink and L. Isaacson, J. Chem. Phys. 46, 603 (1967).

[12] H.A. Gondal, W. Rohrbeck, W. Urban, R. Blankert and J.M. Brown, J. Mol. Spectrosc. 1. 290 (1983).

[13] G. Hancock, P.D. Harrison and A.J. MacRobert, J. Chem. Soc. Faraday Trans. 2 82, 647 (1986).

FIGURE CAPTIONS

Figure 3.1 Part of the LIF excitation spectrum of CF($A^2\Sigma^+$ $v'=1$ – $X^2\Pi$ $v''=0$), showing the P_{11} band head used for lifetime measurements, and the lack of fluorescence from species other than CF. The radical was produced by an RF discharge in 50 mTorr CF_4.

Figure 3.2 Measured LIF signal as a function of time following excitation of CF($A^2\Sigma^+$ $v'=1$) at 223.82 nm produced by an RF discharge in 50 mTorr CF_4. The points represent measured data averaged over 500 laser shots together with 1σ error bars: the solid line is the best fit convolution of the measured laser pulse shape (also shown in the Figure) with a single exponential decay.

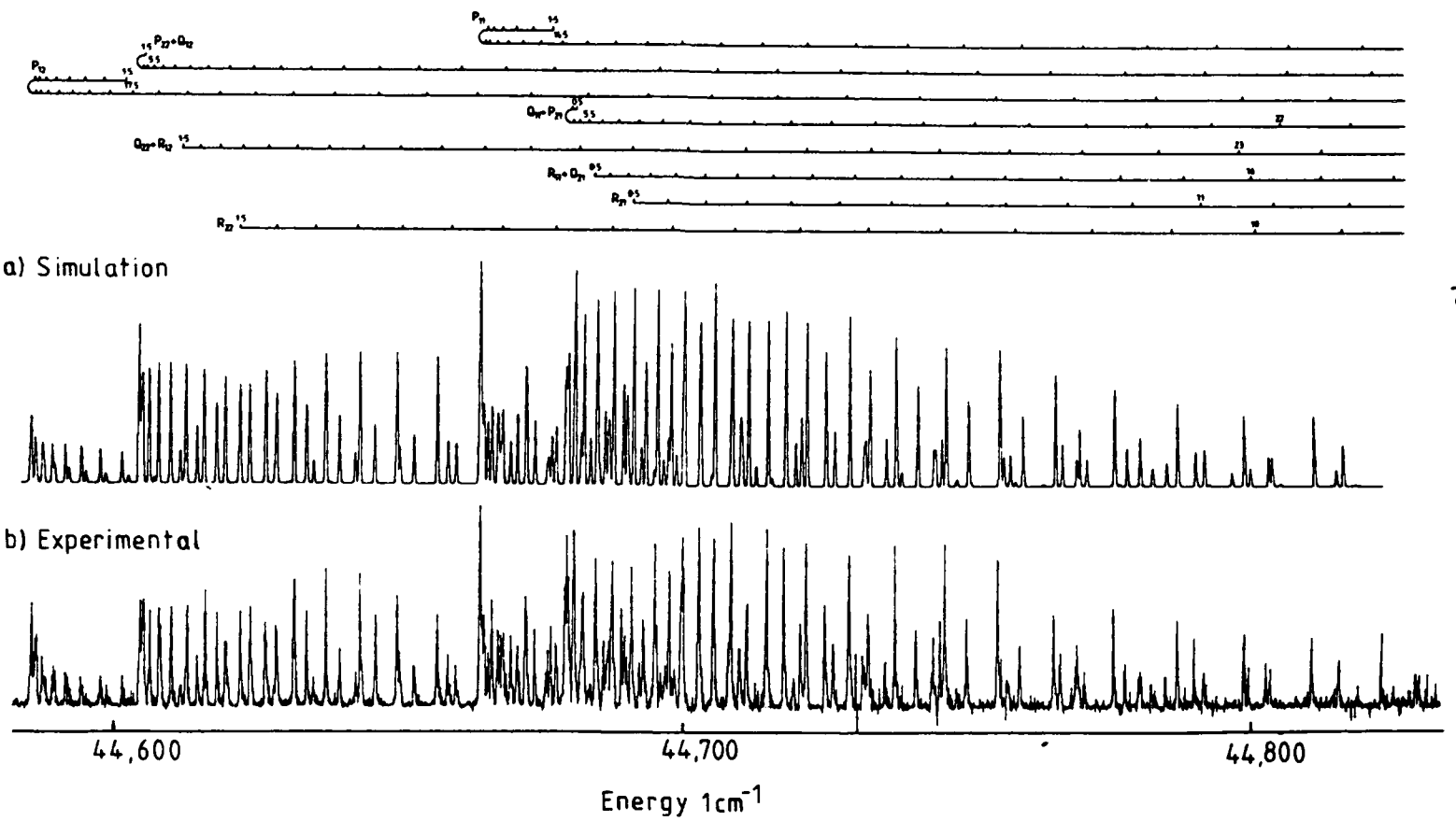

Fig 3.1

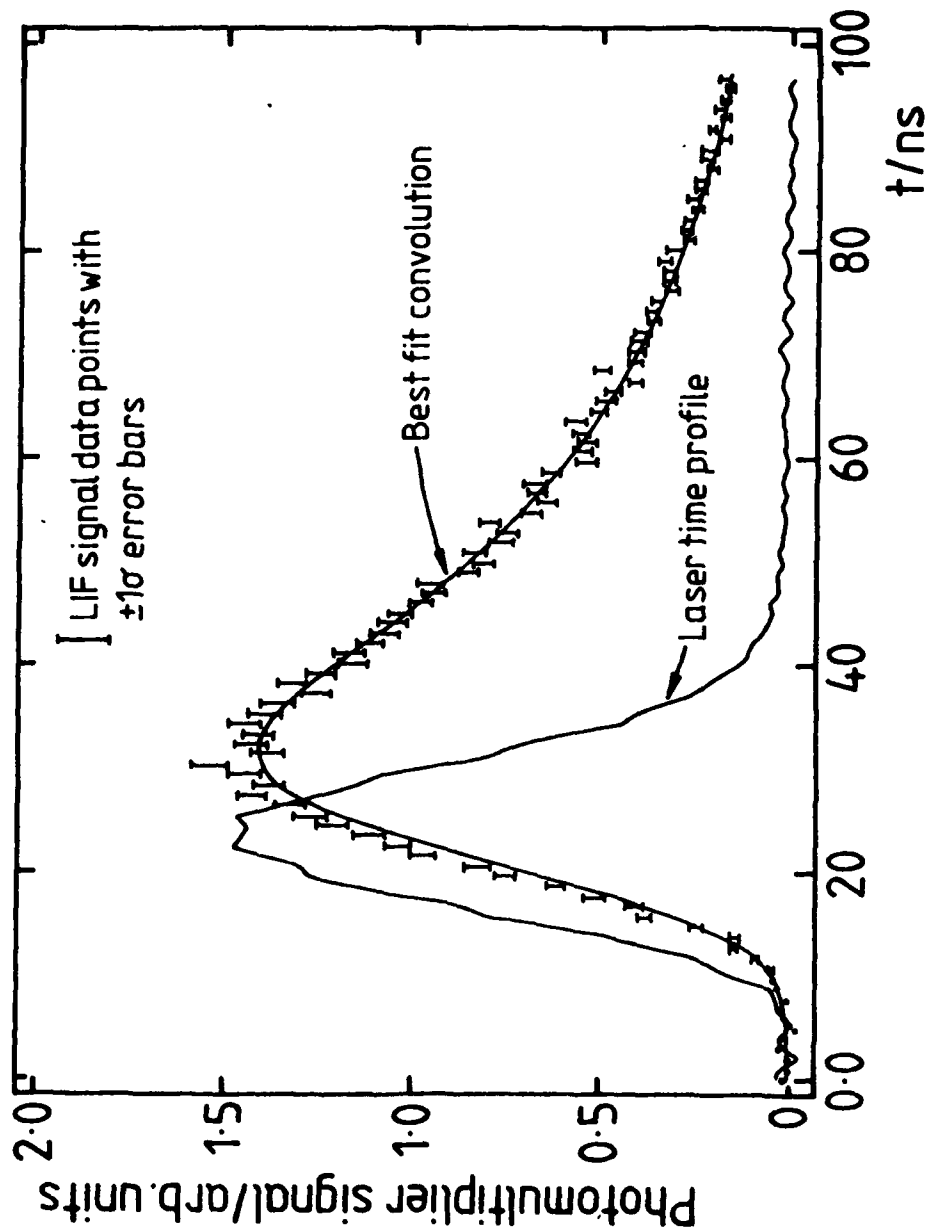
Photomultiplier signal/arb. units
2·0
1·5
1·0
0·5
0
0·0
20
40
60
80
100
t/ns
LIF signal data points with ±1σ error bars
Best fit convolution
Laser time profile

Fig 3.2

4. Additional Photochemical Studies

4.1 The O + CS Reaction

One of the aims of the work set out during the reporting period was to observe the nascent rotational distribution on the $CO(X^1\Sigma^+)$ product of the O + CS reaction. This work is still in progress, and the following sections summarise the most important findings so far.

(a) The rotational distribution at a total pressure of 1.5×10^{-4} Torr has been measured for both $v''=12$ and 14. This does not change when the pressure is increased by a factor of 10: at present we are attempting to improve the sensitivity of the experiment to achieve lower pressures to be able to ensure that the distribution is nascent. All the present indications are that we have succeeded in obtaining the nascent distributions.

(b) Marked differences in the intensities of LIF in P,R lines compared with Q lines have been seen in the lowest pressure experiments as a function of the angle between the polarisation vector of the LIF beam and the plane containing the relative velocity vector of the O and CS reagent beams. These are preliminary data but suggest that we are observing alignment effects (the P,R branch lines probe CO molecules with $\underline{J}$ perpendicular to the transition moment, $\underline{\mu}$, whereas Q branches probe molecules with $\underline{J}$ parallel to $\underline{\mu}$), and that these effects are easily destroyed by relatively efficient collisional processes.

4.2 Photoaffinity Labelling

For part of the grant period, an academic visitor, Professor J.B. Halpern from Howard University in Washington DC, worked on the H_2O and D_2O photolyses mentioned earlier. For part of this time in Oxford, Professor Halpern was supported by funds from the grant. He also collaborated with colleagues from the Organic Chemistry Department in studies carried out in our laboratory on the liquid phase photolysis of an azirine ring containing compound to produce a carbene radical on a species bound to an enzyme (Isopenicillin N Synthetase). Rapid reaction of the carbene with the enzyme to give degradation products (enzyme cleavage) then takes place, and the identification of these products provides information on the active site of the enzyme. A publication from this work has been submitted to Biochemical Journal.

5. Publications and Theses resulting from this work

5.1 Publications (a–d) are included with this Report.

(a) The Radiative Lifetime of CF($A^2\Sigma^+$).
J.P. Booth and G. Hancock, Chem. Phys. Letters 150, 457 (1988).

(b) Two Photon Dissociation of H_2O at 266 nm.
C.G. Atkins, R.G. Briggs, J.B. Halpern and G. Hancock, Chem. Phys. Letters 152, 81 (1988).

(c) Photodissociation of D_2O in the Second Continuum by Two Photon Absorption at 266 nm.
R.G. Briggs, J.B. Halpern, G. Hancock, N. Shafizaden, J. Rostas, J.L. Lemaire and F. Rostas, submitted to Chem. Phys. Letters.

(d) Photoaffinity Labelling of Isopenicillin N Synthetase by Laser Flash Photolysis.
J.E. Baldwin, J.B. Coates, J.B. Halpern, M.G. Maloney and A.J. Pratt, submitted to The Biochemical Journal.

In preparation

(e) A Time Resolved Fourier Transform Spectrometer for Kinetic Studies of Atom plus Radical Reactions.
P. Biggs, G. Hancock and D.E. Heard.

(f) Polarisation and Laser Induced Fluorescence Measurements on the Products of the Two Photon Dissociation of H_2O at 266 nm.
R.G. Briggs, J.B. Halpern and G. Hancock.

(g) Infrared Emission in the O + CF_2 and O + CHF Reactions.
G. Hancock and D.E. Heard.

5.2 Theses

Part II theses (one year projects carried out by all Oxford undergraduates in their fourth and final year of the Chemistry course).

J. Wild	1986	"Ultraviolet Laser Excitation of Gas Phase Species" (work on CF).

D. Heard	1986	"The Kinetics of Species Produced by Infrared Laser Photolysis" (IR emission from O + CF_2, O + CHF).

Mr. Heard is now continuing this work in his D.Phil. thesis, which will be completed in October 1989.

R.G. Briggs	1987	"Ultraviolet Excitation of Gas Phase Species" (H_2O and D_2O photolysis).
A.J. Orr–Ewing	1988	"Laser Induced Fluorescence Studies of Reaction Dynamics" (O + CS reaction).

Mr. Orr–Ewing is now continuing this work for his D.Phil. to be completed in October 1991.

J.P. Booth	D.Phil. 1988	carried out much of the work concerning the CF radical measurements.

THE RADIATIVE LIFETIME OF CF($A\,^2\Sigma^+$)

J.P. BOOTH and G. HANCOCK
Physical Chemistry Laboratory, South Parks Road, Oxford OX1 3QZ, UK

Received 27 June 1988

The radiative lifetimes of the $v' = 0$ and 1 levels of CF($A\,^1\Sigma^+$) in the gas phase have been measured by observing the fluorescence decay following pulsed laser excitation. The values, 26.7 ± 1.8 and 25.6 ± 1.8 ns respectively, are some 30% larger than those previously observed.

1. Introduction

The measurement of absolute concentrations of free radicals by laser-induced fluorescence (LIF) is most conveniently carried out using a "fluorescence actinometer", i.e. by comparing the magnitude of the LIF signal from the radicals with that from a species at known concentration excited under the same conditions. We have recently used this method to determine the absolute concentration of CF($X\,^2\Pi$) and $CF_2(\tilde{X}\,^1A_1)$ radicals in rf plasmas of fluorinated hydrocarbons under conditions similar to those used in the reactive ion etching of Si and SiO_2 features in VLSI manufacture [1]. For CF($X\,^2\Pi$, $v'' = 0$) the most convenient actinometer is NO($X\,^2\Pi$, $v'' = 1$), with the latter concentration known from the thermal population of a measured NO pressure at room temperature. Both species can be excited to their $A\,^2\Sigma^+$ upper states at similar wavelengths (232.9 nm for the CF(0, 0) band, 236.1 nm for the NO(0, 1) band). To relate the LIF signals to the CF concentration, values of the transition dipole moments are needed, and these can be deduced from the radiative lifetimes of the $A\,^2\Sigma^+$ upper states. For NO($A\,^2\Sigma^+$, $v' = 0$) the lifetime is well known [2]: this report describes a direct measurement of the CF $A\,^2\Sigma^+$ radiative lifetimes τ_R for the $v' = 0$ and $v' = 1$ levels.

Two previous measurements of τ_R have been reported, both from time-resolved emission following pulsed electron impact excitation of fluorinated hydrocarbons, giving values of 19 ± 2 ns for $v' = 1$ [3] and 18 ± 2 ns for $v' = 0$ [4]. In addition, two shock tube measurements of the transition dipole moment have resulted in values (2.31 [5] and 2.3 D [6]) corresponding to $\tau_R = 20$ ns. The direct measurement of τ_R reported here is some 30% greater than these results, with the discrepancy larger than the combined error limits.

2. Experimental

The reaction vessel used was a commercial plasma etching chamber (Plasma Technology RIE 80). The CF radical was generated by a 13.56 MHz discharge (25 to 250 W) in a volume of 2.3 ℓ of pure CF_4 at pressures between 50 and 1000 mTorr, measured with a capacitance manometer (Baratron 220AHS). Radiation at 220–240 nm was generated by an excimer-pumped dye laser operating at 50 Hz (Lambda Physik EMG201MSC and FL2002), using coumarin 47 dye, and frequency doubled with a potassium pentaborate (KPB) crystal. Fluorescence emitted perpendicular to the laser beam was collected and focused with two spectrasil B lenses into a monochromator (Edinburgh Instruments 121S15, $f/4$, resolution 1.5 nm with 0.25 mm slits), and detected with an EMI 9813QKB photomultiplier. Special attention was paid to the design of the photomultiplier voltage divider chain to ensure rapid linear response.

For recording the fluorescence excitation spectra the photomultiplier output was terminated to ground with a 3 kΩ resistor, giving a time response of 3 μs. This signal was recorded with a dual channel tran-

0 009-2614/88/$ 03.50

sient digitiser (Datalab DL912) interfaced to an IBM PCXT computer, and the signal integrated over the peak for 1 μs to measure the total emitted fluorescence. The energy of the ultraviolet laser beam was monitored with a photodiode (Vactec VTB6061UV) connected to the second channel of the digitiser, allowing shot-by-shot normalisation of the signal. Typically the signal was averaged for 50 shots of the laser for each point in the spectrum, before changing the dye laser wavelength in increments of 3.5×10^{-4} nm. For the lifetime measurements, a fast gated sampler (Stanford Research Systems SR 255, 1 ns gate) was used to monitor the time behaviour of the photomultiplier output. The sampler was triggered by a signal from a photodiode illuminated by a small portion of the output from the excimer beam.

In order to remove interference from the intense cw emission from the plasma, the rf power was modulated off for a period of 300 μs every 20 ms, and the laser was fired 200 μs into this period. The continuous emission from the plasma decays to zero after 50 μs, whereas the concentration of the ground state CF decays in an approximately exponential fashion with a time constant of about 2 ms. The sampling gate delay was scanned from 0 to 100 ns in 0.5 ns intervals, incrementing after each shot, and repeating the scan 500 times to allow averaging and estimation of the uncertainty of the measurement at each point, whilst eliminating systematic errors due to slowly varying fluctuations in conditions. Careful attention was paid to the method used for subtraction of the background noise level, caused by electrical interference from the excimer laser discharge, and instability of the zero signal level of the sampling gate output. For the smallest signals measured it was necessary to use a synchronised chopper (Rofin 7500) to block the laser beam on alternate shots to allow background subtraction. Signal due to scattered laser light was negligible.

The combination of the laser pulse shape and the time response function of the measuring system was estimated by filling the chamber with atmospheric pressure air and tuning the monochromator to resonance with the laser frequency to observe scattered light radiation.

3. Results and discussion

Fig. 1 shows part of the excitation spectrum of CF as the laser wavelength is tuned through the $A\,^2\Sigma^+$–$X\,^2\Pi$ (1, 0) transition, with the monochromator set to pass (1, 1) emission. Assignments shown were taken from the data of Porter et al. [7]. In this spectral region no fluorescence was observed which could be assigned to species other than CF, and thus the strong P_{11} band head at 223.82 nm was used for the lifetime measurements. In contrast the (0, 0) excitation spectrum showed additional bands which were attributed to CF_2 $\tilde{A}\,^1B_1$–$\tilde{X}\,^1A_1$ (0, 11, 0)–(0, 0, 0) and (0, 12, 0)–(0, 0, 0) transitions around 234.2 and 231.5 nm respectively [8]. In order to avoid any fluorescence contribution from CF_2 to the observed signal an isolated CF feature, an overlap of the $Q_{21}+R_{11}(14.5)$ and $Q_{22}+R_{12}(21.5)$ lines, was chosen for the lifetime measurements.

Fig. 2 shows the measured laser pulse shape and the LIF decay for (1, 0) excitation. The measured pulse shape, a convolution of the true pulse width with the photomultiplier response function, is ap-

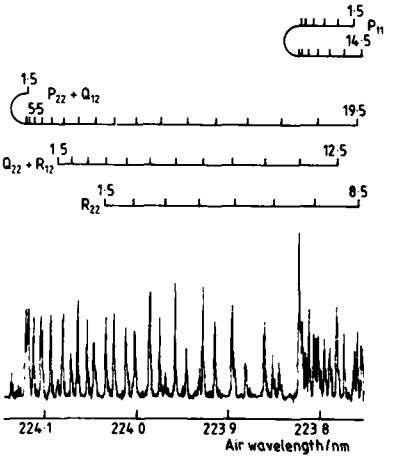

Fig. 1. Part of the LIF excitation spectrum of CF($A\,^2\Sigma^+$, $v'=1$–$X\,^2\Pi$, $v''=0$), showing the P_{11} band head used for lifetime measurements, and the lack of fluorescence from species other than CF. The radical was produced by an RF discharge in 50 mTorr CF_4.

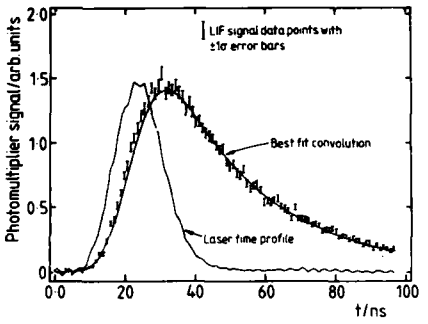

Fig. 2. Measured LIF signal as a function of time following excitation of CF($A\,^2\Sigma^+$, $v'=1$) at 223.82 nm produced by an RF discharge in 50 mTorr CF_4. The points represent measured data averaged over 500 laser shots together with 1σ error bars: the solid line is the best fit convolution of the measured laser pulse shape (also shown in the figure) with a single exponential decay.

proximately Gaussian with a full width at half maximum of ≈ 16 ns. Values of the fluorescence lifetime (which are of the same order as this measured pulse width) were extracted by non-linear least-squares fitting a single exponential decay convoluted with the measured laser pulse shape to the experimentally observed time dependence of the CF fluorescence signal. An example of the experimental data together with 1σ error bars and the best fit convolution is shown in fig. 2. A series of measurements at 50 mTorr total pressure showed no systematic variation of the observed lifetime with applied rf power over the range 25–250 W, and under these conditions the fluorescence lifetime was measured to be 25.6 ± 1.8 ns. The error quoted is twice the standard deviation of the weighted mean of a series of measurements, the weighting being derived from the standard deviations of the non-linear least-squares fitting to the observed time profiles, together with an estimate of the uncertainty in the time measurement in the gated sampler.

At a pressure of 50 mTorr CF_4, collisional quenching of the CF($A\,^2\Sigma$) upper state would need to proceed at a rate constant of 2×10^{-10} cm^3 molecule^{-1} s^{-1} (i.e. the gas kinetic rate) in order to shorten the true radiative lifetime by 1%. Measurements were carried out at CF_4 pressures between 50 and 1000 mTorr. At the higher pressures the quality of the fits was not as good as those at 50 mTorr, but it was apparent that between these limits there was no systematic lowering of the fluorescence lifetime. We conclude that at 50 mTorr quenching by CF_4 or by other species in the plasma is negligible. Shortening of the true lifetime by predissociation was also eliminated: predissociation in CF $A\,^2\Sigma^+$, $v''=2$ has been reported [9], but for $v'=1$ laser excitation spectra were observed with J' values $\leqslant 29.5$ with no deviations seen from the calculated line intensities. We conclude that the value observed represents the true radiative lifetime τ_R of CF($A\,^2\Sigma^+$, $v'=1$).

For $v'=0$ excited at 232.15 nm, a lifetime of 26.7 ± 1.8 ns was obtained under the same conditions. At other wavelengths contributions from underlying $CF_2(\tilde{A}\text{–}\tilde{X})$ LIF were observed, lengthening the observed decay times. As a check on the behaviour of the fluorescence detection system the fluorescence lifetime of the CF_2 $\tilde{A}\,^1B_1(0, 2, 0)$ level was measured as 51 ± 2 ns, in good agreement with the value of 50 ± 5 ns obtained recently [10].

Our values for τ_R are thus approximately one third larger than those previously observed, with the discrepancy being outside the range of the combined error limits. In the electron impact experiments, cascading of population from levels above CF $A\,^2\Sigma^+$, $v'=0$, 1 would tend to make the measured value of the fluorescence lifetime an overestimate of τ_R and thus cannot explain the discrepancy: such cascading was observed [3] when CF was produced from electron impact dissociation of perfluorobutadiene. Electron impact spectra of CF precursors do show evidence of continuous emission in the CF(A–X) region [4], and a contribution from this, were it to arise from a state of short lifetime and be observed together with the CF(A–X) emission, would lead to an underestimate of τ_R for the $A\,^2\Sigma^+$ state. The shock tube studies, which produce radiative lifetimes some 25% smaller than the present measurements, depend upon values of the heats of formation of radical species to calculate the absolute CF concentrations, and any uncertainties in these values can lead to marked differences in the estimated transition moment [11].

Acknowledgement

The research reported herein has been sponsored in part by the United States Army through its European Research Office.

References

[1] J.P. Booth, G. Hancock, M.J. Toogood and N.D. Perry, Proc. Mat. Res. Soc. Symp. 117 (1988), to be published.
[2] G.D. Greenblatt and A.R. Ravishankara, Chem. Phys. Letters 136 (1987) 501.
[3] J.E. Hesser and K. Dressler, J. Chem. Phys. 45 (1966) 3149; J.E. Hesser, J. Chem. Phys. 48 (1968) 2518.
[4] H.A. Van Sprang, H.H. Brongersma and F.J. DeHeer, Chem. Phys. 35 (1978) 51.
[5] J. Harrington, A.P. Modica and D.R. Libby, J. Chem. Phys. 44 (1966) 3380; 45 (1966) 2720.
[6] A.P. Monyakin, I.A. Svyatkin, N.G. Ovsyannikova, L.A. Kuznetsova and Yu.Ya Kuzyakov, Moscow Univ. Chem. Bull. 32 (1977) 38.
[7] T.L. Porter, D.E. Mann and N. Acquista, J. Mol. Spectry. 16 (1965) 228.
[8] C.W. Mathews, Can. J. Phys. 45 (1967) 2355.
[9] W.P. White, Ph.D. Dissertation, Ohio State University (1971).
[10] W. Hack and A. Wilms, J. Phys. Chem. 90 (1986) 4007.
[11] T. Wentink and L. Isaacson, J. Chem. Phys. 46 (1967) 603.

TWO-PHOTON DISSOCIATION OF H_2O AT 266 nm

C.G. ATKINS [1], R.G. BRIGGS, J.B. HALPERN [2] and G. HANCOCK
Physical Chemistry Laboratory, Oxford University, South Parks Road, Oxford OX1 3QZ, UK

Received 12 August 1988

The rotational energy distribution in the OH $A\,^2\Sigma^+$ fragment of the two-photon dissociation of H_2O at 266 nm has been measured. The form of the distribution is very similar to that following single-photon excitation at approximately the same energy, but the alignment of the photofragment is considerably less. Possible dissociation mechanisms for the two-photon excited molecules are discussed.

1. Introduction

The energy required to produce electronically excited $OH(A\,^2\Sigma^+)$ radicals from the photolysis of H_2O corresponds to the absorption of a single photon of wavelength $\leqslant 137$ nm. The absorption spectrum of H_2O below this wavelength consists of a diffusely structured band peaking at around 130 nm, and assigned to a $\tilde{B}\,^1A_1 \leftarrow \tilde{X}\,^1A_1$ transition which at lower wavelengths is overlapped by sharp bands associated with Rydberg transitions [1], and the dissociation dynamics in this region have been extensively studied, largely through measurements of the $OH(A\,^2\Sigma^+)$ internal state distributions [2–6] and alignments [5–8]. Although the $\tilde{B}$ state correlates adiabatically with $OH(A\,^2\Sigma^+)$, the quantum yield for production of the excited species is low ($\leqslant 10\%$) [3,9], with the majority of dissociating molecules crossing to the H_2O $\tilde{A}\,^1B_1$ or $\tilde{X}\,^1A_1$, states, and forming ground state $OH(X\,^2\Pi)$ [10]. Recently this channel has been explored for the first time through measurements of the photofragment spectroscopy of the H atom following photodissociation at ≈ 125 nm [11].

Both $OH(A\,^2\Sigma^+)$ and $(X\,^2\Pi)$ state fragments produced from photolysis via the $\tilde{B}$ state show a high degree of rotational excitation, with this being particularly marked for photolysis at wavelengths shorter than the $\tilde{B}$ state maximum absorption [2–6,11]. The development of potential energy surfaces for the $\tilde{B}$, $\tilde{A}$ and $\tilde{X}$ states [12–14] has stimulated trajectory calculations [15–17], leading to predicted energy distributions in the OH $A\,^2\Sigma^+$ and $X\,^2\Pi$ states. Particularly impressive agreement has been found between theory [17] and experiment [5,11] for excitation near 125 nm, where approximately 1 eV of energy is available for partitioning in the $H+OH(A)$ products, and where rotational distributions peak close to the maximum allowed by energy conservation. At wavelengths above 130 nm (where only one experimental study of rotationally resolved fragment distributions has been reported [5]), calculations for dissociation on the $\tilde{B}$ state surface have shown that trajectories are either direct or can undergo at least one vibration within the deep $\tilde{B}$ surface well [15,18]. The influence of these so-called trapped [15] or indirect [18] trajectories on the diffuse structure of the $\tilde{B}$ state absorption spectrum [18] and on the $OH(A\,^2\Sigma^+)$ rotational energy distribution [15] has been calculated, with the latter study showing a marked effect of the form of the distribution on the precise region of the surface accessed by absorption (and thus on the photodissociation wavelength) [15].

This report describes the rotational energy distribution in $OH(A\,^2\Sigma^+)$ produced by the two-photon dissociation of H_2O at 266 nm. The motivation was twofold: first to test whether the distribution resem-

[1] Present address: BT Research Laboratories, Martlesham Heath, Ipswich IP5 7RE, UK.
[2] Permanent address: Department of Chemistry, Howard University, Washington, DC 20059, USA.

0 009-2614/88/$ 03.50

bled the one-photon case near this dissociation energy (the nearest such study being at 130.4 nm [5]) or whether the distribution was "cooler" because of a trapped trajectory (predicted to occur near 133 nm [15]), and secondly to see if the energy distribution or the OH($A\,^2\Sigma^+$) alignment gave any indication of the involvement of a state other than $\tilde{B}\,^1A_1$ in the two-photon absorption step. A state of $^1A_1$ symmetry has long been predicted to exist in this energy region [13,19] and suggestions have been made about its influence on the H_2O electron impact [20,21] and multiple photon ionisation [22] spectra and on the OH($A\,^2\Sigma^+$) fluorescence polarization [7] and rotational energy distributions [4]. No direct evidence for this $^1A_2$ state has been found, although the other two components arising from the promotion of an electron in the ground state $1b_1$ orbital to a 3p orbital (the $\tilde{D}\,^1A_1$ and $\tilde{C}\,^1B_1$ states corresponding to the $3pb_1$ and a_1 components respectively) are known [1,22], and a state of A_2 symmetry at higher energies, assigned as a $3db_2 \leftarrow 1b_1$ transition, has been identified [22]. Single-photon absorption from the ground $^1A_1$ state to a $^1A_2$ state is forbidden, but it can be accessed (as can the $\tilde{B}\,^1A_1$ state) by two-photon excitation, and in principle it might be expected that the influence of this state would be revealed by differences in the $A\,^2\Sigma^+$ rotational state distributions and alignments between one- and two-photon excitation. For dissociation energies corresponding to single-photon absorption near 124 nm, alignment studies have shown that the $^1A_2$ state is not involved, the $\tilde{B}$ state being the principal carrier of the two-photon continuum in this region [6]. Our results show a rotational distribution very similar (when scaled to the fractional energy appearing in rotation) to the single-photon case at 130.4 nm [5]. Our preliminary data for the OH A–X polarization however show that the alignment is considerably lower than that observed in the one-photon case [5,8].

2. Experimental

Gas phase H_2O was photolyzed in a stainless steel chamber using the frequency-quadrupled output of a Nd^{3+}:YAG laser (J.K. Lasers 2000 L). The linearly polarised laser output (≈ 40 mJ pulse^{-1}) was focused into the vessel with a 20 cm focal length spectrosil lens, and the fluorescence output detected at right angles to both the laser beam propagation axis and its electric vector via a monochromator (Spex 1870 C) fitted with a cooled EMI 9816 QKB photomultiplier. In the experiments reported here emission was detected with no deliberate selection of its polarization vector: the detection system was polarization sensitive (mainly due to the monochromator) but, as discussed below, the effect of product alignment (and thus the polarization of the emission) on the fluorescence spectra was negligible.

Experiments were carried out at H_2O pressures up to 250 mTorr. Under these conditions any effect of collisional scrambling of either the upper state OH population or its polarization is negligible [5] due to the very rapid electronic quenching of OH($A\,^2\Sigma^+$). The monochromator was operated typically with 100 μm slit width, giving a resolution of ≈ 0.1 nm at 300 nm. The voltage output from the detection system was digitised, corrected for variations in the laser intensity, and summed for a preset number of shots at each wavelength setting.

3. Results and discussion

Fig. 1 shows the fluorescence spectrum in the region 306–314 nm, with features clearly identified as arising from the formation of OH($A\,^2\Sigma^+$) with values of N' between 0 and 10. The signal was found to vary with the square of the laser power (and this dependence was used in the normalisation of the signal for fluctuations in the laser intensity), and the rotational levels populated are consistent with those expected for the two-photon dissociation of H_2O at 266 nm. The available energy from this process for partitioning into the H+OH($A\,^2\Sigma^+$) fragments is 1503 cm^{-1} if internal energy in H_2O is neglected, and this is enough to populate $N'_{max} = 9$ in OH($A\,^2\Sigma^+$): the small population observed in $N' = 10$ is presumably the result of a contribution from internally excited H_2O molecules.

Fluorescence from electronically excited species generated by photolysis is expected to be polarized, and the degree of poiarization can be a sensitive function of the level excited and of the branch observed [23]. Extraction of populations from such fluorescence spectra thus need to take polarization

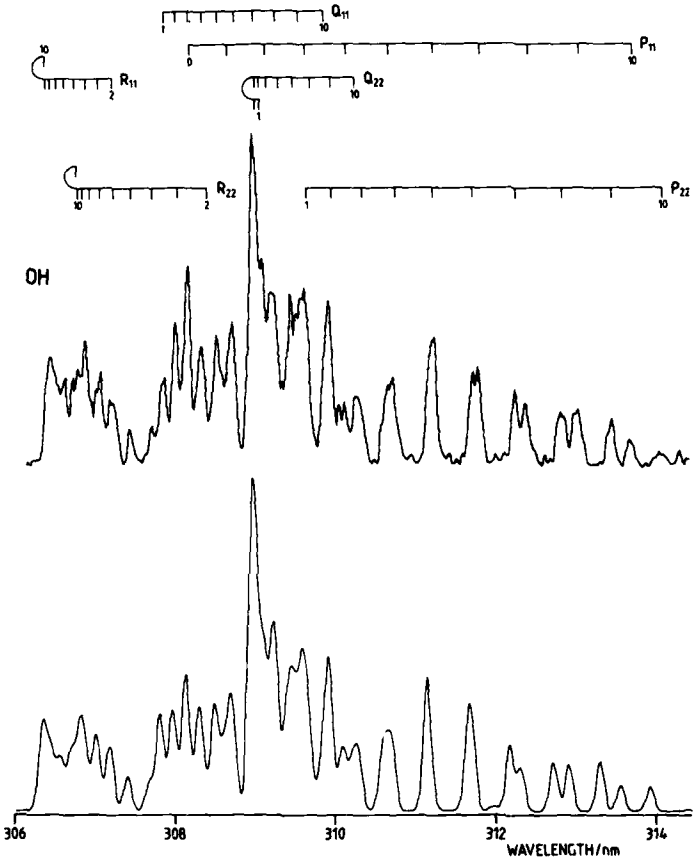

Fig. 1. OH($A\,^2\Sigma^+$) fluorescence spectrum following two-photon excitation of H_2O at 266 nm. Upper trace is the experimental spectrum, lower trace is that simulated using the populations shown in fig. 2. The assignments show the branches numbered with N' values.

into account, particularly (as in the present case) if the detection system is polarization sensitive. Separate measurements on the degree of polarization on isolated features of the spectrum shown in fig. 1 indicate that the polarization index R_ϵ (defined as $(I_\parallel - I_\perp)/(I_\parallel + 2I_\perp)$ where $I_\parallel$ and $I_\perp$ are the intensities of emission parallel and perpendicular to ϵ, the electric vector of the photolysis beam) is close to zero for all wavelengths studied, and that such corrections were unnecessary. Populations in the F_1 and F_2 components of the N' levels were extracted by measuring the intensities of isolated features in spectra such as that of fig. 1 (at higher resolution where necessary). In some cases peak intensities were due to emission from a single upper level (for example, for the high P_{11} lines at long wavelengths). For peaks which consisted of overlapped lines (either from satellite branches at the same value of N' but different

J', or from sets of lines at different N') peak intensities were expressed as sums of contributions from different levels, and resultant sets of simultaneous equations were solved for the upper state populations. In all cases intensities were related to populations by using the Einstein A coefficients of Chidsey and Crosley [24]. Table 1 shows the populations derived for separate F_1 and F_2 components. Spectral simulations carried out with these values were indistinguishable, within the accuracy of the experimental data, from those in which both components were set at the average of those in table 1, and these average values are shown in fig. 2 as a plot of relative population versus N'/N'_{max}, with $N'_{max}=9$. Fig. 1 shows a simulation carried out using these values (with populations for the undetermined $N'=0$ and 2 levels interpolated from the data of fig. 2) showing excellent agreement with the experimental data.

Fig. 2 also shows that the population distribution obtained from the one-photon dissociation of H_2O at 130.4 nm by Simons and co-workers [5], when scaled to the same N'_{max} value, is very similar to that of the present study, apart from a rather higher population observed at low N' values (0–2) in the latter case. Both distributions peak at $\approx 75\%$ of the maximum value, somewhat less than the very high rotational energies seen at lower photolysis wavelengths [2,3,5,6]. If the difference in excitation energies in the two cases is neglected, then at first sight this result would be consistent with the same dissociation dynamics for one- and two-photon excitation, i.e.

Table 1
Relative populations in the F_1 and F_2 components of OH($A\,^2\Sigma^+$, N') produced by the two-photon dissociation of H_2O at 266 nm

N'	Populations	
	F_1	F_2
1	0.53	0.57
2	–	–
3	–	0.65
4	0.89	0.72
5	0.83	0.86
6	1.00	0.80
7	0.87	0.95
8	0.69	0.60
9	0.70	0.76
10	0.36	0.38

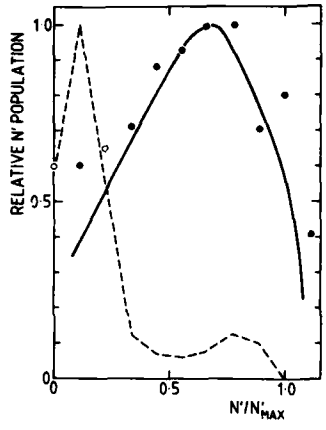

Fig. 2. Rotational populations in OH($A\,^2\Sigma^+$) plotted as a function of N'/N'_{max}, where N'_{max} is the maximum value of N' allowed by energy conservation for dissociation of H_2O with zero internal energy. The experimental points from the present study are given as filled circles (obtained as described in the text), the two open circles are interpolated values to give the best fit to the experimental data. The solid line is the single-photon dissociation result of Simons et al. at 130.4 nm [5], the dashed line is the predicted distribution for dissociation at a "resonance" at 133.7 nm by Segev and Shapiro [15].

both initially populating the $\tilde{B}\,^1A_1$ state from which $A\,^2\Sigma^+$ OH fragments are formed. However, marked differences in the fragment fluorescence polarization are seen in the two cases. Single-photon excitation of H_2O to produce OH($A\,^2\Sigma^+$) via a state of $^1A_1$ symmetry can produce a limiting value of -0.4 for $A_0^{(2)}$, the quadrupole moment of the J' vectors of OH relative to ϵ, which is directly related to the experimentally measured R_ϵ [5,23]. Simons et al. found $A_0^{(2)}$ to be a function of N', decreasing from -0.1 at low N' to a minimum of -0.35 at N'_{max}, close to the limiting value [5]. The lower alignment at low N' was attributed to H_2O molecules with trapped trajectories on the $\tilde{B}$ state surface (as predicted by Segev and Shapiro [15]) and thus with relatively long lifetimes, reducing the $A_0^{(2)}$ value. *Two*-photon excitation to the $\tilde{B}\,^1A_1$ state would predict a limiting value for $A_0^{(2)}$ of $+1.14$ [25] if the intermediate (virtual) state were of $^1B_1$ symmetry, and this has been suggested to be the case for two-photon excitation to the

continuum at energies corresponding to a single-photon absorption near 124 nm, with the $\tilde{A}\,^1B_1$ state making the major contribution to the transition moment as an intermediate [6]. Excitation to a $^1A_2$ state was eliminated as a possibility in this study [6], as the maximum value of $A_0^{(2)}$ experimentally found, 0.6 at high N', was larger than the limiting value of 0.29 expected for $^1A_2$ $\tilde{X}\,^1A_1$ excitation with two photons [25]. Our preliminary polarization results, although presently subject to considerable experimental uncertainty, show $A_0^{(2)}$ lying between the limits ± 0.2 at high N' (where extraction of alignment parameters is less affected by degradation of the polarization by electronic and nuclear spin coupling [5]). These results, although lying closer to the $^1A_2$ limiting value than the $^1A_1$, are unable to distinguish between the two, as lifetime lengthening could be invoked in either case to bring the predicted values into the experimental range (in contrast to the clear distinction possible following excitation near 124 nm [6]).

We make the following points:

(i) If excitation is to the $\tilde{B}\,^1A_1$ state, then a mechanism is needed to reduce the anisotropy (i.e. to make $A_0^{(2)}$ closer to zero) from values seen, at high N', following single-photon dissociation at 130.4 nm. Long-lived trajectories have been suggested to reduce the anisotropy at low N' values in the single-photon case [5], but are calculated to lead to high populations in low N' levels (if predissociation of the $\tilde{B}$ state is neglected): Fig. 2 shows the predicted distribution at 133.7 nm where such trajectories lead to a resonance [15], which is clearly different from the present results (although it should be pointed out that two-photon excitation at 266 nm corresponds to absorption on the shoulder of this predicted resonance, where a higher rotational excitation would occur). Predissociation of the $\tilde{B}$ state has been suggested to explain the lack of low N' population generally observed in the $OH(A\,^2\Sigma^+)$ state [5,26], as longer-lived trajectories which lead to low N' values have a higher probability of crossing from the $\tilde{B}$ state to, for example, the $\tilde{A}\,^1A_1$ state to form ground state products [26]. However, the present results would require $\tilde{B}$ state H_2O molecules leading to high N' fragments to be longer lived than those following 130.4 nm excitation: long-lived behaviour is predicted to be more important as the excitation energy decreases [18], but whether this is sufficient to explain the present behaviour is unclear.

(ii) If excitation is to the $^1A_2$ state, then less reduction in the anisotropy is required, but a crossing to the $\tilde{B}\,^1A_1$ surface is needed for OH $A\,^2\Sigma^+$ fragments to form (the $^1A_2$ state does not correlate adiabatically with $OH(A\,^2\Sigma^+)$ [27]). A crossing at large HO–H distances between the $\tilde{B}\,^1A_1$ and $^1A_2$ states (which now become $^1A'$ and $^1A''$ in C_s symmetry) has been predicted [28].

(iii) An alignment factor close to zero could occur by fortuitous cancelling of alignments of different sign in the two-photon absorption to the $\tilde{B}\,^1A_1$ state, the differences caused by differing intermediate state symmetries. This could occur for the sequences $^1A_1 \leftarrow (^1A_1 \text{ or } ^1B_2) \leftarrow {}^1A_1$ and $^1A_1 \leftarrow (^1B_1) \leftarrow {}^1A_1$ which yield limiting $A_0^{(2)}$ values of -0.57 and $+1.14$ respectively [25]. The former would thus need to dominate (presumably via the $\tilde{X}\,^1A_1$ ground state as intermediate), in contrast to two-photon excitation near 124 nm, where the predominant intermediate state is clearly $\tilde{A}\,^1B_1$ [6].

Further alignment data, and results on D_2O, on the formation of ions and on attempts to observe LIF on the $OH(X\,^2\Pi)$ fragment will be presented in a future publication [27]. Whilst this manuscript was in preparation, we became aware of a similar study by Shafizadeh et al. [29] which, although at lower resolution, shows an OH fluorescence spectrum similar to that reported here.

Acknowledgement

The research reported herein has been sponsored in part by the United States Army through its European Research Office. JBH is grateful to the SERC for the award of a Visiting Fellowship.

References

[1] M.N.R. Ashfold, M.T. Macpherson and J.P. Simons, Topics Current Chem. 86 (1979) 1.
[2] T. Carrington, J. Chem. Phys. 41 (1964) 2012;
H. Okabe, J. Chem. Phys. 72 (1980) 6642;
A. Gedanken, J. Mol. Spectry. 82 (1980) 246.
[3] I.P. Vinogradov and F.I. Vilesov, Opt. Spectry. 40 (1976) 32; 44 (1978) 653.

[4] C. Fotakis, C.B. McKendrick and R.J. Donovan, Chem. Phys. letters 80 (1981) 598;
R.J. Donovan, C. Fotakis, A. Hopkirk, C.B. McKendrick and A. Torre, Can. J. Chem. 61 (1983) 1023.
[5] J.P. Simons, A.J. Smith and R.N. Dixon, J. Chem. Soc. Faraday Trans. II 80 (1984) 1489.
[6] A. Hodgson, J.P. Simons, M.N.R. Ashfold, J.M. Bayley and R.N. Dixon, Chem. Phys. Letters 107 (1984) 1; Mol. Phys. 54 (1985) 351.
[7] M.T. Macpherson and J.P. Simons, Chem. Phys. Letters 51 (1977) 261.
[8] J.P. Simons and A.J. Smith, Chem. Phys. Letters 97 (1983) 1.
[9] L.C. Lee, L. Oren, E. Phillips and D.L. Judge, J. Phys. B 11 (1978) 47;
L.C. Lee, J. Chem. Phys. 72 (1980) 4334;
O. Dutuit, A. Tabche-Fouhaile, I. Nenner, H. Frohlich and P.M. Guyon, J. Chem. Phys. 83 (1985) 584;
L.C. Lee and M. Suto, Chem. Phys. 110 (1986) 161.
[10] R.N. Dixon, Mol. Phys. 54 (1985) 333;
M.P. Docker, A. Hodgson and J.P. Simons, Mo . hys. 57 (1986) 129.
[11] H.J. Krautwald, L. Schnieder, K.H. Welge and M.N.R. Ashfold, Faraday Discussions Chem. Soc. 82 (1986) 99.
[12] F. Flouquet and J.A. Horsley, J. Chem. Phys. 60 (1974) 3767.
[13] G. Theodorakopoulos, I.D. Petsalakis and R.J. Buenker, Chem. Phys. 96 (1985) 217.
[14] V. Staemmler and A. Palma, Chem. Phys. 93 (1985) 63.
[15] E. Segev and M. Shapiro, J. Chem. Phys. 77 (1982) 5604.
[16] L.D. Dunne, H. Guo and J.N. Murrell, Mol. Phys. 62 (1987) 283.
[17] K. Weide and R. Schinke, J. Chem. Phys. 87 (1987) 4627.
[18] R. Schinke, V. Engel, S. Hennig, K. Weide and A. Untch, Ber. Bunsenges. Physik. Chem. 92 (1988) 295.
[19] J.W.C. Johns, Can. J. Phys. 41 (1963) 209; 49 (1971) 944;
R.J. Buenker and S.D. Peyerimhoff, Chem. Phys. Letters 29 (1974) 253;
N.W. Winter, W.A. Goddard and F.W. Bobrowicz, J. Chem. Phys. 62 (1975) 4325;
G. Theodorakopoulos, I.D. Petsalakis, R.J. Buenker and S.D. Peyerimhoff, Chem. Phys. Letters 105 (1984) 253;
G. Theodorakopoulos, C.A. Nicolaides, R.J. Buenker and S.D. Peyerimhoff, Chem. Phys. Letters 89 (1982) 164.
[20] D. Yeager, V. McKoy and G.A. Segal, J. Chem. Phys. 61 (1974) 755.
[21] F.W.E. Knoop, H.H. Brongersma and C.J. Oosterhoff, Chem. Phys. Letters 13 (1973) 20.
[22] M.N.R. Ashfold, J.M. Bayley and R.N. Dixon, Can. J. Phys. 62 (1984) 1806.
[23] C.A. Greene and R.N. Zare, Ann. Rev. Phys. Chem. 33 (1982) 119;
M.T. Macpherson, J.P. Simons and R.N. Zare, Mol. Phys. 38 (1979) 2049.
[24] I.L. Chidsey and D.R. Crosley, J. Quant. Spectry Radiat. Transfer 23 (1980) 187.
[25] G.W. Loge and J.R. Wiesenfeld, J. Chem. Phys. 75 (1981) 2795.
[26] R.N. Dixon, Mol. Phys. 54 (1985) 333.
[27] C.G. Atkins, R. Briggs, J.B. Halpern and G. Hancock, to be published.
[28] S. Tsurubuchi, Chem. Phys. 10 (1975) 335.
[29] N. Shafizadeh, J. Rostas, J.M. Lemaire and F. Rostas, Chem. Phys. Letters 152 (1988) 75.

Photodissociation of D_2O in the second continuum by two photon absorption at 266 nm

R.G. Briggs, J.B. Halpern [a] , G. Hancock

Physical Chemistry Laboratory Oxford University
South Parks Road, Oxford OX1 3QZ, U.K.

N. Shafizadeh[1,2], J. Rostas[2], J.L. Lemaire [1,b] , F. Rostas[1]

1: DAMAp et UA 812 du CNRS
Observatoire de Paris, 92195 Meudon Cedex, France
2: Laboratoire de Photophysique moléculaire du CNRS
B[t] 213 Université de Paris-Sud, 91405 Orsay, France

Abstract

The rotational population distribution of $OD^*(A^2\Sigma^+)$ fragments produced by two photon photodissociation of D_2O at 266 nm has been determined from an analysis of the $A^2\Sigma^+ - A^2\Pi$ fluorescence. The distribution obtained seems to confirm the existence of long lived trajectories when the dissociation process of H_2O or D_2O is initiated with a small energy excess above the threshold for production of excited OH (OD) fragments.

II - 22/12/88

a) Permanent adress: Dept. of Chemistry, Howard University, Washington DC.

b) On leave from Université de Paris VII

1. Introduction

In two recent papers (1,2) reporting independent work, the authors pointed out the interest of studying the photodissociation of H_2O (D_2O) at excitation energies corresponding to the "second continuum" ($\tilde{B}^1A_1 \leftarrow \tilde{X}^1A_1$) near the threshold for production of OH (OD) excited in the $A^2\Sigma^+$ state.

Theoretical studies of this process (3,4) in H_2O predict structure in the absorption cross sections for wavelengths between 130 and 137 nm, corresponding to the maximum of the band and the threshold for OH^* ($A^2\Sigma^+$) production respectively. This structure has been attributed to so called trapped (3) or indirect (4) trajectories of the dissociating system, which are associated with specific rotational populations of the OH radicals formed.

In the experiments reported previously (1,2), H_2O was excited by light at 266 nm, with two-photon absorption (at an energy corresponding to a single 133 nm photon) followed by dissociation on the $\tilde{B}\ ^1A_1$ state surface. The channel leading to excited OH was monitored via the $A^2\Sigma^+ \rightarrow X^2\Pi$ fluorescence of the OH radical. The OH rotational population distributions observed in these experiments are rather broad, peaked near the highest energetically accessible rotational quantum numbers. They are similar to those obtained by one photon excitation at 130.4 nm (5) but quite different from those obtained with two photons at 248 nm (6). In the latter case there is a complete lack of population in the lower half of the rotational level range while at 130.4 and 133 nm (2 photons at 266 nm) this range is quite sizeably populated.

It was felt that these results could be interpreted as indicating that the lowest range of rotational energies was favoured when the excess excitation energy was decreased. As the experiments were carried out at a fixed excitation frequency it was not possible to determine if the rotational distribution changed markedly with frequency, and if such changes could be correlated with predicted "resonances" in the absorption spectrum (3). However, repeating the same experiment with D_2O amounts to changing the excitation energy and gives another chance of observing such an effect. This was done independently in both laboratories before they joined efforts to analyse the data.

2. Experimental results

The apparatus used in Oxford and in Meudon are identical to the ones described in the previous papers (1,2). D_2O is excited at 266 nm by a quadrupled YAG laser and the fluorescence is observed at right angle through a short focal length monochromator. The working resolution was 0.1 nm at Oxford and 0.3 nm at Meudon. The former is sufficient in OH to obtain relative populations by comparison of line intensities. Indeed for most N'

values there is at least one feature whose intensity depends on one, or at most two, N' values. The 0.3 nm resolution, on the other hand, is insufficent to resolve any but the highest N' lines of the P branch.

In the previously reported experiments (1) the rotational population distribution was deduced from the low resolution spectra by a trial and error procedure where simulated spectra obtained from trial populations distributions were compared to the experimental spectrum until the best fitting population was determined.

In OD the spectral line density is about twice as large as in OH and for similar experimental conditions the signal is significantly lower. Therefore the Oxford spectra could not be analyzed safely by the intensity ratio technique used previously (2) and the Meudon spectra had a poorer signal to noise ratio. Considering the very good agreement reached for OH by the two methods applied independently (1,2), it was decided to analyze the best resolved experimental spectra with the fitting technique used earlier on the least resolved ones.

The necessary OD spectroscopic constants were redetermined from the original optical data (7) of the $A\ ^2\Sigma^+ - X\ ^2\Pi_i$ (0-0) band. As for OH, the model Hamiltonians used for the $^2\Sigma^+$ and $^2\Pi$ states were written in the N^2 formalism. The parameters of the ground state were fixed to the values derived by Brown et al. (8) from the best available microvawe, laser magnetic resonance and far infrared data. The complete set of parameters is given in Table I. These parameters were then used with the same Hamiltonian matrices to calculate the line positions and intensities. Synthetic spectra were produced after introducing the relevant instrumental width. It was found that the higher resolution spectra were best reproduced using a 0.07 nm wide gaussian instrumental function.

Figure 1 shows the experimental spectrum obtained and the best fitting simulated spectrum. The corresponding rotational population distribution is shown in Figure 2 and compared to the one found by the same method for OH (i.e. the simulated spectrum technique applied to the best resolved data*). A very similar population distribution is found when starting from the lower resolution spectrum which, conversely, is very well fitted by the degraded synthetic spectrum determined from the higher resolution data.

3. Discussion

At first sight the rotational population distribution of the OD product is similar to that of OH. However its peak is sharper and somewhat displaced towards lower values of N'. A relatively long "tail" not seen in OH extends to N'=11 although the highest energetically

* This distribution differs slightly from the one obtained from the low resolution data and presented in (1).

accessible level is N'=8 if the rotational energy of D_2O is neglected. This tail clearly appears as related to the initial thermal energy of H_2O when the population distributions are plotted on a linear energy scale (Figure 3). The tails in OH and OD become approximately parallel in this representation, showing that the average excess rotational energies in the two fragments due to parent internal energies are the same.

The dynamical effects occuring during dissociation are better displayed on population plots involving a relative scale where the rotational quantum number N' is normalized to N'_{max}, the highest energetically accessible rotational level (N'_{max}=8 for OD and 9 for OH). On such a scale population distributions can be compared for the two isotopes and for different excitation energies. It can be seen (Figure 4a) that apart from a rather more pronounced peaking in the OD data, the two distributions are very similar for $N'/N'_{max} \leq 1$, showing maxima at $N'/N'_{max} \cong 0.8$ and with a plateau at $N'/N'_{max} \cong 0.4$.

These experimental results can be compared to those of Simons et al. (5) where excitation was achieved by one photon at 130.4 nm and those of Hodgson and al. (6) where two photons at 248 nm were used to excite the $\tilde{C}^1B_1$ state which is predissociated by the $\tilde{B}^1A_1$ state. In these two experiments the excess energy was 0.5 and 1 eV respectively. Comparing Figures 4b and 4a, it can be clearly seen that the distributions at 0.5 eV (130.4 nm) are similar to the ones observed at 0.2 eV (2 x 266↔133 nm) whereas at 1 eV (2 x 248↔124 nm) the distributions also peak around N'/N'_{max}=0.75 but the low rotational levels are completely unpopulated.

The presently available theoretical results are compared on Figure 4c. The results of Segev and Shapiro (3) and Schinke (9) for OH at 0.2 eV, although not in good agreement, clearly show a trend to low N' population while the calculation of Weide and Schinke (10) at 0.5 eV result in a high N' peak. At 0.2 eV, the population distribution of Segev & Shapiro corresponds to an excitation at exact resonance (133.7 nm) while that of Schinke was calculated for an energy corresponding to 133 nm and was not meant to be exactly on resonance. It must also be kept in mind that both calculations were done for zero rotational excitation of the parent molecule.

The experimental and theoretical results reviewed above seem to sustain the view that, while photodissociation of H_2O (D_2O) at relatively high excess energy (≥0.5 eV) tends to proceed through direct trajectories (10), a decrease of the excess excitation energy below 0.5 eV progressively favours long lived ones (3,4). The direct trajectories are associated to high rotational excitation of OH (OD) and the long lived trajectories give rise to low rotational states and to the absorption resonances. Experiments at fixed frequency and with room temperature H_2O cannot be expected to display in an obvious fashion the effect of resonances on the rotational distribution. However it seems that the contribution of long lived trajectories (i.e. low N') is more and more important as one decreases the excitation

energy. The low energy excitation experiments are in fact strongly influenced by these trajectories although they are probably discriminated against by non adiabatic transfer. Indeed, as pointed out by Dixon (11), the $\tilde{B} \rightarrow \tilde{A}$ transitions which can take place each time the molecule crosses the seam connecting the two surfaces in the linear geometry, will cause a large part of the molecules which oscillate on the $\tilde{B}$ surface to dissociate to ground state rather than to "cool" excited OH radicals.

The fact that such fragments form a sizeable part of the OH formed by low excess energy excitation would indicate that in this case, even away from resonance, long lived trajectories constitute an important part of all the trajectories initiated.

4. Conclusion

The present study of the OD rotational population distribution resulting from D_2O photodissociation at 133 nm equivalent energy is interpreted as a confirmation of the importance of long lived trajectories in the photodissociation process below 0.5 eV excess energy. This is an encouragement to pursue the planned experiments to detect the variation of product distribution with excitation energy by direct VUV excitation of jet cooled H_2O.

Acknowledgements

The authors wish to thank Professor J.P. Simons for initiating the contacts between the two laboratories and providing helpful suggestions. The research reported herein has been sponsored in part by the United State Army through its European Research Office. JBH is grateful to the SERC for the award of a Visiting Fellowship. Specific funding by Observatoire de Paris and CNRS is also acknowledged.

References

(1) N. Shafizadeh, J. Rostas, J.L. Lemaire, F. Rostas, Chem. Phys. Lett. 152 (1988) 75

(2) C. G. Atkins,R.G. Briggs,J.B. Halpern, G. Hancock Chem. Phys. Lett. 152 (1988) 81

(3) E. Segev, M. Shapiro, J. Chem. Phys. 77 (1982) 5604

(4) R. Schinke, V. Engel, S. Hennig, K. Weide, A. Untuch, Ber. Bunsenges. Phys. Chem. 92 (1988) 295

(5) J.P. Simons, A.J. Smith, R.N. Dixon, J. Chem. Soc., Faraday II 80 (1984) 1489

(6) A. Hodgson, J.P. Simons, M.N.R. Ashfold, J.M. Bayley, R.N. Dixon, Mol. Phys. 54 (1985) 351

(7) M. A. A. Clyne, J.A. Coxon, A.R. Woon Fat, J. Mol. Spec. 46 (1973) 146

(8) J. M. Brown, J.E. Schubert, C.E. Brown, J.S. Geiger, D.R. Smith, J. Mol. Spec. 114, (1985) 185

(9) R. Schinke, Private communication

(10) K. Weide, R. Schinke, J. Chem. Phys. 87 (1987) 4627

(11) R.N. Dixon, Mol. Phys. 54 (1985) 333

(12) G.H. Herzberg Molecular Spectra and Molecular Structures, Vol. III. Van Nostrand, New York (1966) p. 585

Table I – Molecular parameters in cm^{-1} for the $A^2\Sigma^+$ and $X\ ^2\Pi$ states of OD.

		$A\ ^2\Sigma^+$	$X\ ^2\Pi$
	T	32487.17(2)	0.0
	A	–	-139.01607
	B	9.04357(5)	9.87879
	D	0.0005783(19)	0.000538309
10^6	H	0.0171(2	0.01935005
	γ	0.1188(8)	-0.064289
10^4	γ_D	-0.129(14)	0.069
10^7	γ_H	–	–
	p	–	0.125481
10^4	p_D	–	-0.145
10^8	p_H	–	0.050
	q	–	-0.0109
10^4	q_D	–	0.0220
10^8	q_H	–	-0.02735

The ground state parameters were held fixed to the values of Ref. (8) in the least squares fitting procedure. Using the resulting set of parameters, together with the Hamiltonian matrix elements derived in the N^2 formalism, the (0-0) wavenumbers of the (A-X) transition of OD are calculated to better than 0.1 cm^{-1} up to N=30.

Parenthetical figures indicate the uncertainties (1σ) in units of the least significant figure.

Figure captions

Figure 1:

Experimental and best fitting simulated fluorescence spectrum of OD following dissociation of D_2O by two photons at 266 nm. Spectral resolution: 0.07 nm.

Figure 2:

Rotational population distribution of the OH and OD fragments. The OH distribution results from applying the trial and error fitting procedure to the experimental spectrum of Ref. (2).

Figure 3:

Rotational population distribution of OH and OD ($A^2\Sigma^+$, v'=0). The rotational energies of the two radicals are placed on the same scale which has its origin on the OH X $^2\Pi_{3/2}$ (v"=0, J"=3/2) level. The OH and OD energies are set on the common scale by placing the H_2O and D_2O zero point energies in coïncidence. The dissociation energy of H_2O is taken to be 5.113_6 eV (12) from which that of D_2O is deduced to be 5.20_2 eV from tabulated spectroscopic data and isotopic shifts.

Figure 4:

Rotational populations vs. reduced rotational number (N'/N'_{max})

a) Experimental populations for OH and OD

b) Experimental populations resulting from excitation of H_2O and D_2O at 0.5 eV excess energy (one photon at 130.4 nm, Ref. (5)) and 1 eV excess energy (2 photons at 248 nm, Ref. (6))

c) Theoretical results: "Shapiro 0.2 eV": Ref. (3); "Schinke 0.2 eV": Ref. (9); "Schinke 0.5 eV": Ref. (10)

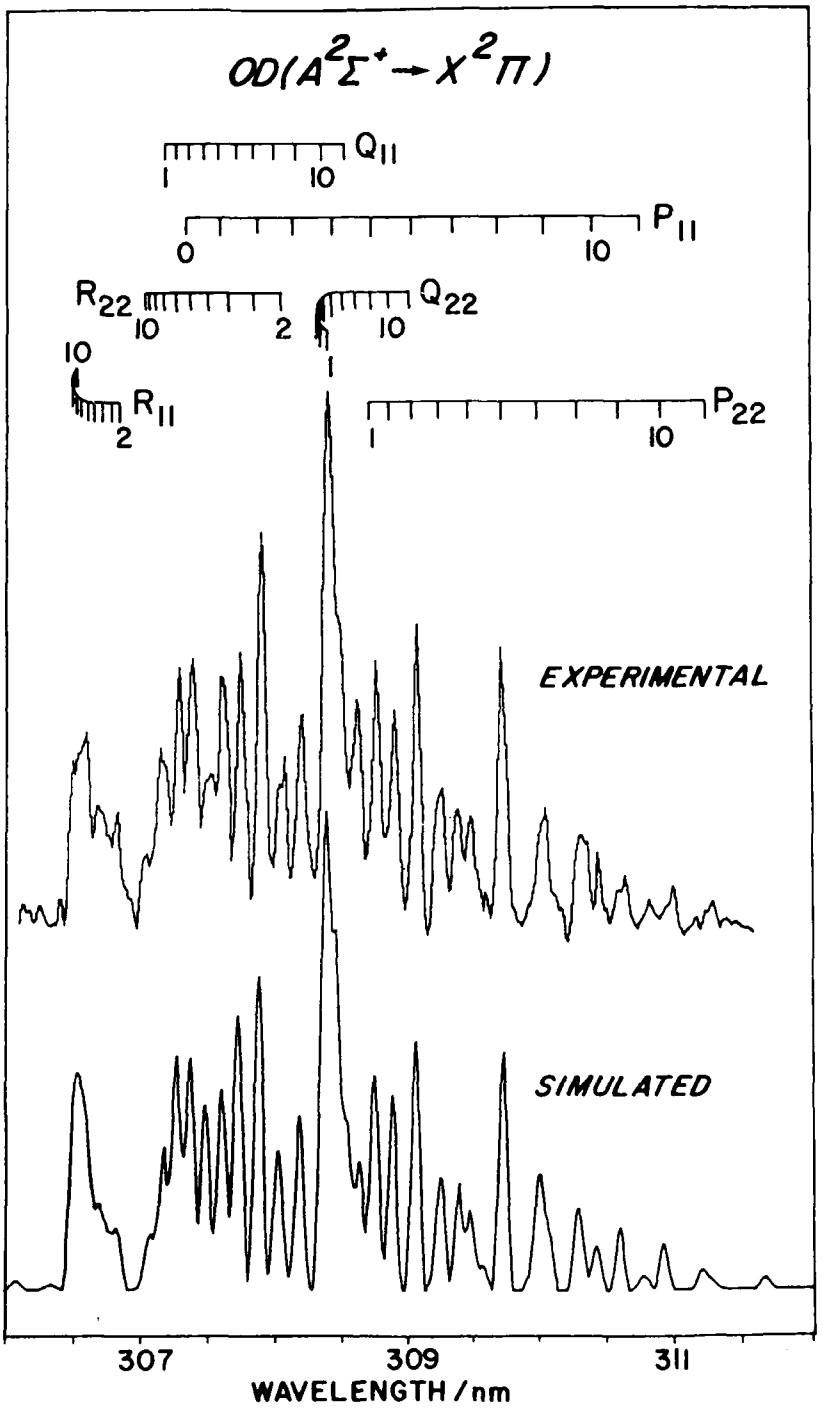
OD($A^2\Sigma^+ \rightarrow X^2\Pi$)
Q_{11}
1
10
P_{11}
0
10
R_{22}
10
2
Q_{22}
10
1
10
R_{11}
2
P_{22}
1
10
EXPERIMENTAL
SIMULATED
307
309
311
WAVELENGTH / nm

FIG 1

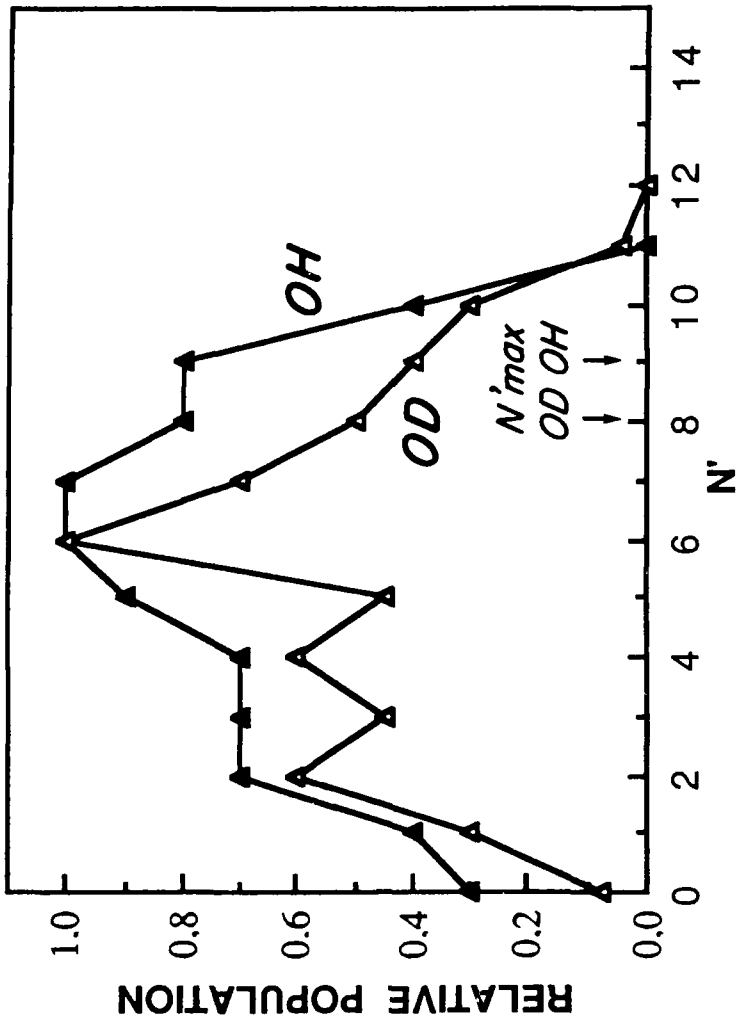
RELATIVE POPULATION
1.0
0.8
0.6
0.4
0.2
0.0
0
2
4
6
8
10
12
14
N'
OH
OD
N'max
OD OH

FIG 2

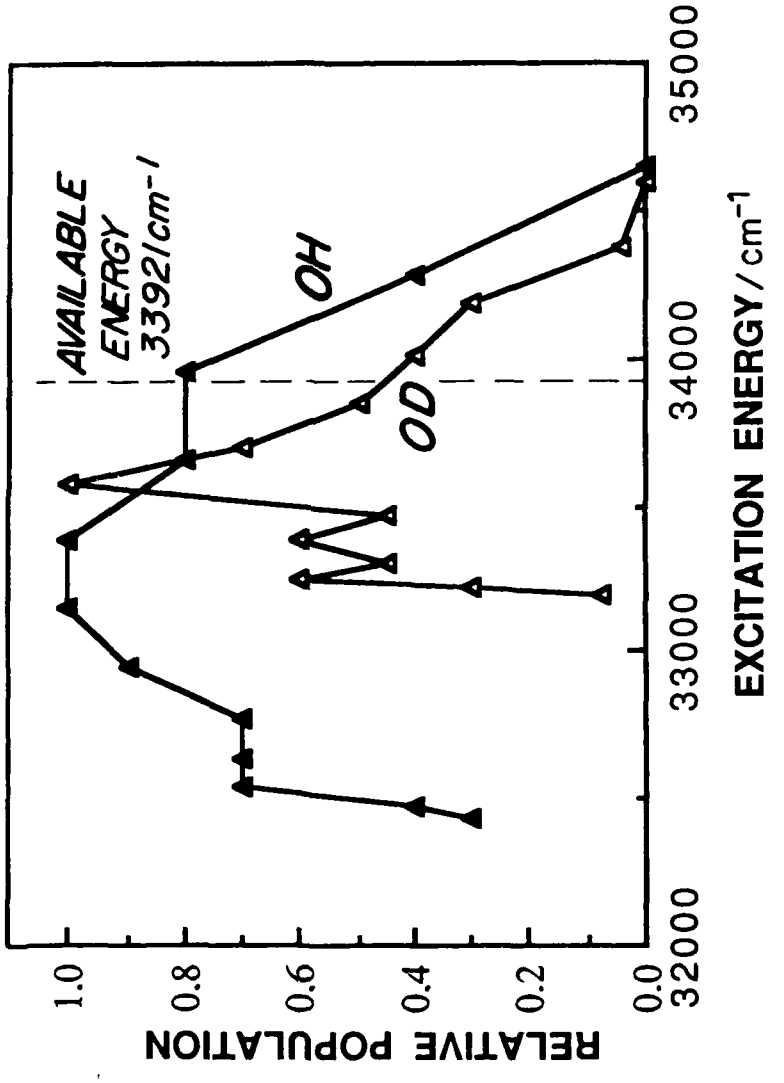
AVAILABLE ENERGY 33921cm⁻¹
OH
OD
RELATIVE POPULATION
0.0
0.2
0.4
0.6
0.8
1.0
32000
33000
34000
35000
EXCITATION ENERGY / cm⁻¹

FIG 3

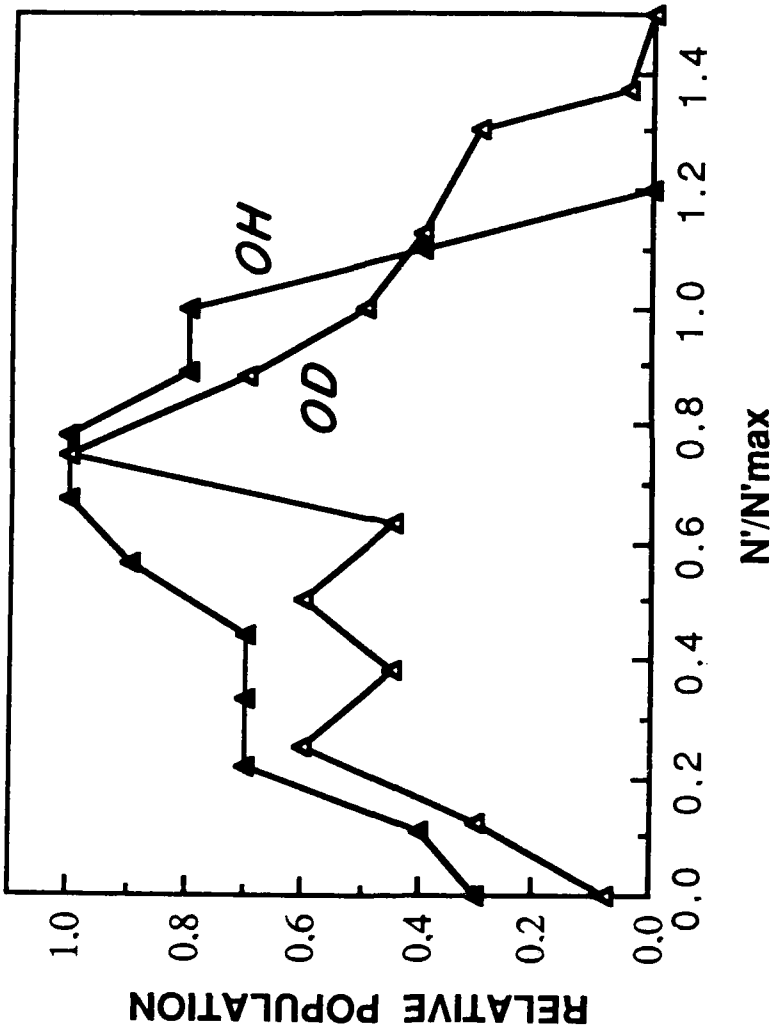
RELATIVE POPULATION
1.0
0.8
0.6
0.4
0.2
0.0
0.0
0.2
0.4
0.6
0.8
1.0
1.2
1.4
N'/N'max
OH
OD

FIG 4a

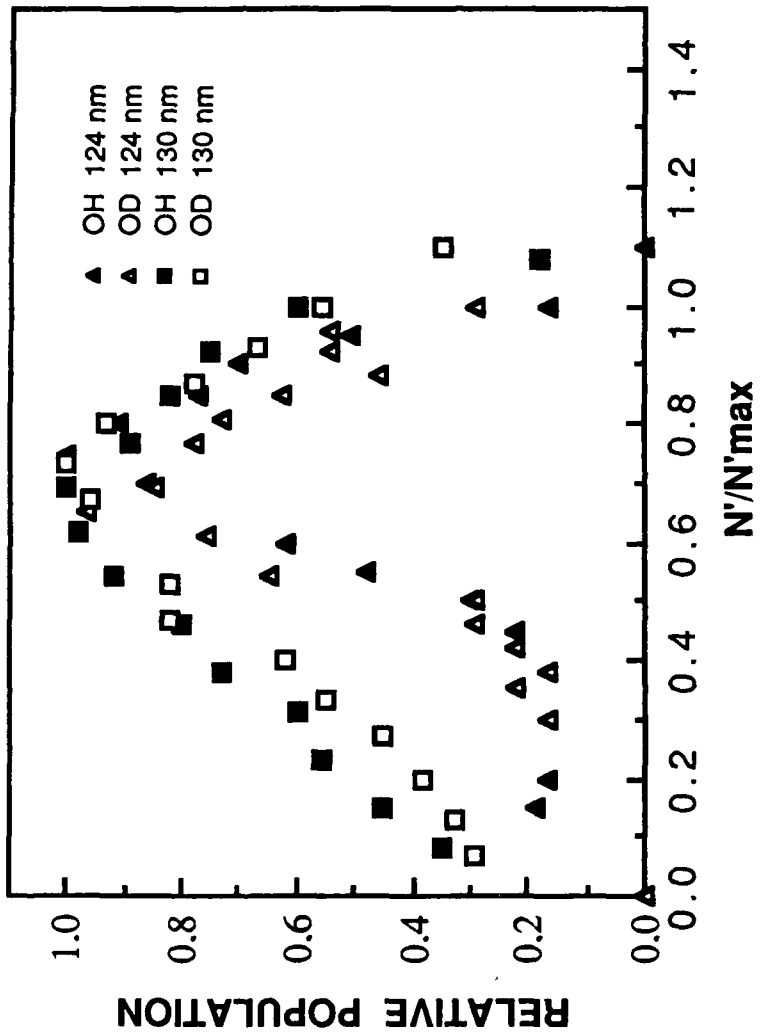
OH 124 nm
OD 124 nm
OH 130 nm
OD 130 nm
RELATIVE POPULATION
N'/N'max
0.0
0.2
0.4
0.6
0.8
1.0
1.2
1.4

FG 4b

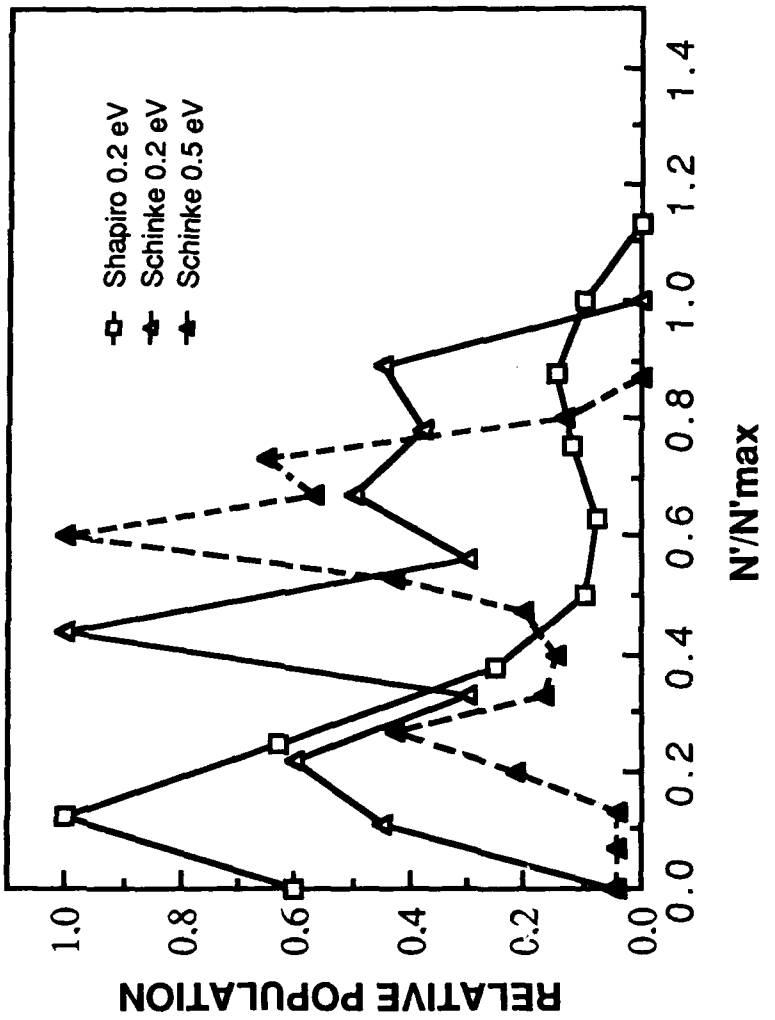
Shapiro 0.2 eV
Schinke 0.2 eV
Schinke 0.5 eV
RELATIVE POPULATION
N'/N'max
0.0
0.2
0.4
0.6
0.8
1.0
1.2
1.4

Fig 4c

PHOTOAFFINITY LABELLING OF ISOPENICILLIN N SYNTHETASE BY LASER FLASH PHOTOLYSIS

Jack E. Baldwin*, Janice B. Coates*, Joshua B. Halpern+# , Mark G. Moloney* and Andrew J. Pratt*.

*The Dyson Perrins Laboratory, University of Oxford, South Parks Road, Oxford, OX1 3QY, U.K., and +The Physical Chemistry Laboratory, University of Oxford, South Parks Road, Oxford, OX1 3QZ, U.K.

SUMMARY

Isopenicillin N synthetase (IPNS), from *Acremonium chrysogenum*, has been photolabelled by laser flash photolysis in the presence of a diazirinyl-containing substrate, DCV (3). Labelling of IPNS by DCV can be inhibited by 52% in the presence of a 13-fold excess of ACV (1a), the natural substrate. In the absence of light, DCV is converted to the corresponding penicillin with comparable K_m but significantly depressed V_{max} relative to ACV. Selective incorporation of [^{14}C]-DCV(5) into IPNS has been demonstrated by fluorography of IPNS analysed by SDS-PAGE. Scintillation counting of labelled IPNS purified on an ion-exchange FPLC column confirms this result. This methodology is applicable for locating the substrate binding site of IPNS.

INTRODUCTION

Isopenicillin N Synthetase (IPNS) is the enzyme responsible for the conversion of L,L,D-α-Aminoadipoyl-cysteinyl-valine (ACV) (1a) to Isopenicillin N (2a) by both filamentous fungi (e.g. *Acremonium chrysogenum*) and streptomycetes (Scheme 1) [1]. In studies aimed at understanding the nature of the enzyme-catalysed reaction, IPNS has been shown to convert a wide variety of analogue substrates into β-lactams, thereby providing routes to a range of new antibiotics [1]. IPNS has been cloned and expressed in an active form at high levels in *E. coli* (*ca.* 20% total protein) [2]. Although its amino acid sequence is known, there are no data currently available about the 3-dimensional structure of IPNS.

It has previously been shown that analogues of ACV with aromatic side chains

---

Abbreviations used: ACV, L,L,D-α-aminoadipoyl-cysteinyl-valine; VCV, L,D-phenoxyacetyl-cysteinyl-valine ; DTT, dithiothreitol; IPNS, isopenicillin N synthetase; DCV, L,D-2-[3-(3-trifluoromethyl-3H-diazirin-3-yl)phenoxy]acetyl-S-carbomethoxy-sulphenyl-cysteinyl-valine; 6-APA, 6-aminopenicillanic acid; [^{14}C]-DCV, L,D-2-[3-(3-trifluoromethyl-3H-diazirin-3-yl)phenoxy][2-^{14}C]-acetyl-S-carbomethoxysulphenyl-cysteinyl-valine.

#Present address: Department of Chemistry, Howard University, Washington D.C. 20059, USA.

(e.g. L,D-phenoxyacetyl-cysteinyl-valine (VCV)(**1b**)) are substrates for IPNS and that these substrates have similar Michaelis constants (K_m) to the native substrate ACV but considerably smaller maximal rate parameters (V_{max}); under identical incubation conditions this results in poor conversion yields [3]. However aryl-substituted substrates are more readily accessible, and produce β-lactams of significantly higher antibiotic activity, than aminoadipate-derived peptides. We are therefore interested in altering the substrate specificity of IPNS *via* mutagenesis to favour aryl-substituted peptide substrates, and are investigating photoaffinity labelling as a means of providing relevant structural information for this and other aspects of IPNS research.

Photoaffinity labelling [4] was chosen as a suitable technique for the identification of the side-chain binding site of IPNS. Photolysis of photoaffinity reagents generates highly reactive species which label regions of the protein in contact with the bound inhibitor, irrespective of the nature of the amino-acid residues present. Although azides have been widely used for the photoaffinity labelling of enzymes [4], they are readily reduced by thiols, so that their application to labelling studies of IPNS, which requires a reducing environment to remain active, was inappropriate. Diazirines, however, have found widespread utility in such work, since they are readily accessible, chemically and thermally inert, stable to physiological conditions, and can be cleanly photolysed at wavelengths in the near-ultraviolet [4]. Their suitability for studies with IPNS was evident, and L,D-2-[3-(3-trifluoromethyl-3H-diazirin-3-yl)phenoxy]acetyl-S-carbomethoxy-sulphenyl-cysteinyl-valine (DCV) (**3**) has been synthesised as a potential photoaffinity inhibitor of IPNS [5]. We herein report the kinetic data for conversion of DCV into the corresponding penicillin (**4**) and the successful photoaffinity labelling of IPNS with this reagent.

MATERIALS AND METHODS

L,D-2-[3-(3-Trifluoromethyl-3H-diazirin-3-yl)phenoxy]acetyl-S-carbomethoxy-sulphenyl-cysteinyl-valine (DCV) was prepared according to the literature method [5], and reduced to the free thiol *in situ* with dithiothreitol (DTT). DTT and Trizma base were from Sigma Chemical Company, Poole, Dorset, U.K. ACV and 6-amino-penicillanic acid were gifts from Eli Lilly and Co., and other chemicals were from BDH Chemicals, Poole, Dorset, U.K., or Aldrich Chemical Company Ltd., Gillingham, Dorset, U.K.

Irradiations were performed with a mercury source (Mineralight lamp) at 254 nm, or a frequency-tripled neodymium - YAG laser at 355 nm (SX lasers System 2000, Cambridge, England). Quartz cells, either 1 mm or 1 cm path length, were used for the irradiations. The power output of the laser at 355 nm was measured using a Photon Control (Cambridge, England) Power Meter, and found to be 21 +/- 2 mJ/pulse, at a repetition rate of 10 Hz.

Radiochemical activity measurements were made by liquid scintillation counting with an LKB 1215 Rackbeta instrument, and LKB "Optisafe" scintillation fluid.

Preparation of Cell-Free Extracts of IPNS

IPNS, isolated from *Acremonium chrysogenum*, was prepared according to the published procedure [6]. This fungal enzyme had a specific activity of 0.023 $IUmg^{-1}$, and was estimated to be approximately 60% pure by SDS-PAGE . Recombinant IPNS, cloned from *A. chrysogenum*, was isolated from *E. coli* by the published procedure [7]. This partially purified IPNS was obtained with a specific activity of 0.45 $IUmg^{-1}$, and was estimated to be approximately 80% pure by SDS-PAGE.

Substrate Incubation Method with IPNS

The reaction mixture, containing enzyme, the substrate (ACV or DCV, 0.38 mM), DTT (11 mM), ascorbic acid (1.1 mM) and ferrous sulphate (0.1 mM) in 50 mM ammonium bicarbonate buffer (pH 7.9) with a final volume of 300µl, was incubated at 27°C in an orbital incubator, shaking at 250 $rev.min^{-1}$ for 10-30 min. The reaction was quenched by the addition of acetone (300µl), which precipitated the protein. The sample was centrifuged, and the acetone removed from the supernatant by a stream of air. An aliquot (100µl) from the supernatant was then bioassayed, as described below.

Bioassay of Penicillin Products

Microbiological assays were performed by the hole-plate method [8] using the test organism *Staphylococcus aureus* N.C.T.C. 6571. Solutions (100 µl) to be tested for penicillin content were loaded into wells in bioassay plates, and incubated overnight at 37°C. The diameters of the resultant inhibition zones were measured, and amounts of product estimated by reference to standards prepared using Cephalosporin C.

SDS-Polyacrylamide Gel Electrophoresis (SDS-PAGE)

Analytical electrophoresis was carried out by the method of Laemmli [9] in a slab-gel apparatus (Bio-Rad Laboratories, Richmond, CA, USA) using 10% (w/v) polyacrylamide gels containing SDS (0.1%). Gels were stained with Coomassie Blue R 250 dye.

Fluorography

After destaining, the SDS-gels were soaked in Amplify™ (Amersham) and dried. The gel was then fluorographed using intensifying screens on Fuji X-Ray film at -78 °C for 14 weeks.

Synthetic Methods

Standard chemical procedures as previously described were used [5]. Melting points were recorded on a Buchi 510 apparatus and are uncorrected. I.r. spectra were recorded on a Perkin-Elmer model 681 spectrophotometer. U.V. spectra were recorded either on a Pye Unicam PU 8800 UV-VIS spectrophotometer or a Perkin-Elmer 555 UV-VIS spectrophotometer. ^1H n.m.r. spectra were recorded on a Bruker WH 300 MHz or

AM 250 MHz spectrometer. Mass spectra were recorded on VG Analytical Ltd., ZAB 1F MM 30F mass spectrometers.

Benzhydryl iodoacetate (6)

A solution of iodoacetic acid (500 mg, 2.8 mmol) in acetone (10 ml) was treated with diphenyldiazomethane (650 mg, 3.4 mmol) [10] in acetone (10 ml), and the mixture stirred at room temperature for 2 h. The solvent was removed and the crude material purified by flash chromatography [11] (dichloromethane/light petroleum (1:10, then 1:1, v/v) to give the *title compound* (**6**) as a colourless oil (780 mg, 80% yield). $C_{15}H_{13}O_2I$ requires C, 51.2; H, 3.72%. Found C, 51.1; H, 3.76%. ^1H n.m.r. δ (p.p.m.) (300 MHz, [^2H]chloroform) 3.69 (2H, s, ICH_2), 6.78 (1H, s, $CHPh_2$), 7.16-7.30 (10H, m, ArH). ^{13}C n.m.r. δ (p.p.m.) (62.85 MHz, [^2H]chloroform) -5.4 (t, CH_2I), 78.5 (d, $CHPh_2$), 127.1, 128.1, 128.5 (all d, ArC), 139.4 (s, 4° ArC), 167.5 (s, C(O)O). I.r. (chloroform) 1730 (s), 1495 (m), 1450 (m), 1415(m), 1260 (s), 1085 (s), 980 (m), 700 (s)cm^{-1}. m/z (FI) 352 (M^+).

Benzhydryl 3(3-Trifluoromethyl-3H-diazirin-3-yl)phenoxyacetate (7)

Benzhydryl iodoacetate (**6**) (293 mg, 0.83 mmol), 3-(3-hydroxyphenyl)-3-trifluoromethyl-3H-diazirine [5] (140 mg, 0.69 mmol) and potassium carbonate (143 mg, 1.0 mmol) in acetone (5 ml) were stirred overnight at room temperature. The solvent was removed, and the crude product purified by flash chromatography (dichloromethane, then dichloromethane/light petroleum (1:1, v/v)) to give the *title compound* (**7**) as a colourless oil (360 mg, 99% yield). $C_{23}H_{17}F_3N_2O_3$ requires C, 64.8; H, 4.0; N, 6.6%. Found C, 65.0; H, 4.0; N, 6.7%. ^1H n.m.r. δ (p.p.m.) (300 MHz, [^2H]chloroform) 4.75 (2H, s, OCH_2), 6.75 (1H, s, H2), 6.86 (1H, ddd, J=8.4Hz, H4 or H6), 6.92 (1H, ddd, J=7.5 Hz, H6 or H4), 7.04 (1H, s, $CHPh_2$), 7.27-7.40 (11H, m, ArH). ^{13}C n.m.r. δ (p.p.m.) (62.85 MHz, [^2H]chloroform) 65.5 (t, OCH_2), 78.0 (d, $OCHPh_2$), 113.3 (d), 115.7 (d), 119.8 (d), 124.2 (s), 127.1 (d), 128.2 (d), 128.6 (d), 130.1 (d), 130.8 (s), 139.3 (s), 158.0 (s), 167.5 (s, C(O)O). I.r. (chloroform) 1760 (s), 1605 (m), 1580 (m), 1495 (m), 1450 (m), 1435 (w), 1350 (w), 1340 (w), 1265 (m), 1245 (m), 1085 (m), 700 (s) cm^{-1}. U.V. λ_{max} (methanol) 268 nm (log ε 3.2), 252 (2.4). m/z (field desorption) 426 (M^+).

3(3-Trifluoromethyl-3H-diazirin-3-yl)phenoxyacetic Acid (8)

To the ester (**7**) (100 mg, 0.23 mmol) was added anisole (10 mg, 0.09 mmol), redistilled trifluoroacetic acid (2 ml) and dichloromethane (2 ml), and the mixture stirred at room temperature for 20 min. The solvent was removed *in vacuo*, and the residue treated twice with toluene, and dried under vacuum. The crude product was purified by flash chromatography (dichloromethane then methanol/dichloromethane (1:10, v/v)) to give the *title compound* (**8**) as a white solid (30 mg, 50% yield), m.p. 75-80°. ^1H n.m.r. δ (p.p.m.) (300 MHz, [^2H]chloroform) 4.50 (2H, s, OCH_2), 6.66 (1H, s, H2), 6.80 (1H, d, J=7.8 Hz, H4 or H6), 6.85 (1H, d, J=8.2 Hz, H6 or H4), 7.23 (1H, dd, J=8.0 Hz, J'=8.0 Hz, H5). ^{13}C n.m.r. δ (p.p.m.) (62.85 MHz, [^2H]chloroform/[^2H]methanol) 65.4 (t, OCH_2),

113.5 (d), 119.7 (s and d), 124.2 (s), 130.1 (d), 130.7 (s), 158.0 (s), 171.8 (s, C(O)OH). I.r. (chloroform) 3000 (b), 1740 (s), 1610 (s), 1585 (s), 1495 (m), 1435 (m), 1345 (m), 1295 (m), 1250 (m), 1080 (m) cm^{-1}. U.V. λ_{max} (methanol) 274 nm (log ε 3.2), 352 (2.44). m/z (fast atom bombardment) 260 (M^+, 10%), 232 (54), 175 (46), 174 (28), 157 (100), 145 (53), 138 (45), 131 (54), 127 (32), 115 (65), 109 (22), 107 (37), 103 (37), 87 (24), 75 (28), 69 (30), 63 (27), 57 (47).

(2S,5R,6R)-1-Aza-3,3'-dimethyl-7-oxo-6-[3(3-trifluoromethyl-3H-diazirin-3-yl)phenoxyacetamido-4-thia-bicyclo[3.2.0.]heptane-2-carboxylic acid (4)

Acid (8) (30 mg, 0.12 mmol) in dry toluene (3 ml) and dimethylformamide (2 drops) was treated with oxalyl chloride (18 mg, 0.14 mmol) at 0°C, and stirred for 1 h. The solvent was removed *in vacuo*, and the residue dissolved in acetone (3 ml).

To a solution of 6-aminopenicillanic acid (25 mg, 0.12 mmol) in 4% (w/v) potassium hydrogen carbonate (3 ml) and acetone (3 ml) was added dropwise with stirring and cooling the above acid chloride solution over 10 min., and the solution stirred at 0°C for 1h. The solution was lyophilized, redissolved in 4% potassium hydrogen carbonate solution, and extracted with dichloromethane. The aqueous phase was layered with dichloromethane, and acidified to pH 2 (5M sulphuric acid) and the layers separated. The aqueous phase was washed with dichloromethane, dried over sodium sulphate, and the solvent removed, to give the *title compound* (4) (40 mg, 75% yield.). ^1H n.m.r. δ (p.p.m.) (300 MHz, [^2H]chloroform) 1.61 (6H, s, Me), 1.65 (3H, s, Me), 4.50 (1H, s, H3), 4.58 (1H, d, OCH_a), 4.60 (1H, d, OCH_b), 5.58 (1H, d, J=4.3 Hz, H5), 5.74 (1H, dd, J=4.3 Hz, J'=9.1 Hz, H6), 6.76 (1H, s, H2'), 6.88 (1H, d, J=7.8 Hz, H4' or H6'), 6.98 (1H, dd, J=2.5 Hz, J'=6.9 Hz, H6' or H4'), 7.37 (1H, dd, J=8.0 Hz, J'=7.2 Hz, H5'), 9.01 (2H, bs, COOH and NH). I.r. (chloroform) 3400 (m), 3020 (m), 1785 (s), 1740 (s), 1690 (s), 1610 (s), 1585 (s), 1520 (s), 1440 (m), 1290 (s), 1080 (m), 690 (m) cm^{-1}. U.V. λ_{max} (methanol) 274 nm (log ε 3.17), 352 (2.30). m/z (fast atom bombardment) 459 (M^+ + 1, 2%), 175 (15), 160 (100), 157 (77), 137 (24), 114 (38), 87 (23), 70 (26), 69 (23), 55 (21).

L,D-Iodo[2-^{14}C]acetyl-(S-diphenylmethyl)cysteinyl-valine benzhydryl ester

To a solution of L,D-S-(diphenylmethyl)-cysteinyl-valine benzhydryl ester [5] (70 mg, 0.13 mmol), iodoacetic acid (20 mg, 0.11 mmol) and 1-ethoxycarbonyl-2-ethoxy-1,2-dihydroquinoline (EEDQ)(40 mg, 0.16 mmol) in dichloromethane (1 ml) was added iodo[2-^{14}C]acetic acid (50μCi) in dichloromethane (2 ml), and the mixture stirred at room temperature overnight. The reaction mixture was diluted with dichloromethane, washed with saturated aqueous sodium bicarbonate solution, 10% citric acid solution, and dried over sodium sulphate. The solvent was removed *in vacuo*, and the crude product purified by flash chromatography (dichloromethane then ethyl acetate/dichloromethane (1:20, v/v)) to give the title compound as a white solid (73 mg, 96% yield), which was identical by t.l.c. to an authentic sample [5] (R_f 0.5 in ethyl

acetate/dichloromethane (1:20, v/v)).

L,D-2-[3-(3-Trifluoromethyl-3H-diazirin-3-yl)phenoxy][2-^{14}C]-acetyl-S-carbomethoxysulphenyl-cysteinyl-valine ([^{14}C]-DCV)

The above dipeptide (73 mg) was converted to the title compound [^{14}C]-DCV in 3 steps according to the literature method [5] in 80% overall yield. The radiochemical specific activity of the product [^{14}C]-DCV was found to be 240 mCi.mol^{-1}, giving a radiochemical yield of 40% from iodo[2-^{14}C]-acetic acid. A U.V. spectrum of [^{14}C]-DCV showed the characteristic diazirine absorption at 350 nm.

Incubation of [^{14}C]-DCV with IPNS and cofactors under the normal conditions followed by bioassay produced an inhibition zone on *S. aureus* plates, with the corresponding penicillin produced in 0.04% yield.

Determination of K_m and V_{max} Data for the conversion of DCV by IPNS

K_m and V_{max} data were obtained by the method of Baldwin *et.al* [3]: A mixture of IPNS (0.75 IU), DCV (0.33-1.6 mM), DTT (18 mM), ascorbic acid (1.8 mM) and ferrous sulphate (0.18 mM) in 50 mM ammonium bicarbonate buffer pH 7.9 (total volume 550 µl) was incubated at 27°C and shaken at 260 rev.min^{-1} for 5 min. Samples (100 µl) were withdrawn after 40, 60, 90, 120 and 300 sec. intervals, and immediately added to acetone (100 µl) to quench the reaction. The precipitated protein was separated by centrifugation, and the acetone removed by a stream of air. The supernatant volume was adjusted to 100 µl with 50 mM ammonium bicarbonate buffer pH 7.9, and then bioassayed.

Photolysis of DCV

The concentration of DCV in solutions during photolyses was estimated from the intensity of the diazirine absorption of 350 nm in the UV spectrum. This absorption decreases on decomposition of the diazirine group (see Fig. 1).

(i) A solution of DCV (2.5 mM) and DTT (8.4 mM) in 28 mM Tris-HCl buffer pH 7.7 and 14 mM ammonium bicarbonate buffer pH 7.9 (total volume 357 µl) was irradiated at 254 nm using the Mineralight lamp, over a 2h period at 4°C. See Fig.1.

(ii) A solution of DCV (6 mM) and DTT (8.4 mM) in 32 mM ammonium bicarbonate (total volume 157 µl) was irradiated at 355 nm using the YAG laser at 10°C over 10 min. During irradiation, nitrogen gas was seen to be evolved. See Fig. 1.

Photo-inactivation of IPNS by DCV

A pair of incubation mixtures was prepared. Both contained DTT (22 mM) and recombinant IPNS (0.038 IU, 0.07 mg) in 50 mM ammonium bicarbonate (total volume 157 µl); one contained DCV (6 mM) and the other did not. After pre-incubation at 0°C for 10 min., both of these mixtures were irradiated at 355 nm (YAG laser) for 6 min. Another pair of samples were also prepared as above, except that, instead of being

irradiated, they were kept in the dark. The enzyme was subsequently concentrated by centrifugation using Amicon Centricon™-10 Microconcentrators (5000xg/4°C/1h), and washed twice with 50 mM ammonium bicarbonate buffer (50 µl). The enzyme solution was then diluted to 200 µl with 50 mM ammonium bicarbonate; 180 µl of this solution was incubated with a mixture of ACV disulphide (1.6 mM), DTT (10.5 mM), ascorbic acid (1.1 mM) and ferrous sulphate (0.11 mM) and made up to a total volume of 330 µl with 50 mM Tris-HCl buffer pH 7.7. The solution was shaken at 27°C for 15 min., and the yield of isopenicillin N determined by bioassay in the usual manner. These values were used to calculate the extent of loss of activity of IPNS during irradiation in the absence or presence of DCV.

The dependence of photo-inactivation on DCV concentration was determined by comparing the IPNS activity (by bioassay) of both irradiated and non-irradiated samples at different levels of DCV. Samples of IPNS were photoinactivated as described above, except that the DCV concentration was varied between 0 and 5.7 mM.

Protection of IPNS by ACV Against Photo-inactivation by DCV

Mixtures of DTT (63mM), recombinant IPNS (0.050 IU, 140µg), DCV (5.6mM), either with or without ACV (74mM), were irradiated. An additional pair of control samples were prepared, but kept in the dark. The enzyme solution was then concentrated, washed and assayed as described above.

Incorporation of [^{14}C]-DCV into IPNS

In a typical experiment, a mixture of [^{14}C]-DCV (5.6 mM), DTT (45 mM) and fungal IPNS (0.11 IU, 0.20 mg) in 50 mM ammonium bicarbonate buffer (total volume 330 µl) was prepared. Two fractions were taken (150 µl each), one of which was irradiated for 7.5 min. (YAG laser) and the other of which was kept in the dark. Each of these solutions contained 0.1 µCi of ^{14}C. The molar ratio of [^{14}C]-DCV to IPNS was 360:1. The protein in both solutions was then concentrated by centrifugation in Amicon Centricon™-10 Microconcentrators (5000xg/4°C), and washed seven times with DTT (250 mM) in 50 mM ammonium bicarbonate . The ^{14}C content of the washings was determined by the addition of Optisafe (3ml), followed by liquid scintillation counting. The radioactive content of the last wash filtrate was less than 0.5% of the ^{14}C initially added. The protein was isolated, and examined by SDS-PAGE and fluorography. See Fig. 2.

Photoaffinity Labelling of IPNS by [^{14}C]-DCV

In a typical experiment, a mixture of [^{14}C]-DCV (0.71 mM), DTT (91 mM) and recombinant IPNS (0.3 IU, 2.0 mg) in 50 mM ammonium bicarbonate buffer (total volume 330 µl) was prepared. Two fractions were taken (150 µl each), one of which was irradiated for 7.5 min. (YAG laser) and the other of which was kept in the dark. Each

of these solutions contained 0.15 μCi of ^{14}C. The molar ratio of [^{14}C]-DCV to IPNS was 4.7:1. After this treatment the protein in both solutions was concentrated by centrifugation in Amicon Centricon™-10 Microconcentrators (5000xg/4°C), and washed seven times with DTT (250 mM) in 50 mM ammonium bicarbonate. The ^{14}C content of the washings was determined by liquid scintillation counting. The radioactive content of the last wash filtrate was less than 1.2% of the ^{14}C initially added. The protein was then purified by ion exchange chromatography on a Pharmacia FPLC system. A Mono Q 5/5 anion exchange column was used, developed at a flow rate of 1ml.min^{-1} at room temperature, with a linear gradient of sodium chloride (0-220 mM) in 20 mM Tris-HCl buffer (pH 7.7), and the eluate monitored at 280 nm. The radioactive content of the eluate fractions (1ml) was determined by the addition of Optisafe (6ml), followed by liquid scintillation counting. The results are shown in Fig. 3.

Protection of IPNS by ACV Against Photoaffinity Labelling by [^{14}C]-DCV

A mixture of ACV (0, 1.45, or 14.5 mM), DTT (152mM) and recombinant IPNS (0.3 IU, 2.0mg) in 50mM ammonium bicarbonate buffer (total volume 280 μl) was pre-incubated at 20 C for 5 min. [^{14}C]-DCV(final concentration 0.71mM) was added to give a total volume of 330μl, and each of the solutions divided into 2 fractions (150 μl each), one of which was irradiated for 7.5 min (YAG laser), and the other of which was kept in the dark. Each of these solutions contained 0.25μCi of ^{14}C. The molar ratio of DCV to IPNS was 4.7:1. The protein was purified by washing in Amicon Centricon™-10 Microconcentrators, followed by separation by ion exchange FPLC, as described above. The eluate was monitored at 280nm. The radioactive content of the eluate fractions (1ml) was determined by the addition of Optisafe (6ml), followed by liquid scintillation counting. The amount of IPNS protein eluted from the ion exchange column was estimated from the area of the A_{280} peak corresponding to IPNS. The incorporation of radioactivity per unit of IPNS protein was calculated for each sample at 0, 1.45 or 14.5mM ACV levels with or without irradiation.

RESULTS AND DISCUSSION

DCV was shown to be a substrate for IPNS in the following manner. Incubation of DCV with IPNS in the absence of U.V. irradiation gave rise to a product which was antibiotically active against *S. aureus* by a hole-plate assay, and sensitive to penicillinase (*B. cereus I*). DCV incubated in the presence or absence of cofactors and boiled IPNS showed no bioactivity. These results are consistent with enzyme-mediated formation of the expected penicillin (4) (Scheme 2).

An authentic sample of penicillin (4) was prepared by acylation of 6-aminopenicillanic acid (6-APA) with the appropriate acid chloride (Scheme 3). The biological activity of authentic penicillin (4) was equivalent to that of the incubation product and allowed quantification of the conversion yield of DCV. Antibiotic activity

against *S. aureus* was found to be one tenth that of Penicillin V and 100 times that of Cephalosporin C. The enzymatic conversion yield of DCV was 0.25% relative to the conversion of ACV; the kinetic parameters of the conversion were determined by a stopped bioassay technique [3]. These results, which are shown in Table 1, indicate that substitution of the aromatic ring by the photolabile group does not significantly affect the yield from the enzymatic conversion (entries 2 and 3). However, both L,D-phenoxyacetyl-cysteinyl-valine and DCV gave much lower conversion yields than the natural substrate ACV (entry 1, Table 1).

U.V. irradiation of DCV with a Mercury lamp at 254 nm showed approximate first order decomposition with a half-life of *ca.* 30 minutes (Fig. 1). However this method of photolysis proved unsatisfactory in subsequent experiments, since the prolonged exposure to this wavelength (required to produce complete decomposition of DCV) caused up to 80% loss of the catalytic activity of IPNS. Although literature reports have described extensive studies of the decomposition of diazirines to the corresponding carbenes using laser flash photolysis [12,13], this technique has not been widely used for photoaffinity labelling studies [14-18]. A frequency-tripled Neodymium-YAG laser provides high intensity monochromatic light at 355nm, corresponding closely to the diazirine absorption maximum (λ_{max} 350 nm) but not to that of proteins (λ_{max} *ca.* 280 nm), and therefore offers the possibility of selective generation of the reactive carbenes. Laser flash photolysis (pulse energy 21 +/- 2 mJ, repetition rate 10 Hz) of DCV gave complete decomposition of the diazirine group in 7 minutes under conditions which had no effect on IPNS activity (Fig. 1). Under these conditions, IPNS was inactivated upon irradiation at 355nm in the presence of DCV and dithiothreitol (DTT), and at least a 250-fold molar excess of DCV over IPNS was required in order to achieve complete inactivation.

The relatively low affinity of DCV for IPNS, as indicated by its K_m value (entry 3, Table 1), necessitates the use of a large excess of the labelling reagent in order to achieve complete inactivation of the protein. This could lead to non-specific labelling of the protein [4], and in order to investigate this possibility, a protection experiment was carried out. Thus, a labelling experiment in the presence of the natural substrate, ACV was conducted. Under these conditions, the label, DCV, is expected to be displaced from the active site, and specific labelling prevented [4], resulting in retention of activity of the enzyme. When a mixture of ACV, DCV, DTT and IPNS was incubated under the normal irradiation conditions (the ratio of ACV to DCV was 13:1), bioassay showed that 48% of the activity of IPNS was retained, compared with its activity in a non-irradiated sample. Under the same conditions, but in the absence of ACV, complete inactivation of IPNS resulted. The most likely explanation for these results is that ACV is protecting the active site from labelling by DCV. The incomplete retention of activity by IPNS may be due to the fact that both ACV and DCV have a relatively weak affinity for IPNS (entries 1 and 3, Table 1). However, it could also be due to the

modest excess of ACV used, since protection experiments of this kind have been reported where up to a 500-fold excess of the protecting agent (normally the natural substrate) was required in order to achieve complete protection [19, 20].

[^{14}]C-DCV was then used to demonstrate photoaffinity labelling of IPNS directly. Irradiation of IPNS in the presence of [^{14}C]-DCV and 100mM DTT was followed by concentration and desalting of the mixture in an Amicon Centricon™ - Microconcentrator (10,000 Dalton molecular weight cut-off). Thorough washing with 250mM DTT was carried out to remove non-covalently bound [^{14}C]-DCV. A non-irradiated control was also prepared and the IPNS protein washed as described above. Fluorography of SDS-polyacrylamide gels showing samples from both the irradiated and non-irradiated mixtures indicated that IPNS from the irradiated sample showed incorporation of radioactivity ; that is, photolabelling of IPNS had occurred (Fig. 2). This labelling of IPNS was highly selective, although not totally specific, since only IPNS and one other protein in the partially purified fungal extract (which contained 6 other protein species) were labelled under these conditions. The heavy band appearing in the fluorogram at the gel front is not protein, since it does not stain with Coomassie Blue dye. Similar examples of the incomplete specificity of photoaffinity labels for the targets for which they were designed have been reported [20, 21].

In order to confirm that the incorporation of radioactivity into IPNS occurs only in the irradiated sample under these conditions, an alternative approach was adopted. In this experiment, mixtures of IPNS and [^{14}C]-DCV (both irradiated and non-irradiated, as described above) were thoroughly washed using Amicon Centricon™-10 Microconcentrators, the enzyme was isolated, and purified by ion-exchange FPLC . A radioactively-labelled protein was isolated, which eluted in the position expected for IPNS, and which appeared identical to both untreated IPNS, and to IPNS from the non-irradiated control sample, when examined by SDS-PAGE . The data are shown in Fig. 3; in the non-irradiated solution (*-hV*) there has been no uptake of radioactivity into the IPNS. The irradiated sample (*+hV*) clearly demonstrates radiochemical incorporation into IPNS. The radiochemical specific activity of the labelled IPNS was found to be 2.8mCi.mol^{-1}, corresponding to a 21% incorporation of the label into the protein on a molar basis.

The specificity of the incorporation of [^{14}C]-DCV was investigated further, by means of an ACV protection experiment, similar to that described above. In the presence of ACV, with a ratio of ACV relative to [^{14}C]-DCV of 2:1, the uptake of [^{14}C]-DCV was 76% of that in the absence of ACV, and a 20:1 ratio of ACV:[^{14}C]-DCV gave only a 41% uptake. This confirmed the earlier bioassay results for the retention of activity of IPNS when the irradiations were performed using DCV in the presence of ACV, and is consistent with protection of the active site against labelling by DCV.

Thus using [^{14}C]-DCV , the selective, light-dependent, covalent incorporation of the modified substrate into IPNS, using laser photolysis, has been demonstrated. Unfortunately, the low radiochemical specific activity of the [^{14}C]-DCV meant that it was not practicable to attempt to localise the point of insertion of the radioactive label by digestion of the ^{14}C-labelled IPNS, followed by sequencing of the radioactive fragments. However, we have recently prepared a tritiated derivative of DCV, which has a much higher radiochemical specific activity, and are currently examining its utility in order to locate the point of attachment of DCV to IPNS.

ACKNOWLEDGEMENTS

The authors would like to thank Drs R.M. Adlington and M.J.C. Crabbe for helpful discussions, Dr G. Hancock (Physical Chemistry Laboratory, Oxford) for use of the laser equipment, and Mr C. Astbury and Mr D. Heard for assistance with the laser experiments. Financial support was provided by the Science and Engineering Research Council and Eli Lilly and Company. JBH acknowledges financial support from the United States Army European Office (contact number; DAJA 45-85-C-0034). MGM acknowledges financial support from Glaxo Group Research Ltd. (U.K.).

REFERENCES

[1] Baldwin, J.E. (1985) in 'Recent Advances in the Chemistry of β-Lactam Antibiotics'. Third International Symposium, 1984. (Brown A.G. and Roberts S.M., eds.), pp. 62-85, The Royal Society of Chemistry, London.

[2] Samson, S.M., Belagaje, R., Blankenship, D.T., Chapman, J.L., Perry, D, Skatrud, P.L., VanFrank, R.M., Abraham, E.P., Baldwin, J.E., Queener, S.W. and Ingolia, T.D., (1985) *Nature* **318**, 191-194.

[3] Baldwin, J.E., Abraham, E.P., Burge, G.L. and Ting, H-H. (1985) *J.Chem.Soc., Chem.Commun.*, 1808-1809.

[4] Bayley, H., (1983) "Photogenerated Reagents in Biochemistry and Molecular Biology", North-Holland/Elsevier, Amsterdam.

[5] Baldwin, J.E., Pratt, A.J. and Moloney, M.G. (1987) *Tetrahedron* **43**, 2565-2575.

[6] Pang, C-P., Chakravarti, B., Adlington, R.M., Ting, H-H., White, R.L., Jayatilake, G.S., Baldwin, J.E. and Abraham, E.P. (1984) *Biochem.J.* **222**, 789-795.

[7] Baldwin, J.E., Killin, S.J., Pratt, A.J., Sutherland, J.D., Turner, N.J., Crabbe, M.J.C., Abraham, E.P. and Willis, A.C. (1987) *J.Antibiot.* **40**, 652-659

[8] Smith, B., Warren, S.C., Newton, G.G.F. and Abraham, E.P. (1967) *Biochem.J.* **103**, 877-890.

[9] Laemmli, U.K. (1970) *Nature* **227**, 680-685.

[10] Miller, J. (1959) *J.Org.Chem.* **24**, 560-561.

[11] Still, W.C., Kahn, M. and Mitra, A., (1978), *J.Org.Chem.* **43**, 2923-2925.

[12] Turro, N.J., Lehr, G.F., Butcher, J.A., Moss, R.A. and Guo, W. (1982) *J.Am.Chem.Soc.* **104**, 1754-1756.

[13] Liu, M.T.H. (1982) *Chem.Soc.Rev* . **11**, 127-140.

[14] Rak, S.F., and Schuster, G.B. (1987) *Photochem. Photobiol.* **45**, 439-43.

[15] Hucho, F., Muhn, P., and Fahr, A. (1986) *J. Protein Chem.* **5**, 99-107.

[16] Weber, H., Junge, W., Hoppe, J., and Sebald, W. (1986) *FEBS Lett.* **202**, 23-6.

[17] Fahr, A., and Hucho, F. (1986) *J. Neurosci. Methods* **16**, 29-38.

[18] Muhn, P., Fahr, A., and Hucho, F. (1984) *Biochemistry* **23**, 2725-2730.

[19] Ray, R., Holick, S.A., Hanafin, N., and Holick, M.F. (1986) *Biochemistry* **25**, 4729-4733.

[20] Link, R.P., Kutner, A., Schnoes, H.K., and DeLuca, H.F. (1987) *Biochemistry* **26**, 3957-3964.

[21] Harter, C., Bachi, T., Semenza, G., and Brunner, J. (1988) *Biochemistry* **27**, 1856-1864.

Table 1. Yields and kinetic data for enzymatic conversion of various substrates by IPNS to the corresponding penicillins.

Entry	Substrate	Yield (%)	K_m (mM)	V_{max} ($\mu molmin^{-1}\mu mol^{-1}$)
1	ACV	100	0.16	1.64
2	VCV	0.04	0.50	0.80×10^{-3}
3	DCV	0.25	0.77	0.75×10^{-3}

Fig. 1. Photolyses of DCV solutions.

-⊙- , mercury lamp photolysis at 254nm ; -◆- , frequency tripled neodymium-YAG laser at 355nm. For details, see the text.

Fig. 2. Incorporation of [^{14}C]-DCV into IPNS

Fungal IPNS was incubated with [^{14}C]-DCV and DTT , and either kept in the dark (-) or irradiated (+) with a Neodymium-YAG laser. Washed protein samples were freeze dried, separated by SDS-PAGE , stained with Coomassie Blue (a), and then fluorographed at -78°C for 14 weeks (b). For details, see the text.

(M), molecular weight markers { albumin (bovine serum; 66.2 kDa), ovalbumin (hen's egg; 45kDa), carbonic anhydrase (bovine erythrocyte; 30kDa), myoglobin (horse; 17.2 kDa) and cytochrome *c* (horse; 12.3 kDa)}.

Fig. 3. Photoaffinity Labelling of IPNS by [^{14}C]-DCV

Recombinant IPNS was incubated with [^{14}C]-DCV and DTT , and either kept in the dark (*-hV*) or irradiated (*+hV*) with a Neodymium-YAG laser. Each sample was washed, loaded onto a Mono Q 5/5 anion exchange FPLC column, and eluted with a sodium chloride gradient. The radioactive content of each fraction was determined by liquid scintillation counting. For details, see the text. IPNS protein elutes in Fractions 22-26. The peak of radioactivity eluting from 43-50ml arises from the final wash of the column with 400mM NaCl, and appears not to be associated with protein. —— , A_{280}; o—o ^{14}C cpm; - - -, [NaCl] (M).

FIGURES ETC

Scheme 1

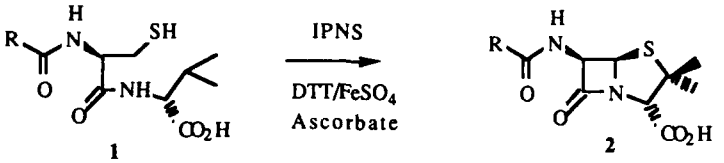

Scheme 2

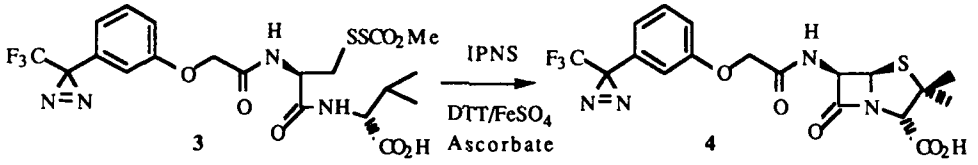

Scheme 3

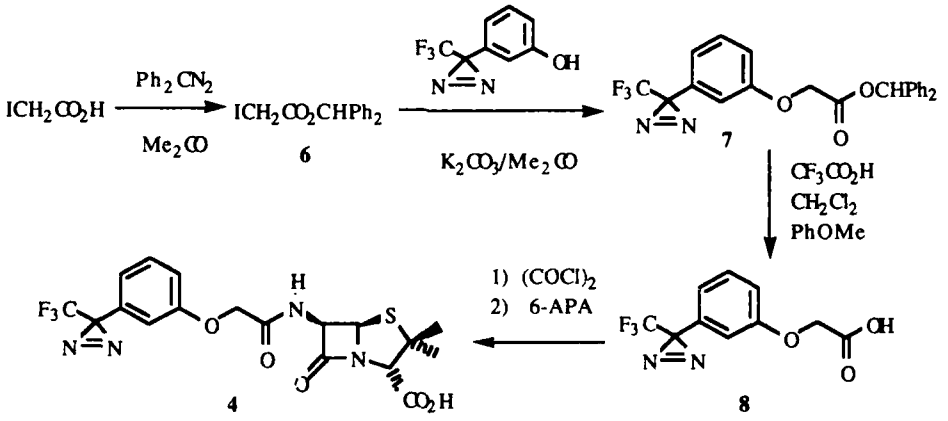

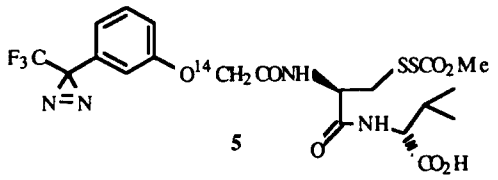

5

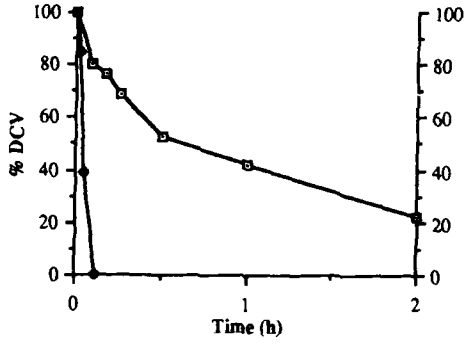

Fig. 1. Photolyses of DCV(3) solutions.

⊙ , mercury lamp photolysis at 254nm ; ◆ , frequency tripled neodymium-YAG laser at 355nm. For details, see the text.

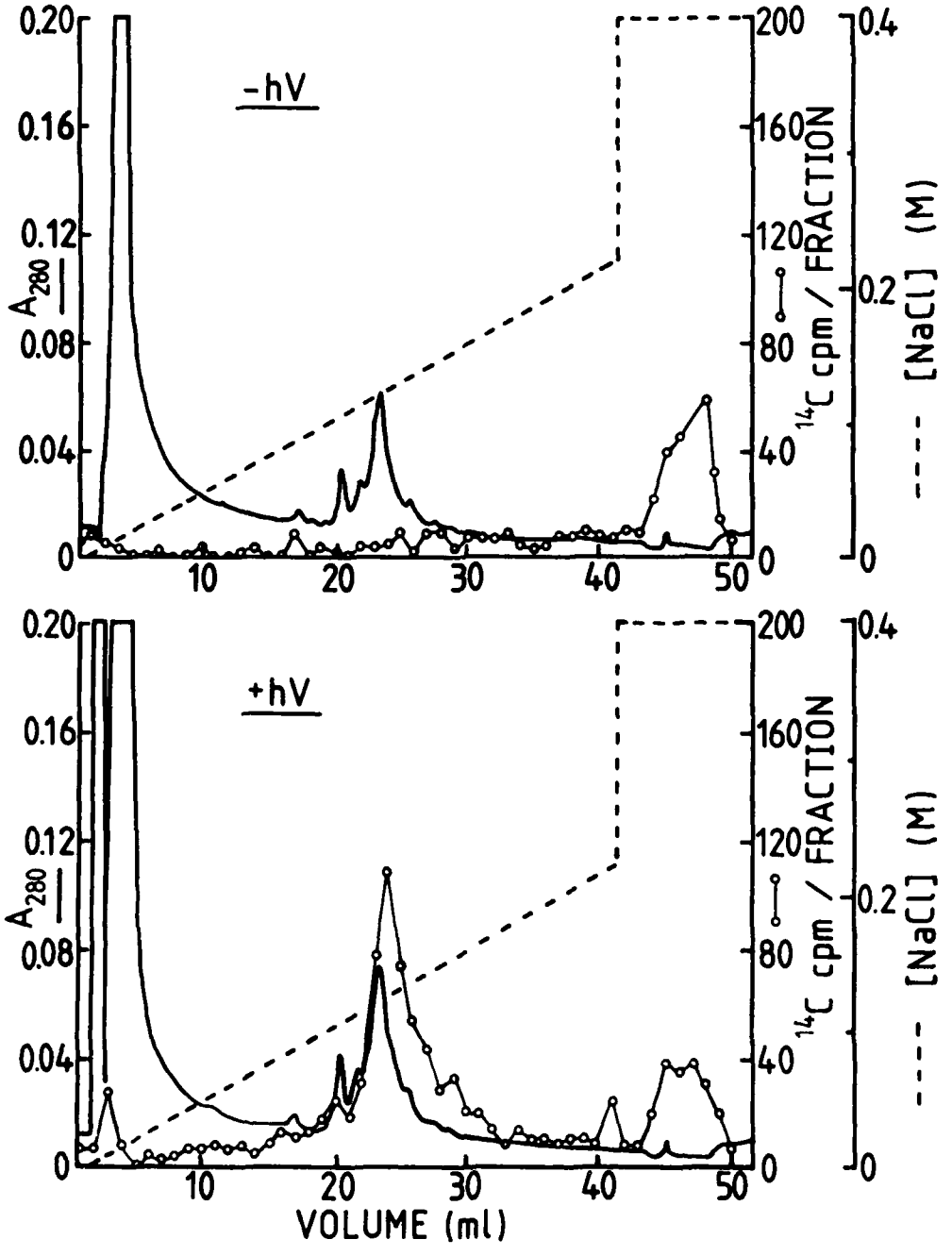
-hV
+hV
A_{280}
^{14}C cpm / FRACTION
[NaCl] (M)
VOLUME (ml)
0.20
0.16
0.12
0.08
0.04
0
200
160
120
80
40
0.4
0.2
10
20
30
40
50